



CENTRO DE INVESTIGACIÓN Y DE ESTUDIOS AVANZADOS DEL INSTITUTO
POLITÉCNICO NACIONAL
Unidad Mérida

DEPARTAMENTO DE FÍSICA APLICADA

**“Systematic Exploration of the Potential Energy Surfaces of
Molecular Clusters”**

TESIS

Que presenta

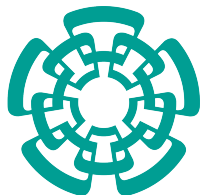
Alba Margarita Vargas Caamal

Para obtener el grado de

Doctora en Ciencias
en
Fisicoquímica

Director de Tesis:

Dr. José Gabriel Merino Hernández



**CENTRO DE INVESTIGACIÓN Y DE ESTUDIOS AVANZADOS DEL INSTITUTO
POLITÉCNICO NACIONAL**
Unidad Mérida

DEPARTAMENTO DE FÍSICA APLICADA

**“Exploración de la superficie de energía potencial de cúmulos
moleculares”**

TESIS

Que presenta

Alba Margarita Vargas Caamal

Para obtener el grado de

Doctora en Ciencias
en
Fisicoquímica

Director de Tesis:

Dr. José Gabriel Merino Hernández

*A las mujeres de mi vida,
por haberme construido**

**Alba María, Isabel, Lisbeth, Magui, Angeles, Rosario, Ángela, Carolina, Reyna, Liz, Maricruz, Pety, Isabel C., Violeta, Stephanie, Izari, Ixaura, Lupita, Mariana, Melissa, Fairoja, Marissa, Ritzabel, Melina, Gaby, Helen.*

AGRADECIMIENTOS

En el aspecto profesional quiero dar gracias a mi asesor, Dr. Gabriel Merino.

Por sus enseñanzas, por creer en mí e impulsarme en el camino científico.

También a todos los colaboradores de los artículos publicados, cuyas aportaciones han sido clave para el desarrollo de este trabajo. De manera especial agradezco a los doctores Albeiro Restrepo, Cristina Vargas, Filiberto Ortiz Chí, y Romeo de Coss por su disponibilidad y apoyo como sinodales.

Gracias al Cinvestav por darme el privilegio de esta formación académica y al

Conacyt por la beca otorgada, por ayudarme a alcanzar esta meta.

Y de modo personal quiero dar gracias a Dios por iluminar mi camino. A mi madre Alba María por su amor y maravilloso ejemplo. A mis hermanos, especialmente a Isabel y Lisbeth por darme fortaleza y apoyarme, su cariño y consejo me han impulsado en todo momento. A mis sobrinos, por su hermosa amistad y apoyo, cuenten conmigo siempre.

To Jürgen, you give more light and inspiration to my life, for this love that crosses oceans, ILD.

A mis amigos por su cariño, consejos y apoyo: Gely, Rosario, Ángela, Caro, Reyna, Leandro, Liz, Isabel, Stephanie, Izari, Violeta. Ustedes y mi familia son mis ángeles en la Tierra.

RESUMEN

En esta tesis se presenta el resultado de estudios teórico-computacionales sobre cúmulos que van desde dímeros de etanol y metallocenos hasta sistemas que resultan de la microsolvatación de haluros de hidrógeno. Esto permitió conocer las estructuras de mayor estabilidad, la naturaleza de las interacciones que mantienen los cúmulos como unidades discretas y contestar la pregunta ¿cuántas moléculas de agua se necesitan para disociar un ácido?. Para esto se llevó a cabo la exploración sistemática de las superficies de energía potencial (PES, por sus siglas en inglés), empleando el programa GLOMOS, métodos *ab initio* y la teoría de los funcionales de la densidad. Además de los resultados geométricos y energéticos, las discusiones sobre las interacciones se basaron en la información obtenida mediante el índice de interacciones no-covalentes (NCI, por sus siglas en inglés), análisis de descomposición de energía (EDA, por sus siglas en inglés), índices de Wiberg, gráficas Stern-Limbach y cálculo de momentos dipolares, entre otros métodos. En los dímeros de metallocenos, la búsqueda exhaustiva convergió a tan sólo cuatro isómeros cuya estabilidad relativa se modifica con la variación de temperatura. Los resultados del EDA y NCI mostraron que la dispersión tiene la mayor contribución para estabilizar estos sistemas. En contraste, se obtuvieron 153 isómeros de los dímeros de etanol dentro de un rango de tan sólo 6.5 kcal mol⁻¹ y se clasificaron en tres grupos de acuerdo al tipo de interacción dominante. La complejidad de estos sistemas con puentes de hidrógeno también se reflejó en la gran variedad obtenida de la microsolvatación de una molécula HX con hasta siete moléculas de agua, donde se localizaron 3778 cúmulos en un rango de 22 kcal mol⁻¹. Los resultados muestran que el HI se disocia a partir de tres moléculas de agua, HBr con cuatro y HCl con cuatro o cinco dependiendo del factor entrópico mientras que el fluoruro de hidrógeno se disocia sólo parcialmente con siete moléculas de agua. En los cúmulos (HX)_n(H₂O)_n se requirieron tres, dos y dos moléculas de agua, para disociar HCl, HBr y HI respectivamente. Esta disminución en el número de moléculas de agua para obtener la disociación cuando se tiene más de una molécula HX, sugiere efectos cooperativos. Un resultado interesante fue la formación espontánea de aniones bihaluro BrHBr⁻ y IHI⁻, que implican puentes de hidrógeno muy fuertes. En general, las interacciones que estabilizan los cúmulos microsolvatados son: puentes de hidrógeno agua-agua y HX-agua, así como las electrostáticas del par iónico formado entre iones hidronio (cationes Eigen, Zundel y estructuras intermedias de estas especies) e iones haluro.

ABSTRACT

This thesis presents the results of theoretical-computational studies on clusters ranging from dimers of ethanol and metallocenes to systems resulting from the microsolvation of hydrogen halides. Information about the nature of the interactions that keep the clusters as discrete units and the lowest energy structures clusters were obtained. For microsolvated systems, the question: how many water molecules are needed to dissociate an acid? was answered. For this, the systematic exploration of potential energy surfaces (PES) was carried out, using the GLOMOS code, *ab initio* methods, and density functional theory. In addition to the geometric and energetic results, the discussions about the interactions were based on the information obtained through methods such as NCI (Non-covalent interactions index), energy decomposition analysis (EDA), Wiberg bond indices, Stern-Limbach plots and calculation of dipole moments, among others. In the metallocene dimers, the exhaustive search converged to only four isomers whose relative stability is modified by the variation in temperature. The results of the EDA and NCI showed that dispersion has the main contribution to stabilize these systems. In contrast, 153 isomers of the ethanol dimers within a range of only 6.5 kcal mol⁻¹ were obtained and classified into three groups according to the type of dominant interaction. The complexity of these systems with hydrogen bonds was also reflected in the wide variety of clusters obtained from the microsolvation of one HX molecule with up to seven water molecules, whit 3778 structures located in a range of 22 kcal mol⁻¹. The results show that HI dissociates from three water molecules, HBr with four and HCl with four or five depending on the entropic factor while hydrogen fluoride is only partially dissociated with seven water molecules. In the (HX)_n(H₂O)_n clusters, HCl, HBr, and HI achieved dissociation with three, two, and two water molecules, respectively. The decrease in the number of water molecules required for dissociation, when it is compared with clusters with one single HX molecule, suggests cooperative effects. Interestingly, the formation of bihalide anions BrHBr⁻ and IHF⁻, which are species with strong hydrogen bonds, was spontaneous. Microsolvation promotes the formation of Eigen, Zundel and intermediate Eigen-Zundel-like structures, which stabilize the clusters along with water-water and HX-water hydrogen bonds, ionic and long range X...H interactions.

CONTENTS

RESUMEN	7
ABSTRACT	9
OBJECTIVES	14
INTRODUCTION	15
Chapter 1. Conceptual framework	19
Microsolvation	20
Non-covalent interactions	29
Hydrogen and halogen bond	32
Proton transfer and dissociated complexes	34
Structural sampling	38
Experimental methods	41
Chapter 2. Methodology	45
Introduction	46
The GLOMOS code	48
Dispersion corrections	50
Bonding Analysis	52
Wiberg bond index	52
Energy decomposition analysis (EDA)	53
Non-covalent index (NCI)	56
Stern-Limbach plots	59
Appendix A. Methodology	62
Chapter 3. Ethanol dimers	68
Introduction	69

Computational details	71
Results and discussions	72
Potential energy surface analysis	72
Energetics	76
Energy decomposition analysis	80
Conclusions	85
Appendix B. Ethanol dimers.	86
Chapter 4. Metallocene dimers	91
Introduction	92
Computational details	93
Results and discussions	94
Structures and energetics	94
Thermal effects	96
Bonding and EDA	99
Conclusions	105
Appendix C. Metallocene dimers	106
Chapter 5. Microsolvation of HCl	110
Introduction	111
Computational details	112
Results and discussions	113
Structures and energetics	113
Bonding analysis	117
Dipole moment	120
Conclusions	124
Chapter 6. Microsolvation of hydrogen halides HX (X= F, Cl, Br, and I)	125
Introduction	126

Computational details	129
Results and discussions	129
Structures and energetics	129
Bonding Analysis	135
Dipole moment distribution	138
Conclusions	141
Appendix D. Microsolvation of hydrogen halides HX (X= F, Cl, Br, and I).		142
Chapter 7. Acid dissociation in (HX)_n(H₂O)_n clusters		
(X= F, Cl, Br, I; n= 2, 3)	144
Introduction	145
Computational details	147
Results and discussions	147
Structures and energetics	147
Bonding Analysis	152
Conclusions	158
Appendix E. Acid dissociation in (HX) _n (H ₂ O) _n clusters (X= F, Cl, Br, I; n= 2, 3)	159
PUBLICATIONS	167
REFERENCES	168

OBJECTIVES

1. To explore systematically the potential energy surfaces of molecular clusters of different nature to know the lowest energy structures.
2. To analyze the type of interactions that stabilize the clusters.
3. To determine the number of water molecules needed to dissociate the hydrogen halides HF, HCl, HBr and HI.

“Theory without facts is fantasy, but facts without theory is chaos”

Charles O. Whitman

Introduction

In nature, even the simplest phenomenon possesses a high degree of complexity and requires some approaches to be studied. A first intuitive step is to divide the problem into small pieces or propose simplified models. Certainly, experiments have been essential pieces in scientific methodology but in most of the cases, it is difficult to isolate the system and obtain detailed information. Nowadays, computational tools and advanced experimental techniques allow examining chemical issues at a molecular and atomic level, providing the opportunity to use a kind of powerful “microscope” to study phenomena and explain mechanisms. Solvation is a clear example and plays a crucial role in a wide range of physical, chemical and biochemical processes. Clusters formed by interacting solvent and solute molecules depicts the solvation at a molecular level, called microsolvation. Clusters of a variety of molecules have received attention due to they provide convenient and theoretically tractable systems since they are considered a bridge between atoms and their bulk counterpart.¹ Under this perspective, their study is a way to divide the problem and to take a sample or handle it as simplified models of condensed phases. In this sense, computational methods have demonstrated to be successful in predicting the most stable structures and give information about the type of stabilizing interactions.²⁻⁵ Particularly in microsolvation, these studies focus on the number of solvent molecules required to develop bulk-

like behavior.⁶ Thus, water-acid clusters allow to address the issue of dissociation and suggest the question: How many water molecules does it take to dissociate an acid? To answer this question, microsolvation was the center of interest in this work and clusters of hydrogen halides with water molecules were studied. Moreover, the study of the transfer of the proton in water-acid clusters and its evolution as it increases the size of this cluster is intended to answer for the relationship between microsolvation and reactivity because it is possible to gradually follow the progression of intermolecular interactions.⁷ The analysis should consider all possible geometries and not only one structure for a given chemical formula, which involves the full characterization of the Potential Energy Surface (PES)⁸. This can be a difficult task because microsolvation implies to increase the number of solvent molecules until dissociation, carrying to bigger clusters and the non-covalent intermolecular interactions entail complicated search landscapes with large numbers of local minima and small energy barriers.⁹⁻¹⁰

Hence, a beginning with smaller clusters was crucial to try our systematic exploration method and learn about the characterization of structures and interactions. In this sense, dimers were selected as a convenient starting point, since they can be considered the simplest model of interacting molecules. Ethanol dimers were the first system explored because they have a complex potential energy surface and is an advantageous model to study hydrogen bonding. The rich landscape of structures and information obtained, was fundamental for learning on the searching method, classification of structures and analysis bonding to continue with the exploration of clusters with different nature. Then, metallocenes dimers were the next computational defiance because they have transition metals, a high coordination number, and relativistic effects can play a significant role. The result was fruitful, expanding the knowledge about interactions and the use of tools to analyze them. Thereby, with the acquired experience,

the road was ready to take on the next task: microsolvation of hydrogen halides. HCl was the first system chosen due to studies on its dissociation in the condensed phase and in microsolvation environments. In addition, an experimental work was a motivation to start with this species. Afterward, the exploration was extended to the hydrogen halides family because they are considered to form the simplest acids and have a key role in the chemical and atmospheric field.

To present the systematic exploration of the potential energy surfaces of molecular clusters, this thesis is divided into seven chapters. Chapter one provides a conceptual framework of the main topics: microsolvation, clusters, non-covalent interactions, and a perspective of the challenges related to the study of these systems. Water was the solvent used in the microsolvated clusters but an overview of microsolvation studies with nonaqueous solvents also is important owing to their technological applications within fields such as separation chemistry, electrochemical devices or ionic recognition.¹¹

The stochastic, structurally unbiased approach used to sample the PES is described in the second chapter. Moreover, a brief description of the methods used for the analysis bonding is given. The next chapters describe the studies and results of the clusters selected. Thus, a comprehensive characterization of the ethanol dimer PES is presented in Chapter 3, which provides insights into the nature of the interactions that keep the dimers as discrete units as well as highly correlated energies to evaluate relative stabilities while the detailed analysis of the bonding and nature of the ferrocene dimer is contained in Chapter 4 and it will be worth pursuing to understand the pattern of its supramolecular arrangements.

The first topic about microsolvated clusters is in Chapter 5, which is devoted to the exploration of the PES of HCl with one up six water molecules. An analysis of bonding based on energetics, Wiberg Index, average dipole moments, and Stern-Limbach plots was carried out to answer the question about the number of water molecules needed to obtain dissociated complexes and to know the stabilizing interactions in these systems. Following the same methodology, the results obtained of the systematic exploration of the PES for the complete series of hydrogen halides (HX, X= F, Cl, Br, and I) with up seven water molecules is presented in Chapter 6. Finally, the exploration was extended to clusters with more of one HX molecule in the seventh chapter, through the study of $(HX)_n(H_2O)_n$ clusters with $n=2, 3$. This provided new insights into microsolvation since there are few reports regarding the presence of more than one molecule of acid, which expands the variety of interactions and structural richness.

Chapter 1

Conceptual framework

“The role of the infinitely small in nature is infinitely great”

Louis Pasteur

Microsolvation

According to the definition of IUPAC, solvation is *any stabilizing interaction of a solute (or solute moiety) and the solvent or a similar interaction of solvent with groups of an insoluble material (i.e. the ionic groups of an ion-exchange resin). Such interactions generally involve electrostatic forces and van der Waals forces, as well as chemically more specific effects such as hydrogen bond formation.*¹² In a short definition, solvation is the process of surrounding solute particles by solvent (See Figure 1.1).¹³⁻¹⁵ Whereas Florez, *et al.*⁹ defines microsolvation as “the stabilization of solute-solvent complexes because of the explicit intermolecular interactions between the participating moieties.”

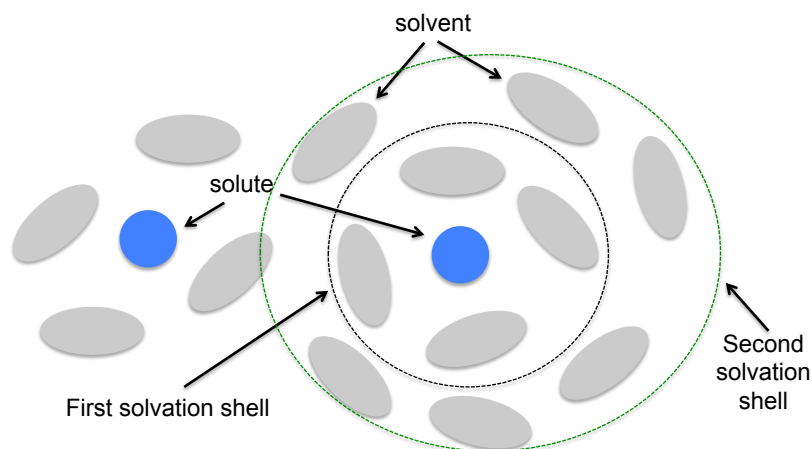


Figure 1.1 Scheme of the solvation process

These definitions contain key concepts as solute (or moiety), solvent, and intermolecular interactions whose stabilizing action keep the parts of the system together (forming complexes). Then, an overview of intermolecular interactions is mandatory to have a complete definition and this topic will be addressed later. First, a brief look at how the solvation effects are performed in computational calculations. Solvation studies can be carried out through two methodologies (and hybrids of these two): microsolvation or explicit solvation, and implicit or continuum solvation (see Figure 1.2).

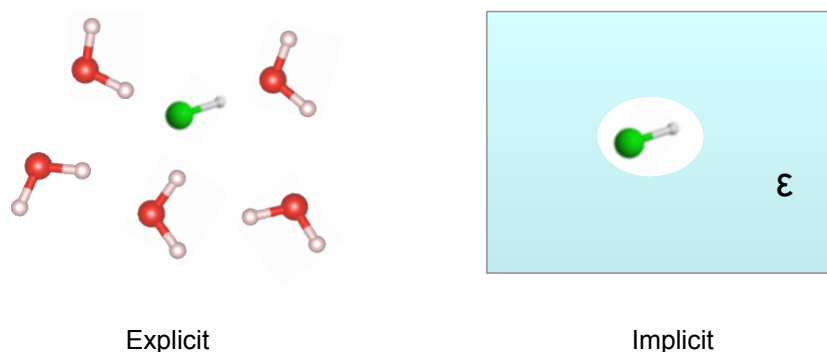


Figure 1.2 Representation of microsolvation (explicit) and implicit solvation.

Microsolvation (or explicit solvation), involves the presence of solvent molecules around the solute molecule, typically about one to ten. In experiments, a solute molecule is surrounded, depending on its size, by a first solvation shell of about six (for a monatomic ion) to probably hundreds or thousands of water molecules for a protein. The first solvation shell is, in turn, solvated by a second shell, and so on. (Figure 1.1) This approach gives more details on the molecular structures and short-range effects but in general carries high computational cost,

which depends on the size and kind of clusters, level of theory and methods employed. In this work, microsolvation was the approach used to study acid dissociation. The methods and computational details will be described in the next chapter.

On the other hand, the implicit solvation uses a continuous medium (a continuum) to “imply” the presence of individual solvent molecules. Consider solvent as uniform polarizable medium or fixed constant ϵ (dielectric constant or relative permittivity), instead of individual solvent molecules and the solute as a molecule in a suitably shaped cavity in the medium (see Figure 1.2) Although for some purposes explicit solvation is needed, particularly where solvent molecules participate in a reaction, continuum methods are widely used due to its lower computational cost.¹⁶

The complexes mentioned in the definition of microsolvation are clusters of solute and solvent molecules. A cluster is a group of atoms or molecules that are formed by means of covalent and non-covalent interactions. Small clusters have been experimentally detected in several environments (laboratory, atmosphere, outer space), thus, it is important to understand their composition, structure, and bonding.⁹ They can be classified as atomic (pure or mixed), see examples of fullerene and CB_4 clusters¹⁷ in figure 1.3; and molecular clusters, homogeneous (one-component) and heterogeneous (two or more component), as clusters with water molecules of Figure 1.3. Dimers studied in this work are homogeneous molecular and the microsolvated clusters are a heterogeneous molecular type.

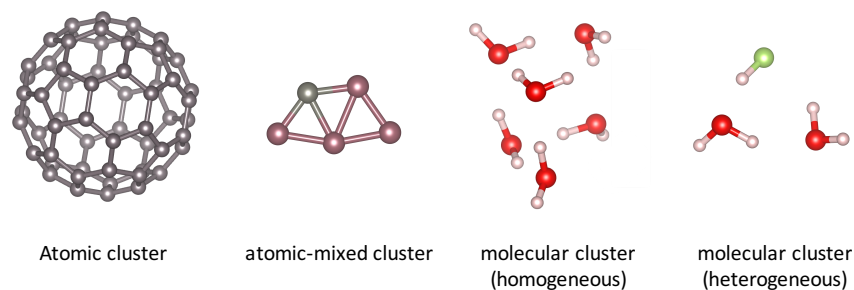


Figure 1.3 Examples of atomic and molecular clusters.

Since most electrolytes are less soluble in nonaqueous solvents than in water, solvation phenomena in nonaqueous solution have been much less investigated compared to those in aqueous solution. However, nonaqueous solutions of electrolytes have been interesting for physical chemistry and bio-disciplines in understanding ion-molecule interactions, protein stabilization as well as enzymatic activity¹⁸ and recognizing their importance in various industries such as material production, electrolysis, and metal plating.¹⁹

Classification of solvents is related to their polar character or value of dielectric constant. Thus, solvents are polar ($\epsilon > 15$) or non-polar ($\epsilon < 15$). A polar solvent can be protic or aprotic; protic solvent contains labile proton (usually has a hydroxyl, carboxyl or amine group); i.e. water, ammonia, and formic acid. Aprotic solvents cannot donate protons, examples: acetone, acetonitrile, and tetrahydrofuran. Alcohols and some nonaqueous solvents such as N, N-dimethylformamide (DMF), dimethyl sulfoxide (DMSO), or acetonitrile (AN) have medium relative dielectric constants $\epsilon = 35-46$ compared with high (water, $\epsilon = 78.4$ at 20 °C) and low (benzene and n-hexane, $\epsilon = 1.9 - 2.3$) dielectric solvents, and many electrolytes can be dissolved in these solvents.¹⁹

Studies on structure and dynamics of electrolytes in nonaqueous solvents are available in literature.^{11, 20-25} Given the vast amount of them, it would be impossible to cover all the solvation studies. A brief outline of some papers is as follows.

Salter *et al.*,²⁴ reported bond dissociation energies as results of calculations on lithium–ammonia clusters and their cationic equivalents with the aim of establishing accurate Li–N bond dissociation energies of these clusters for the first time. Small alkali-ammonia clusters, provide tractable model systems for experimental and theoretical studies that may mimic some aspects of solvated electron behavior. On the other hand, an extensive study on the “isolated” carboxylic (–COOH) and amide (–NH) interactions in neat DMSO using spectroscopic methods and studies along with molecular dynamics (MD) simulations, density functional theory (DFT), and *ab initio* calculations were recently published.²⁵

Nielsen,²³ Marques¹⁰ and their co-workers have studied microsolvated ions in water and methanol. As the methanol molecule combines a hydrophobic part with a hydrophilic OH-group, the structure of (CH₃OH)_n clusters is less dominated by the H-bond network than in the case of water. Acetonitrile is another solvent used in microsolvation of ions, Ayala *et al.*²⁶ explored bromine anion in water, methanol, and acetonitrile to establish the geometrical distribution and solvent-solvent, ion-solvent interactions. One example of experimental-theoretical work was carried out by Dauster *et al.*,²² they generated methanol clusters via supersonic expansion and doped with sodium atoms to determine ionization potentials and compared with quantum-chemical calculations.

In contrast with water or methanol, benzene clusters are prototype systems that can be used to study non-polar environments, which are relevant to understanding the selectivity of

many chemical phenomena occurring in living organisms, since it has been recognized that interactions between aromatic rings contribute, among others, to the base-pair stacking in DNA, to protein structure or to the formation of supramolecular architectures.²⁷ There are studies about solvation of benzene²⁸ and phenol clusters with water and methanol as solvents.²⁸⁻²⁹ In the same way, Barbu *et al.*³⁰ reversed the role of the aromatic molecules and used them to solvate the small anion species, NO⁻ and O⁻². The solvents included benzene, naphthalene, pyridine, and pyrimidine. Another report presented the microsolvation features of three alkali-ion systems (i.e., Na⁺, K⁺, and Cs⁺) solvated with benzene up to 21 molecules.²⁷

Microsolvation of the cation- π interaction has been explored in detail by Sastry and co-workers,³¹⁻³³ they reported that the sequential attachment of water molecules to cation- π (Li⁺-benzene, K⁺-benzene, and Mg⁺²-benzene) systems revealed how solvation of the metal ion decreases its interaction energy with the π system, while the solvation of the π system increased its interaction energy with the metal ion.

The solvated electron is perhaps one of the best-studied species in this area as it is the simplest quantum solute.³⁴⁻³⁵ How chemical environments stabilize excess charges is of critical importance in biology, solution phase chemistry, and condensed matter physics. Microsolvated ions are bare ions that are ligated by one or more solvent molecules. They occur in diverse areas in biochemistry, surface, and atmospheric chemistry. For example, the microsolvation of halide ions is extensive although mostly in an aqueous environment.^{9, 11, 23, 26, 30}

Owing to most biochemical reactions of interest occur in the solution phase, the effects of solvation on biomolecules will be very important. An amino acid, which is the building block of protein, is an ideal system to study the effects of solvation on the biochemical activity due to

their moderate size. Then, microsolvation of amino acids such as glycine, alanine, adenine, cysteine and their zwitterionic complexes is a trend research.³⁶⁻⁴² Ahn and co-workers¹³ carried out calculations for the bare alanine, neutral alanine-(H₂O)_n, and alanine zwitterion (AlaZW)-(H₂O)_n, (*n* = 1 and 2) clusters. Göth *et al.*⁴³ studied the gas-phase structure of ubiquitin and its lysine-to-arginine mutants, ubiquitin is a small protein that plays an important role in signal transduction and post-translational modification of other proteins.

A related issue is the environment of protein chromophores, which is far from bulk solution since only a limited number of water molecules have access to the chromophore. Likewise, the water content inside DNA is limited, about 2.5 water molecules per base pair,⁴⁴ and only during DNA replication where part of the DNA helix is unwinded, there is large exposure to water. In ion transport through membranes, ions have to shed their solvation shell of water, but to lower the energy cost, the membrane protein mimics the solvation shell by replacing the water by e.g. amide groups or alcohol groups of amino acid residues.²³

In the case of mixed solvents, the solutes can be preferentially solvated by either solvent, nevertheless, the solvent-solvent interactions can significantly influence solute-solvent interactions. The organic solvents which are miscible with water are used for these types of experiments.⁴⁵ In this sense, mixed solvents have widely been used in thermodynamic, dynamic, and kinetic studies on ionic interactions in solution with changing solvent properties of the reaction medium. In order to explain the variation of data, the approaches usually assume a homogeneous continuum with specific bulk properties, because theories which can be successfully applied to a neat medium usually fail in mixed solvent systems.¹⁹

Finally, the list of reports about solvation in water is vast: microsolvation of formamide,¹⁴ anions solvated in water,^{9, 15, 26, 46} cations derived from magnesium, lithium, sodium, cesium as well as sulfate, chloride, iodide, and perchlorate anions, reveals that the effect of ions and counterions on water can be strongly interdependent and nonadditive and in certain cases extends well beyond the first solvation shell of water molecules directly surrounding the ion.^{33, 47-48} Although the microsolvation model derived from salt-water clusters is not expected to quantitatively predict the liquid-phase solvation of the salts, it can be used to provide valuable insights into the interactions between the solvent and the solute ions. In this topic, Liu *et al.*⁴⁹ carried out studies on the microsolvation of three different alkali-halide ion pairs, LiI, CsI, and NaCl. They, as well as other researchers,^{1, 50} noticed that the number of water molecules needed to separate one ion pair is coincident with the solvent/solute ratio in corresponding saturated aqueous solutions for some of these salts.⁴⁹

The special case of microsolvation with water as a solvent leads us to one of the central themes of this thesis. Water is considered the universal solvent and plays a central role in our understanding of chemical and biological processes, and it has the special ability to dissociate molecules. Acid dissociation, leading to proton transfer⁵¹⁻⁵² and solvation of the fragments, is one of the most important chemical processes.⁵³⁻⁶³ In accordance with spectroscopic and thermochemical data, gas phase ion chemistry of small water clusters rapidly approaches bulk behavior, if the ion high concentration and pH value of the cluster are taken into account.¹

Despite its apparent simplicity, the mechanism through which an acid dissociates in aqueous environments is not easy to describe at the molecular level because the proton transfer (PT) is a fast reaction depending on several factors such as temperature and this migration becomes more complex after dissociation due to the presence of ions.^{51, 64-70} There are a number

of ground-breaking experimental reports, including those that involve IR spectroscopic data as a function of solvation number and other techniques such as mass spectrometry and beam deflection methods, but there are several troubles when examining this process accurately.^{55-57, 71-}

⁷⁹ As it was mentioned before, the theory provides valuable insight to understanding the transition between microscopic and macroscopic descriptions of acid dissociation.^{59, 62, 80-110} By monitoring cluster properties as a function of the number of water molecules, it is possible to follow the step-by-step progression of intermolecular interactions.¹¹¹

Non-covalent interactions

Non-covalent interactions are involved in a vast number of phenomena related to the bio-disciplines and macromolecular science. They were first recognized by van der Waals¹¹² in 1873 helping in the reformulation of the equation of state for real gases. In 1930, London¹¹³ described these bonds using quantum mechanics.

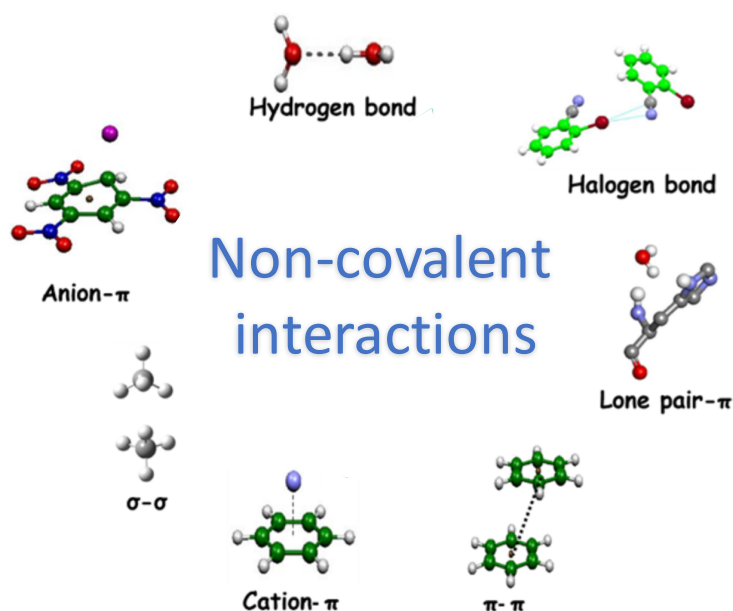


Figure 1.4 Representation of distinct kinds of noncovalent interactions.³³

Non-covalent interactions lead to the formation of molecular clusters as covalent interaction leads to the formation of a classical molecule. While most of these interactions are in general weaker than covalent interactions (main reason to call them “non-covalent”), the strength of some of the bonds such as hydrogen bond, cation- π , and anion- π can have a varied range and

in some particular instances might be even slightly stronger than a weak covalent bond.³³ Moreover, the collective factor is important because although they are individually weak, when they increase in quantity, they become significant and their importance in the biochemical realm is such that many phenomena and mechanisms simply would not occur except for the existence of these interactions.

Figure 1 shows some examples based on the structure of interacting molecules cation- π interaction, π - π stacking, halogen bond, etc. However, the stabilizing origin include electrostatic interactions between permanent multipoles (charge-charge, charge-dipole, charge-multipole, multipole-multipole), interactions between permanent and induced multipoles, dispersion interactions (see Table 1.1), as well as charge-transfer, ionic (electrostatic interaction between the positively and negatively charged species) and metallic interactions, and those leading to formation of hydrogen and halogen bonding.^{4, 114-115}

Non-covalent complexes also are classified with respect to the dominant contribution to stabilization energy or simply by size. According to their size, the classification ranges from small (less of 24 atoms, taking the benzene dimer as the boundary case), to large or extended clusters (more of 24 atoms). Classification based on the dominant contribution is not unique since rarely there is one energy term dominant and most of the clusters exhibit two or more types of intermolecular interaction. However, an example of purely dispersive interaction is the case of noble-gas atoms,⁴ only based on quantum mechanics was possible to theoretically derive the attraction between noble-gas atoms in terms of the London dispersion energy and it is owing to instantaneous multipole-induced multipole moment interactions.¹¹⁴

Although the terms “dispersion” and “van der Waals” are often used synonymously in literature, it is mandatory to clarify that dispersion interactions can be empirically defined as the attractive part of the van der Waals type interaction.¹¹⁶

Table 1.1 Distance dependencies of non-covalent interactions. The table was taken from Knowles and Jacobsen work.¹¹⁵

Noncovalent interaction		Energy dependence on distance
Charge–charge		1/r
Charge–dipole		1/r ²
Dipole–dipole		1/r ³
Charge-induced dipole		1/r ⁴
Dipole-induced dipole		1/r ⁵
Dispersion		1/r ⁶
H-bond		Complicated ~1/r ²
Steric repulsion		1/r ¹²

Hydrogen and halogen bond

Due to their importance in the study of ethanol dimers and acid-water clusters, this section is dedicated to two interactions that, in fact, share certain characteristics: the hydrogen bond (HB) and the halogen bond (XB). Both have been widely investigated but the research about hydrogen bond received more attention a long time.

Hydrogen bond plays a key role in chemistry, physics, and biology. They are responsible for the structure and properties of water and many compounds important for life. The current definition according to the IUPAC recommendations is: *The hydrogen bond is an attractive interaction between a hydrogen atom from a molecule or a molecular fragment X-H in which X is more electronegative than H, and an atom or a group of atoms in the same or a different molecule, in which there is evidence of bond formation.*¹¹⁷ Despite its relevant role, HB does not represent some special type of non-covalent interaction. Any type of H-bonded complex is stabilized by the same energy components as any other non-covalently bonded complex. In general, the hydrogen bond is a composite interaction, which can have pronounced covalent, electrostatic or van der Waals components and consequently spans a wide energy range. However, both the H-bond and the halogen bond have a peculiar directionality and their relevance deserves a special consideration within non-covalent interactions.^{2,4}

Halogen atoms are usually considered as sites of high electron density and under this perspective, they can form attractive interactions by functioning as the electron donor site (nucleophilic site). This is the case when they work as hydrogen bond acceptor sites.¹¹⁸ However, *a halogen bond occurs when there is evidence of a net attractive interaction between an electrophilic region associated with a halogen atom in a molecular entity and a nucleophilic*

region in another, or the same, molecular entity.¹¹⁹ Then, for these cases, a halogen atom acts as electrophile. This behavior can be explained by effects such as charge transfer to the σ^* orbital (σ -hole) of a R–X bond, as well as electrostatic, dispersion, and polarization interactions.¹²⁰ There is an increasing interest in halogen bond in biochemistry and medicinal chemistry because they are present in protein-ligand interactions and environmental reactions.¹²¹⁻¹²²

Figure 1.5 is a schematic representation of the hydrogen bond (HB) and the halogen bond (XB), where the three dots denote the bond. Then, in the first case, **R-H** represents the hydrogen bond donor and the acceptor may be an atom or an anion **Y** or an electron-rich region.¹¹⁷ For the scheme of halogen bonding, **X** is the electrophilic halogen (Lewis acid, XB donor), **Y** is a donor of electron density (Lewis base, XB acceptor), and R is carbon, nitrogen, halogen, etc.¹²⁰⁻¹²⁴

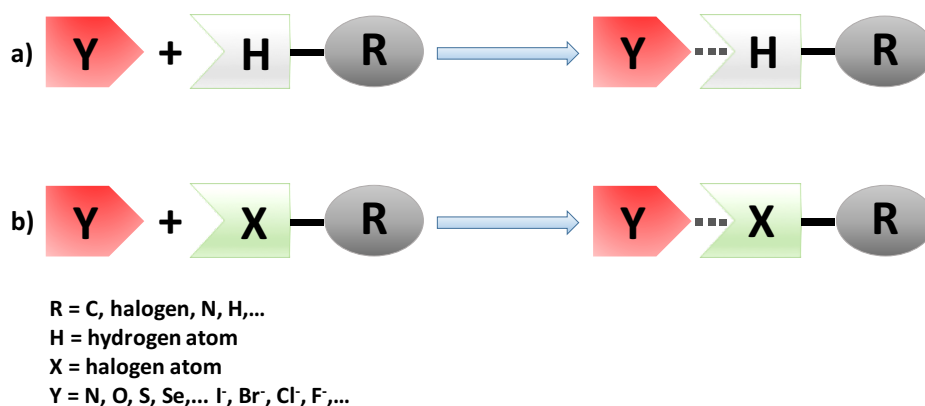


Figure 1.5 Schematic representation of a) Hydrogen bond and b) Halogen bond.

Several articles analyze the competition between hydrogen bonds and halogen bonds in different complexes such as hypohalous acids, methyluracil, phosphine derivatives, etc.¹²⁵⁻¹²⁹ Then, the XB interactions can take an important contribution depending on the atoms or molecules that compose the complex.

The interatomic distances can be useful to distinguish XB interactions since in a typical halogen-bonded complex the interatomic distance between X and the nucleophilic atom Y tends to be less than the sum of the van der Waals radii, for hydrogen bond systems a criterion of distance related to van der Waal radii is not recommended because is true only for strong hydrogen bonding.^{119, 121, 130}

Proton transfer and dissociated complexes

One of the most fundamental aspects associated with liquid water is the spontaneous auto-ionization of a water molecule leading to the proton and the hydroxide ion. It is the dynamic equilibrium between water and these ions that determines the pH of water. Hence, the motion of the proton in water has been a subject of intense investigation. In 1805, Grotthuss¹³¹ proposed a mechanism for proton transport as a result of studies in the electrolysis of metals dissolved in water. In some cases, instead of reducing the dissolved metal, he observed the decomposition of water. By considering water as a mixture of oxygen and hydrogen species (he did not know the chemical formula of water), Grotthuss hypothesized that these elements could be charged by the applied electric field. He imagined that these charge carriers formed “wires” at the anode and cathode along which they continuously move in a domino-like effect (Figure 1.6).

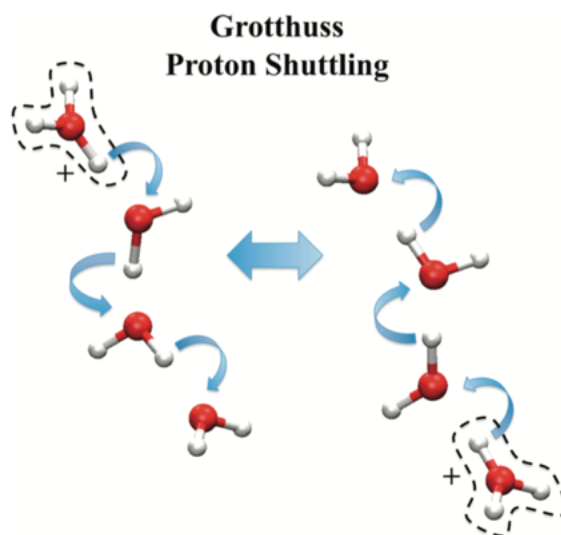


Figure 1.6 Illustration of the Grotthuss shuttling process for the excess proton in a small water wire. Figure from the work of Knight and Voth.¹³²

Grotthuss mechanism was the notion of preferred solvation structures of hydrated protons in the literature, in particular, the complexes proposed by Eigen and Zundel.⁵² An Eigen cation is composed of a central hydronium ion (H_3O^+) solvated by three water molecules (H_9O_4^+) and in a Zundel cation (H_5O_2^+), the excess proton is shared between two water molecules (see Figure 1.7).^{66, 133} Modern research suggests that Grotthuss shuttling occurs by interconversion between these cations and that the dominant state in liquid water is the Eigen cation.¹³² For example, the first molecular dynamics simulations of the excess proton in water were performed classically by Tuckerman *et al.*¹³⁴⁻¹³⁵ in the early 1990s and they found for the hydronium ion a dynamic complex which continuously fluctuates between a Zundel and an Eigen structure as result of proton transfer.

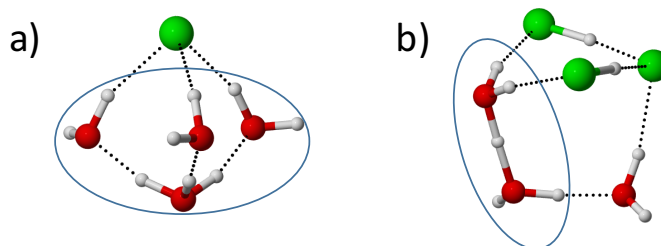


Figure 1.7 Clusters with a) Eigen and b) Zundel cations.

Then, the transfer of a proton starts from an H_9O_4^+ structure. In the first step, one of the outer water molecules loses a hydrogen bond with an external water molecule. This causes the O–O distance of the central water molecule and that outer water molecule decrease and a H_5O_2^+ like structure is formed. The proton can now transfer, without energy barrier, from the first to the second oxygen atom. Hydrogen bonding of the previously central water molecule with an external water molecule leads to an increase of the O–O distance again, forming a new H_9O_4^+ cluster and completing the proton transfer. To think of proton transfer in terms of well-defined structures and transition states can be misleading. One should keep in mind that the behavior of hydrated protons is by nature, very fluxional. In concentrated acid solutions, the situation becomes even more complex. Proton transfer is affected by the presence of counterions and other excess protons. The Eigen-Zundel-Eigen mechanism for proton transport has been statistically validated through advanced molecular dynamics simulations and photoelectron spectroscopy.⁶⁴

133, 136-137

Most of the acid-base chemistry occurs in water in which excess protons move via the Grotthus mechanism.^{52, 64, 133} As additional water molecules are successively incorporated, the X–H distance in the acid increases gradually up to a given cluster size where fully dissociated forms

related to the Eigen and Zundel cations are found. For example, quasi-Eigen¹⁰⁷ (or Eigen-like-type, $\text{H}_7\text{O}_3^+\text{X}^-$) cations, in which an X^- ion replaces to one of the water molecules in the Eigen cation; or the Zundel-type structures, where one or both water molecules are replaced by X^- ion (see Figure 1.7). An alternative name for this kind of complexes is intermediate Zundel-Eigen-type structures.^{66, 87, 93} Excess protons are mostly present both as Eigen and Zundel-like structures, either as a direct hydronium-halide contact-ion pair (CIP) or a solvent-separated ion pair (SIP).^{74,}

¹³⁶ See examples in Figure 1.8.

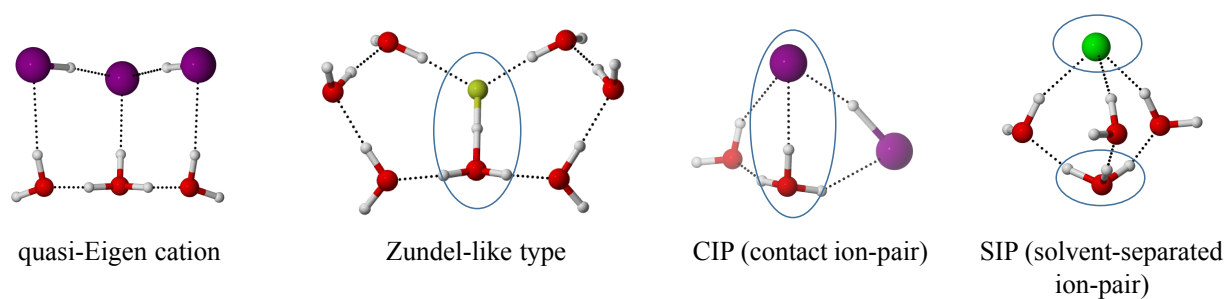


Figure 1.8 Dissociated forms in acid-water clusters.

Structural sampling

A successful way to study clusters and their interactions is the exploration of their potential energy surface (PES), which is a hypersurface defined by the potential energy of a collection of atoms over all possible arrangements and has $3N-6$ coordinate dimensions (for linear molecules $3N-5$), where N is the number of atoms. Owing to a high dimensional PES can not be easily plotted, Figure 1.9 represents a hyperslice through the full PES for a molecule with three atoms (ABC), showing the energy as a function of two coordinates dimensions, for example the AB and BC bond lengths and taking a fixed value for the angle ABC.⁸

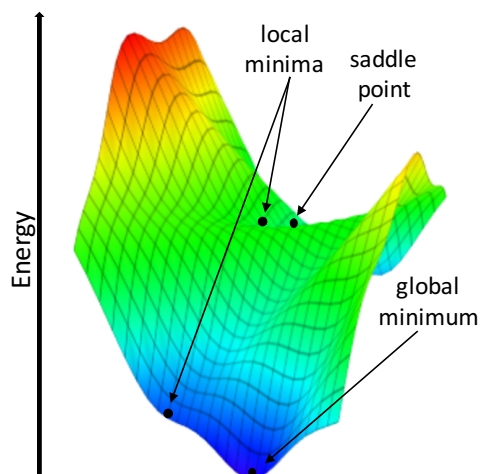


Figure 1.9 Representation of a hyperslice of a potential energy surface.

High-level *ab initio* and DFT (density functional theory) computations on molecular clusters assume a tremendous challenge in producing accurate potential energy surfaces (PESs) for intermolecular interactions owing to the exponential dependency of the number of local

minima on the number of molecules.¹³⁸⁻¹⁴⁰ In most cases, chemical intuition is the weapon of choice to guess the best candidates. However, this biased approach quickly becomes impractical because of the overwhelming number of possibilities, which, even for clusters of relatively small sizes, is bound to miss relevant regions of the corresponding PESs. This is a very sensitive issue, especially in the cases where several local minima are very close in energy to the global minimum without being structurally related.

Microsolvation is a difficult problem from both theoretical and experimental perspectives, as discussed in the recent work by Hadad *et. al.*¹⁴¹ Clearly, the exploration of the PES of clusters is a challenge even for homogeneous systems, water clusters being a clear example of exponentially increasing complexity as a function of size, owing to the availability of multiple hydrogen-bond acceptors, each offering a choice of two lone pairs for hydrogen bonding. This fact and the narrow energy range of local minima severely difficult the characterization of these PESs.^{55, 57, 60, 63, 65, 68, 138, 142-151} As a result, it remains a challenge to locate most, not to say all, of the low-energy configurations of large-size molecular clusters and a systematic procedure is needed. Among the various methodologies proposed in the literature are analytical and stochastic approaches, simulated annealing, and genetic algorithms.¹⁵²⁻¹⁵⁴ Some of them will be discussed in the next chapter.

In many instances to find the “global minimum” is not sufficient to describe the properties of the system because many interactions that contribute significantly to the stabilization of the system appear in various “local” minima. According to Boltzmann distributions, microstates with lower energy will have a higher probability of being occupied than the states with higher energy but at higher temperatures high-energy microstates increase

their probabilities of occurrence. Stability is dictated by the size of the energy barriers that need to be overcome in going from one state to the other, not by the energy difference between states. Expectation values for a given observable are to be calculated as statistically weighted averages of all individual possibilities.¹⁴¹ Additionally, sometimes the global minimum is not clearly defined since it depends on the level of theory or the accuracy of the calculation.¹⁵⁵ Only by a careful and systematic exploration of the PES of the system it is possible to determine the set of geometries representative for the interactions that stabilize the system and provide an adequate description of the association process.

The static view of the energy landscape may be complemented by studying the dynamics of the molecular cluster by starting the simulation from a given minimum that was previously obtained in the global optimization process. The essence of an atomistic MD simulation is, starting from an initial set of positions and velocities, to integrate Newton's equation of motion to obtain the position of each particle as a function of time (a trajectory).^{34, 156-157} Owing the type of information provided by static and dynamic approaches, they should be considered complementary rather than competitive.¹⁴¹

In summary, the study of molecular clusters involves various challenges. The first issue is that the number of local minima increases exponentially with the size of the clusters and many of them could be close in energy. Furthermore, high-level methods are needed for the reliable theoretical investigations of weakly bound molecular complexes since lack of electron correlation effects prevents accurate estimation of the stability and energetics of many of the molecular clusters.^{141, 151} Anharmonic and nuclear quantum effects have been also included in several reports and these aspects have a minimal or important impact depending on the system

treated.^{97, 108, 158-162} All these considerations demand a high computational cost but a systematic exploration with a reliable level of theory is able to provide valuable results and new insights to complement the description of the potential energy surfaces of clusters and their intermolecular interactions.

Experimental methods

Comparison of theoretical and experimental results allows for the testing of the ability and accuracy of newly developed procedures and techniques. The main experimental tools employed to study the non-covalent interactions are combinations of different spectroscopic methods with size-selecting techniques.

Among the diffraction methods stand out X-ray and neutron diffraction. Single-crystal X-ray analysis affords information on the geometrical features of single molecules and their relative arrangement in the crystal. However, diffraction by liquids gives much less information, even when X-ray and neutron diffraction results are combined for simple liquid such as water.^{121-122, 163}

Spectroscopy methods provide information on cluster geometry and frequencies of intermolecular and intramolecular vibrational modes, they are based on exciting the vibrational or rotational energy levels of molecules, resulting in the absorption, or emission of the incident radiation at specific frequencies. This radiation can be electromagnetic or neutrons. Spectroscopy methods include microwave spectroscopy, infrared and Raman, NMR, ZEKE (zero kinetic energy) photoelectron spectroscopy⁴ and other type of spectroscopies.¹⁶³⁻¹⁶⁴ For example, microwave Spectroscopy (MW) is a method of very high resolution optical. It enables

measurement under conditions of effective isolation of molecules, avoiding perturbations of the ground-state structure from either solvent or lattice effects. The observation of the pure rotational spectra in the microwave region can provide rotational constants and thence, the moments of inertia and hence the most probable structure can be obtained. For nonrigid systems, the observed moments of inertia correspond to a vibrationally averaged structure.^{4, 121, 165}

Nuclear magnetic resonance (NMR) generates unparalleled high-resolution structures of dynamic complexes in solution. NMR parameters such as chemical shifts and coupling constants can yield a wealth of information regarding the occurrence, thermodynamics, and local structures.¹²¹⁻¹²² With the advent of soft ionization mass spectrometry tools, namely electrospray ionization (ESI) and matrix-assisted laser desorption/ionization (MALDI), mass spectrometry (MS) has become a tool to investigate non-covalent interactions. ESI is achieved by applying a potential difference between the inlet of the mass spectrometer and a conductive capillary containing the analyte solution.¹⁶⁵ Fourier transform ion cyclotron resonance (FT-ICR) mass spectrometers are also being used to study large proteins assemblies.¹⁶⁵

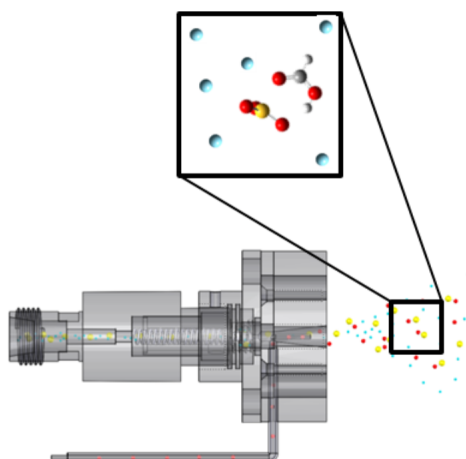


Figure 1.10 Scheme of a supersonic jet expansion, taken from the work of Mackenzie, *et al.*¹⁶⁶

The gas phase molecular clusters are experimentally generated by pulsed supersonic jet expansion techniques (see Figure 1.10). A dilute mixture of the gas under study with an inert gas (such as argon or helium) is allowed to expand through a slit-jet source, leading to the formation of molecular clusters of variable sizes.¹⁶⁷⁻¹⁶⁹ This gas expansion is coupled with a variety of experimental techniques, such as infrared (IR), microwave (MW), and photoelectron spectroscopy for probing the molecular clusters thus generated. The powerful tool of mass spectrometry is often used in conjunction with the above experimental methods for determining the sizes of the clusters.¹⁵¹ This methodology has been used to study the rotational spectra of halogen-bonded complexes.¹²¹

Specific examples about acid-water clusters are the works of Gutberlet *et al.*⁷⁴ and Rizzutto *et al.*¹⁷⁰ The formers studied microsolvation of HCl in He nanodroplets via high-resolution IR spectroscopy. Helium droplets were formed in a supersonic expansion of precooled

(16 K) gaseous He through a nozzle and subsequently were doped with HCl or DCl and H₂O. The complexes were detected in a quadrupole mass spectrometer. The second research used Raman thermometry measurements of freely evaporating microdroplets to determine evaporation coefficients for two different hydrochloric acid solutions. FTIR and Raman spectroscopy measurements in cryogenic solutions using liquefied rare gases yield spectra with sharper bands and thus facilitate assignments.¹²¹

Chapter 2

Methodology

Introduction

Some methods of searching for minimum energy points on a PES include stochastic and Monte Carlo methods, molecular dynamics (MD), simulated annealing,¹⁷¹ genetic algorithms, and stochastic methods. None of these guaranty to find the global minimum, but in many cases they provide an efficient exploration of the PES.¹⁵⁵

Molecular Dynamics (MD) methods solve the Newton equation of motion for atoms on an energy surface. Very small time steps must be used for integrating Newton's equation and different local minima can be generated by selecting configurations at appropriate intervals during the simulation and subsequently minimizing these structures.¹³³ On the other hand, simulated annealing techniques choose high initial temperatures (2000 – 3000 K) to start an MD or Monte Carlo calculation, during which the temperature is slowly reduced.¹⁵⁵

Genetic algorithms are stochastic global optimization methods, loosely inspired by the principles of natural selection and genetics. First generating an initial set of solutions and iteratively improving the solution pool until a termination criterion is met.¹⁰

Stochastic methods are initial-guess-independent, can leap over energy barriers, and are able to sample several wells in the same run.¹⁷² In this work, a stochastic search method was used, which involves repeatedly moving molecules randomly to obtain initial clusters followed by refinement with an optimizer (Figure 2.1).¹⁴⁰ For this type of methods, the computational cost can be high depending on the number of atoms conforming the system. However, in the last years, with the steady growth in computational power at affordable cost, stochastic explorations of moderately sized atomic and molecular clusters using quantum Hamiltonians have become a viable choice for obtaining detailed information on the nature of intermolecular interactions and

to overcome the problems associated with biased initial guesses.

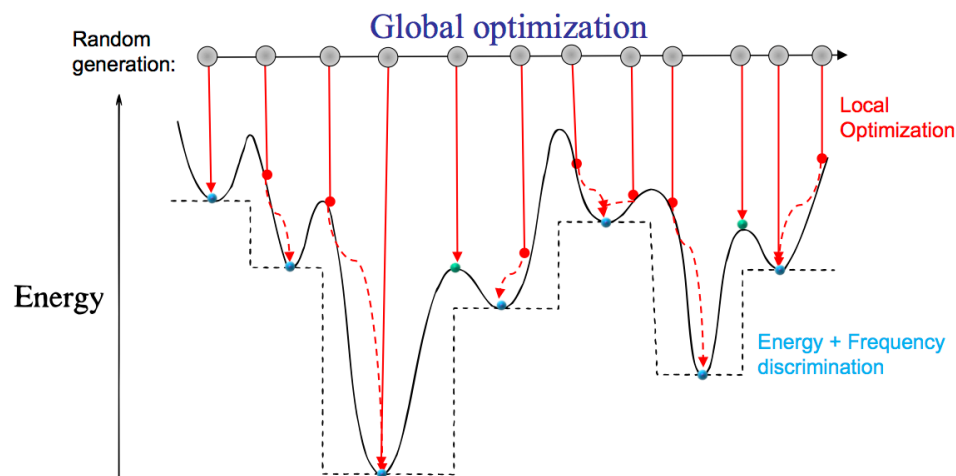


Figure 2.1 Stochastic approach for global optimization.

The methodology used for the study of molecular clusters is described in this chapter. The PESs were explored using the program GLOMOS¹⁷³⁻¹⁷⁴ and the optimizations were done with the *Gaussian 09* (revision D.01) package.¹⁷⁵ All the clusters were characterized as true minima by harmonic vibrational frequencies analysis. Dispersion corrections were included in all the optimization calculations to obtain a better description for non-covalent complexes and the analysis bonding was carried out using Wiberg bond index (WBI), energy decomposition analysis (EDA), non-covalent index (NCI), and Stern-Limbach plots.

The GLOMOS code

GLOMOS employs a modified-kick algorithm; a “kick” operation implies that each atom or molecule is randomly moved.^{140, 173-174} After the generation of initial clusters, GLOMOS include subroutines to submit calculations to programs of electronic structure as *Gaussian*, and for comparison of geometries. The program is available for molecular and atomic clusters and provides a systematic method to explore the PES for a given system (see Appendix A).

In general, the computational procedure for the exploration of PESs using GLOMOS and *Gaussian 09* was as follows (Figure 2.2):

1. Generation of initial structures. The initial populations of clusters were generated via the kick algorithm implemented in the program GLOMOS (see details in the Appendix A).
2. First optimization. This step is also called preoptimization and usually a low level of theory is selected to obtain optimized structures at low computational cost. For the cluster of this thesis, the optimizations were performed with the *Gaussian 09* (revision D.01) package.¹⁷⁵
3. Comparison of structures. The next step was a geometrical and energetic discrimination. Then, preoptimized clusters were compared using hierarchical algorithms for molecular similarity detection. For the microsolvated clusters, a hierarchical algorithm¹⁷⁶ based on the RMSD (Root-Mean-Square Deviation) of intermolecular atomic distances, and relative energy of the complexes were used to determine the structural similarity and remove repeated structures while retaining enantiomeric pairs. Therefore, different candidates were obtained for the final geometry optimization.

Recently, an Ultrafast Shape Recognition algorithm¹⁷⁷ for molecular similarity detection was implemented in GLOMOS, which is briefly described in Appendix A.

4. Reoptimization of the structures. Selected candidates of the previous step were optimized using a higher level of theory to obtain a better description of the systems.

5. Final comparison of structures. After the reoptimization step, it is necessary a second comparison procedure because some structures converge at similar geometries after reoptimization. When the process of comparison and selection concludes, the program provides the final structures and energetic values.

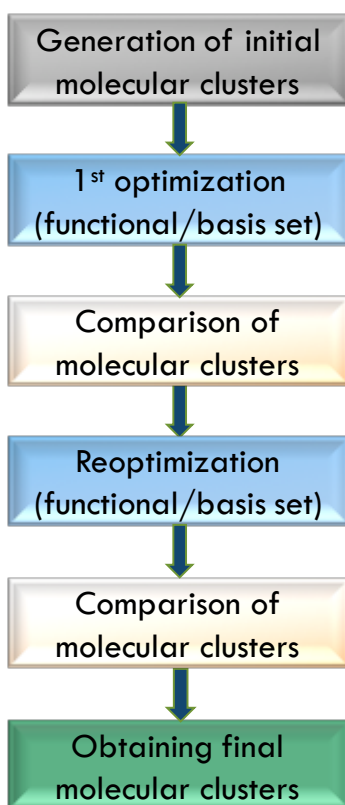


Figure 2.2 Procedure for the exploration of PES.

Afterwards, the coordinates of optimized structures are used to calculate properties and analyze the systems through distances, angles, relative energies, bond order, charges, binding energies, properties related to the electron density, etc.

GLOMOS code, combined with *ab initio* and DFT computations is established as a very reliable procedure for localizing minima and systematic exploration of PESs. Additionally, if the systems studied belong to a group in the periodic table or with similarities, for example the halogen group, it is possible to obtain a more complete population of structures because those isomers that were missing from the stochastic search can be identified in clusters of the other member of the group and generated by hand to have a more complete PES.

Dispersion corrections

Density functionals are not able to describe the long-range dispersion interaction correctly. Therefore, it is necessary to explicitly account for van der Waals interactions. A relatively simple way to modify GGA Exchange-correlation functionals is to add the attractive C_6/R^6 van der Waals term for all atomic pairs. These corrections to the DFT calculations are collectively referred to as DFT-D methods, suggested by Grimme *et al.*^{116, 178-182} Thereby, in the DFT-D2 approach, an empirical atomic pairwise dispersion correction is added to the Kohn-Sham portion of the total energy (EKS-DFT) as

$$E_{\text{DFT-D}} = E_{\text{KS-DFT}} + E_{\text{disp}} \quad (2.1)$$

where E_{disp} is given by

$$E_{disp} = -s_6 \sum_{i=1}^{N_{at}-1} \sum_{j=i+1}^{N_{at}} \sum_g f_{damp}(R_{ij,g}) \frac{C_{6,ij}}{R_{ij,g}^6} \quad (2.2)$$

The sum is over all atoms pairs in the system, C_6 denotes the averaged 6th-order dispersion coefficient for atom pair and R is their internuclear distance. Global scaling factor (s_6) is typically used to adjust the correction to the repulsive behavior of the chosen density functional (for example for PBE functional, $s_6 = 0.75$). Moreover, to avoid near-singularities for small interatomic distances, damping function (f_{damp}) is used, that effectively re-scales interatomic forces to minimize interactions within the bonding distance R which determine the range of the dispersion correction.

A significant improvement over the DFT-D2 method is the DFT-D3 scheme, which is characterized by higher accuracy, a broader range of applicability, and less empiricism compared to the DFT- D2 method. This scheme uses the following form of the dispersion correction

$$E_{disp} = - \sum_{i=1}^{N_{at}-1} \sum_{j=i+1}^{N_{at}} \sum_g f_{d,6}(R_{ij,g}) \frac{C_{6,ij}}{R_{ij,g}^6} + f_{d,8}(R_{ij,g}) \frac{C_{8,ij}}{R_{ij,g}^8} \quad (2.3)$$

where $f_{d,8}$ and C_8 are eighth-order damping function and dispersion coefficients, respectively, for the additional repulsive potential.^{116, 182}

Considerably better results are obtained with DFT-D methods and can be recommended for extended clusters possessing various structural motifs.^{4, 178, 183-185} For this reason, DFT-D2 and

DFT-D3 approaches were used in this work for the exploration of the different clusters. In ethanol dimers, the MP2 (second order Møller-Plesset perturbation theory) and coupled cluster methods were also used for calculation of single points. The computational details will be discussed in the corresponding section of each chapter.

Bonding Analysis

The interactions of dimers and microsolvated clusters were analyzed using tools such as the noncovalent index (NCI), Wiberg bond index, energy decomposition analysis (EDA), and Stern-Limbach plots besides of the geometrical and energetic information of the structures. The analysis of the data obtained after exploration of PES gives valuable insights to understand the interactions that govern these clusters.

Wiberg bond index

Wiberg bond index (WBI) was originally introduced in the framework of the semiempirical CNDO (Complete Neglect of Differential Overlap) theory. It is computable from the wave function and was the first quantum chemical quantity that could be put in correspondence with the classical chemical notion of the bond multiplicity for a multiatomic molecule.¹⁸⁶

Wiberg observed that neither Coulson's bond order nor Mulliken's overlap population could be applied for Pople's CNDO theory, which was in general use at that time. The reason was that neither the individual elements of the density-matrix nor any of their simple combinations have the correct invariance properties when the molecule is rotated as a whole.

Thus, he introduced a new bond index which is quadratic in the density-matrix elements and has the proper invariance:¹⁸⁷

$$W_{AB} = \sum_{\mu \in A} \sum_{\nu \in B} |D_{\mu\nu}|^2 \quad (2.4)$$

Then, Wiberg bond indices are electronic parameters related to the electron density between atoms and have the advantage that for simple systems is consistent with our intuition that bonds come in integers, that is bonds are roughly single, double, and triple.¹⁸⁸ Currently, they can be obtained from a natural population analysis using for example the NBO program¹⁸⁹ and provide a reasonable quantification of bond order in many cases.¹⁹⁰

In this work, Wiberg bond indices of the H-X interactions in clusters with hydrogen halides and water molecules were calculated as a method for monitoring the possible dissociation. These data were used to plot WIB versus number of occurrences, this information allows to visualize how the structures are distributed according their level of dissociation related to the decrease of their Wiberg bond indices and compare the acid series.

Energy decomposition analysis (EDA)

In order to achieve a better understanding of chemical phenomena that give rise to the interactions, it is necessary some methods able to provide readily identifiable values. The development of energy decomposition analysis (EDA) is a valuable tool to quantifying the nature of stabilizing interactions.¹⁹¹⁻¹⁹³ The EDA schemes can be classified by the nature of their

underlying theory, this may be described as either variational in which the interaction energy is decomposed by use of intermediate wavefunctions, or alternatively as perturbation based in which the interaction between the fragments is seen as a perturbation to the non-interacting description, and the interaction is constructed as corrections resulting from different physical effects.¹⁹¹ The variational methods are typically derived from the early energy decomposition analysis of Morokuma¹⁹⁴ and the perturbation approaches from the popular symmetry-adapted perturbation theory scheme (SAPT).¹⁹⁵ For this work variational based EDA methods were used, due to they are available in GAMESS¹⁹⁶ and ADF¹⁹⁷ packages. Moreover, the theory of SAPT is also more complicated than the variational methods and many energy terms can be involved in describing the interaction energy.¹⁹¹

In dimers (ethanol and metallocenes), we have two well defined fragments (monomers). For these clusters, EDAs were carried out in order to know the nature of interactions that keep those monomers together. Additional coupled cluster calculations as CCSD(T) were performed to derive the dispersion to complete the interaction analysis energy (as was accomplished for ethanol dimers). EDA can also be calculated for DFT methods. Thus, if an explicit correction term for dispersion interaction is employed, such as in the methods suggested by Grimme^{116, 178} (case of metallocene dimers), the EDA results remain unchanged and the dispersion correction appears as an extra term.^{193, 198}

The method of Su and Li¹⁹³ used in the chapter 3 for ethanol dimers, can be considered as an extension and modification of the method developed by Kitaura and Morokuma¹⁹⁹ (KM), Ziegler and Rauk,¹⁹⁸ and Hayes and Stone. For HF and KS-DFT methods the total interaction energy is decomposed into electrostatic (ΔE^{ele}), exchange (ΔE^{ex}), repulsion (ΔE^{rep}), polarization + charge transfer (ΔE^{pol}), and dispersion (ΔE^{disp}) terms. Then, in this case, the electrostatic,

exchange, and repulsion terms are isolated, while in KM method, exchange and repulsion are not separated. The polarization energy term is defined as the “orbital relaxation energy” and is equivalent to the to the sum of the polarization, the charge transfer, and the mixing term in the KM EDA.¹⁹³

For metallocene dimers, an EDA based on the approach of Ziegler and Rauk¹⁹⁸ as is implemented in ADF package was used. The procedure is similar to the Su and Li approach with some differences in the energy terms. The bond formation between the interacting fragments is divided into four steps, which can be interpreted in a plausible way. In the first step the fragments, which are calculated with the frozen geometry of the entire molecule, are superimposed without electronic relaxation, yielding the quasiclassical electrostatic attraction ΔE^{ele} . In the second step the product wave function becomes antisymmetrized and renormalized, which gives the repulsive term ΔE^{Pauli} , termed Pauli repulsion. In the third step the molecular orbitals relax to their final form to yield the stabilizing orbital interaction ΔE^{orb} . The latter term can be divided into contributions of orbitals having different symmetries. For these organometallic dimers, the dispersion corrected revPBE-D3 functional was employed, hence the dispersion correction term, ΔE^{disp} , was added to the interaction energy (ΔE^{int}) values to describe the total bond energy as

$$\Delta E^{\text{int}} = \Delta E^{\text{Pauli}} + \Delta E^{\text{ele}} + \Delta E^{\text{orb}} + \Delta E^{\text{disp}} \quad (2.5)$$

ΔE^{int} can be used to calculate the bond dissociation energy, D_e , by adding ΔE^{prep} , which is the necessary energy to promote the fragments from their equilibrium geometry to the geometry in the compounds (equation (2.2)). The advantage of using ΔE^{int} instead of D_e is that the

instantaneous electronic interaction of the fragments is analyzed, which yields a direct estimate of the energy components.

$$-D_e = \Delta E^{\text{prep}} + \Delta E^{\text{int}} \quad (2.6)$$

Thus, the Pauli exchange repulsion term is related to the exchange energy component of the KM EDA approach. The final orbital interaction term contains interaction energy information relating to the charge transfer and polarization interaction components and other orbital mixing interactions. This term is somewhat similar to the mixing term of the KM EDA as it is calculated as a remainder term that is required for the energy components to add up to the full interaction energy.¹⁹¹

Non-covalent index (NCI)

As the name suggests, the NCI method of Johnson and co-workers has been specifically developed to reveal non-covalent interactions.²⁰⁰ In NCI analysis, the mapping of localized binding interactions is done by employing two scalar fields, the electron density (ρ), and its first derivative, the reduced density gradient (s), which is a fundamental dimensionless quantity in DFT used to describe the deviation from a homogeneous electron distribution. These two quantities are connected as:

$$s = \frac{1}{2(3\pi^2)^{1/3}} \frac{|\nabla\rho|}{\rho^{4/3}}, \quad (2.7)$$

where $\nabla\rho$ is the gradient of ρ .

If the reduced density gradient is plotted as a function of the density across a molecule, it can be seen that the main difference between the monomer and dimer cases is the appearance of steep peaks at low density, see example of water dimer (Figure 2.3a and 2.3b). When we search for the points in 3D space giving rise to these peaks, non covalent regions clearly appear in the (supra)molecular complex (Figure 2.3c).

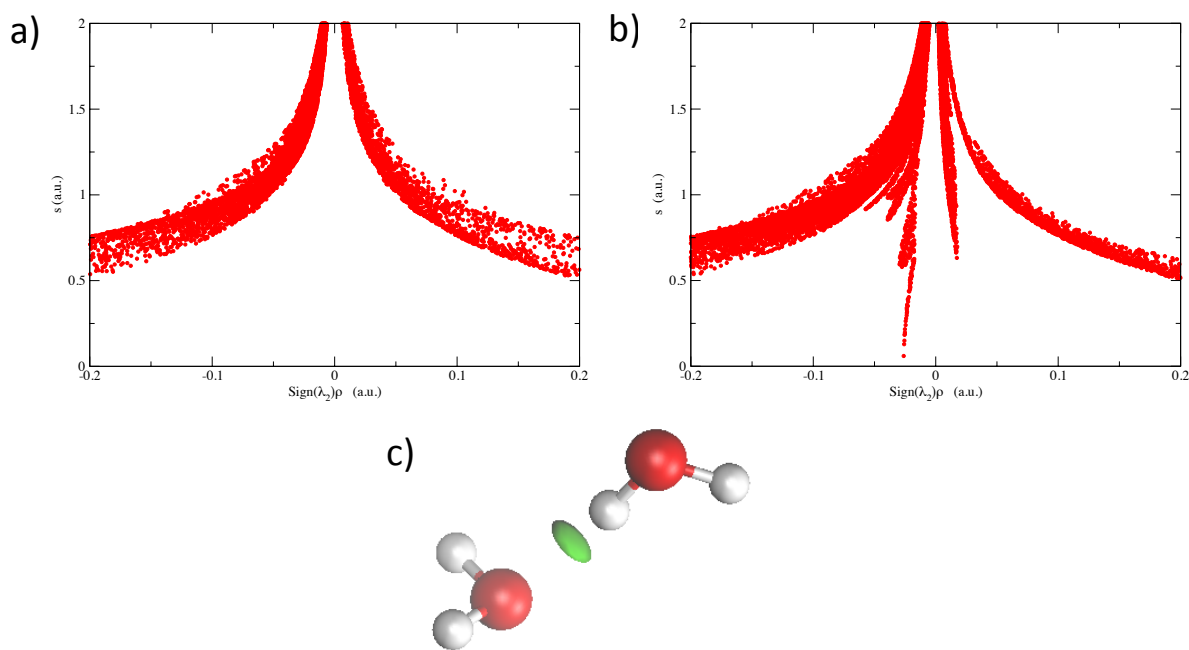


Figure 2.3 Plots of a) water monomer, b) water dimer, and c) NCI isosurface for the water dimer.

In density tails (i.e., regions far from the molecule, in which the density is decaying to zero exponentially), the reduced gradient will have very large positive values. Conversely, the reduced gradient will assume very small values, approaching zero, for regions of both covalent bonding and noncovalent interactions. When there is overlap between atomic orbitals, a trough in

the $s(\rho)$ diagram appears. The points forming this trough can identify the interaction when they are mapped back to real space (Figure 2.3c). This procedure is able to reveal noncovalent interactions, such as hydrogen bonds, steric repulsion, van der Waals interactions, and even covalent bonding.

To distinguish between attractive and repulsive interactions, one must consider accumulation or depletion of density in the plane perpendicular to the interaction. This is mainly characterized by the second eigenvalue, λ_2 , of the electron-density Hessian (second derivative) matrix. Therefore, the color of the isosurfaces is decided by the parameter $\text{sign}(\lambda_2)\rho$. In general, stabilizing hydrogen bonds and van der Waals interactions are represented by blue ($\lambda_2 < 0$) and green color ($\lambda_2 \leq 0$), respectively, whereas destabilizing interactions ($\lambda_2 > 0$) are indicated by red colored surfaces.²⁰⁰⁻²⁰¹

For the metallocene dimers (Chapter 4), a density cutoff of $\rho = 0.01$ a.u. is applied to create isosurfaces with a value of $s = 0.5$ and colored in the $[-0.03, 0.03]$ a.u range. These isosurfaces are computed using the NCIPLOT program.²⁰² Density properties can be integrated within the NCI region to obtain the volume (V_{NCI}) of the isosurface and the charge (q_{NCI}) enclosed within it.²⁰¹

$$V_{\text{NCI}} = \int_{\Omega_{\text{NCI}}} d\vec{r} \quad (2.8)$$

$$q_{\text{NCI}} = \int_{\Omega_{\text{NCI}}} \rho(\vec{r}) d\vec{r} \quad (2.9)$$

To perform such integrations, it is necessary to establish a unique definition of the NCI region. Because the difference between the interacting and noninteracting monomers is directly reflected in the $s(\rho)$ diagram, it is possible to define the NCI region as the points in 3D space with (ρ, s) values lying in the $s(\rho)$ peak. To identify this region, both the monomer and dimer densities must be computed and compared. The lower edge of the monomer $s(\rho)$ curve is splined and all the points of the dimer $s(\rho)$ plot lying below the splined curve are localized in real space. In practice, these integrations are performed numerically, by summation over a cubic grid with 0.1 a.u. increments and cutoffs of $\rho=0.2$ a.u. and $s=2.0$.

Stern-Limbach plots

Stern-Limbach plots were used to correlate the symmetry and of $H\cdots X$ hydrogen bond lengths in the HX -water clusters ($X= F, Cl, Br, I$). In these plots, q_1 measures the displacement of the proton from the center in idealized linear hydrogen bonds, while q_2 quantifies the distance between the two electronegative atoms (see Figure 2.4 for an illustration and definition of variables). r_1 and r_2 are the A-H and H-B distances, respectively. High negative (positive) values of q_1 correspond to hydrogen atoms that are clearly attached to the A (B) atom.

For hydrogen bonds involving equally electronegative atoms (atom A and B = halogen atom X), $q_1 = 0$ indicates the point at which the proton is equally shared by both atoms, while positive or negative values denote that one of the X atoms is more strongly bound to the proton.

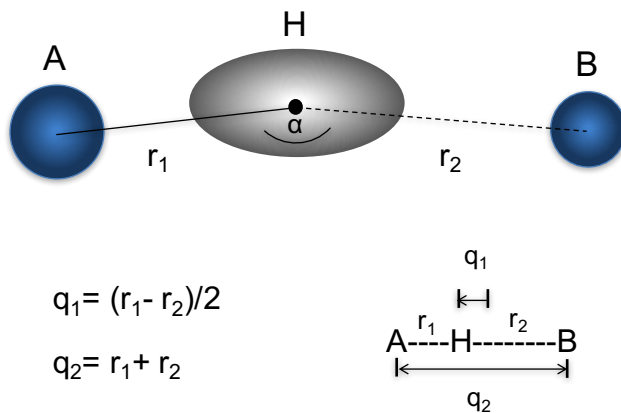


Figure 2.4 Definition of hydrogen bond coordinates q_1 and q_2 . In our case, the A and B atoms are either oxygen or halogen. The large volume associated with the proton intends to suggest a high degree of delocalization.

The Stern-Limbach plots^{107, 203-204} allow to obtain q_2 as a function of q_1 and provide information about proton transfer of studied clusters since the successive increase of water molecules decreases the distances $B \cdots H$ (r_2) and simultaneously increases the distances $H-A$ (r_1).

One example of plot is showed in the Figure 2.5 for systems exhibiting OHO hydrogen bonds in the solid state. In this case r_1 and r_2 are the O-H and H-O distances, respectively. Most of cases, a quadratic correlation is obtained and the points on the curve situate every cluster either is a positive or negative region of q_1 to identify dissociated and undissociated complexes.

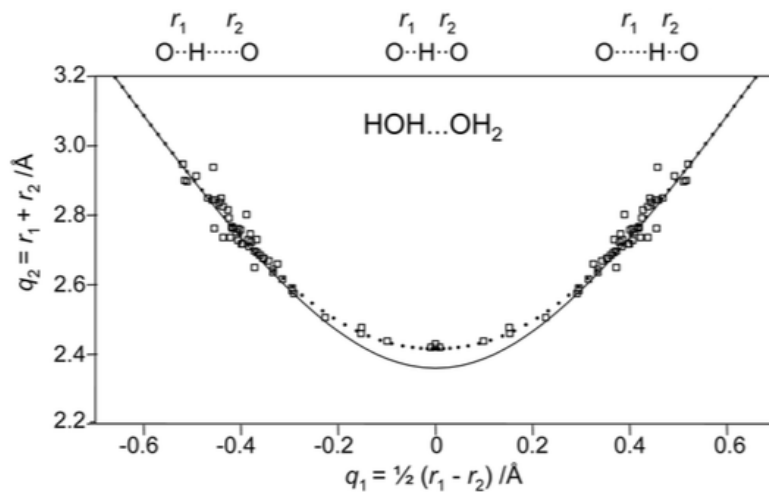


Figure 2.5 Hydrogen bond correlation q_2 vs. q_1 of the neutron structures contained in the Cambridge Structural Database of systems exhibiting OHO hydrogen bonds in the solid state.

Plot and description taken from the work of Limbach, *et al.*²⁰³

Appendix A

The GLOMOS code

In the GLOMOS code, the total energy can be massively evaluated interfaced with a serial/parallel atomic level code that take advantage of the resource managers available on the supercomputers. The stochastic method implemented in GLOMOS, transforms the potential energy landscape into local minima nodes. Initially a specified number of random molecular clusters are generated and geometrically relaxed by local energy minimization at the level of theory selected. There are some important concepts involved in the process to generate structures defined in Figure A-2.1.

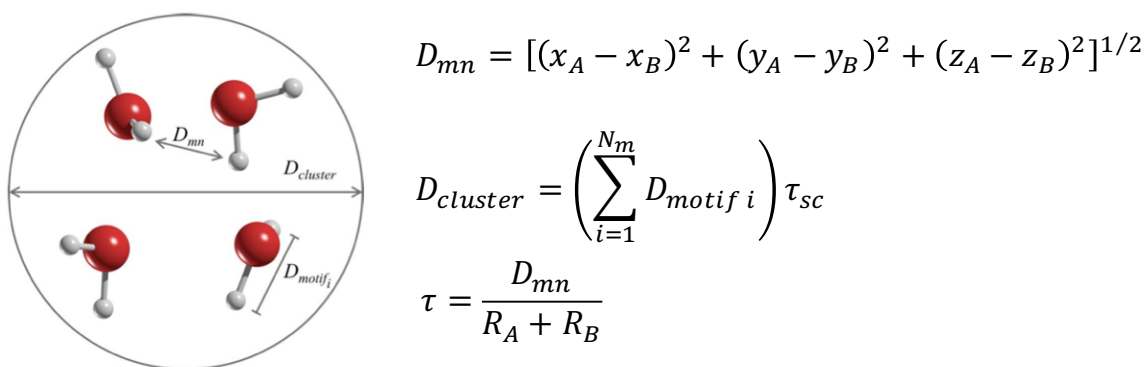


Figure A-2.1 Definition of distances and connectivity criterion for the generation of molecular clusters.

- D_{mn} is the distance between any pair of molecules (A, B), which is defined as the distance between closest atoms of molecules A and B.
- $D_{cluster}$ is the sum of the distances D_{motif} corresponding to the total of molecules N_m in the molecular cluster multiplied by a τ_{sc} factor for estimating the spatial distribution.

- Connectivity criterion applies for the distance D_{mn} . That is, two molecules are “connected” if D_{mn} satisfies the range of factor τ specified in the input. This factor is given by:

$$\tau = \frac{D_{mn}}{R_A + R_B}$$

The range for τ is specified through two values (maximum and minimum) in the input. R_A , R_B are the covalent radii of the closest atoms of the molecules A and B, respectively. For example, when $\tau = 1$ the distance D_{mn} is equal to the sum of covalent radii of the closest atoms of the molecules. If τ_{\max} is too large, the molecules will be far from each other and if τ_{\min} is too small, the molecules will be too close. Both extremes are not convenient for searching clusters. To achieve the connectivity criteria implies being within this range of τ . Usually is recommended to use values into a short range, i.e. $\tau_{\min} = 0.95$ and $\tau_{\max} = 1.2$. Then, we can obtain clusters with a reasonable tolerance of distances between molecules.

The procedure of GLOMOS starts with the random generation of molecular clusters (see the flowchart in Figure A-2.2). The selected molecules must achieve the following conditions:

- ✓ Molecules are located into a spatial distribution (solid sphere, solid disc, planar, linear).
- ✓ The distance between any pair of molecules A, B, must satisfy the connectivity criteria specified in the input data.
- ✓ The total number of molecules must be equal to the number of molecules (N_m) stipulated in the input file.

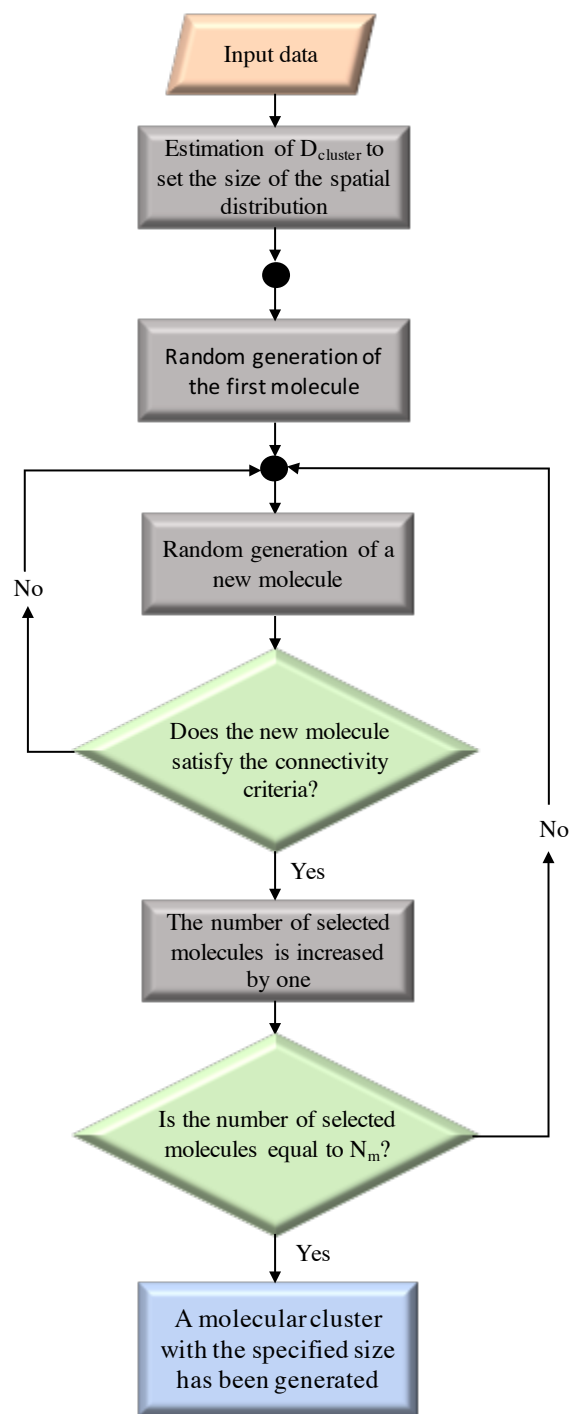


Figure A-2.2 Flowchart for the generation of initial molecular clusters using GLOMOS.

Generation of initial structures

- i. The molecules of the cluster under study are specified in the input file by means of their cartesian coordinates (xyz files) and the number of molecules that constitutes the cluster, N_m . The input file should also include the total number of clusters (initial population), values for connectivity criteria, level of theory for optimizations, and convergency parameters for the comparison of clusters.
- ii. The number N_m , type of molecules and factor τ_{sc} are used to estimate $D_{cluster}$. The spatial distribution can be selected between the options: solid sphere, solid disc, planar and linear. Moreover, the program has the option to combine different spatial distributions, this provides the opportunity to generate a wide variety of structures and explore different morphologies.
- iii. The algorithm “kicks” each molecule into the spatial distribution. For the clusters studied in this work, solid sphere distribution was used. The molecule is translated and rotated randomly by a vector at its three angles by Euler rotations with respect to its center of mass.
- iv. In the same way, other molecules are added to complete the cluster (number of molecules equal to N_m), but every new molecule must satisfy the connectivity criterion. Namely, if the new molecule achieves this connectivity condition then it remains as part of the cluster, otherwise, another molecular orientation is tested (step iii).

The initial population of molecular clusters requested in the input file is generated following the same procedure (steps iii and iv). Subsequently, the clusters are optimized using a program for performing electronic structure computations

In order to improve the efficiency of our approach we discriminate the equivalent configurations implementing the modified version of the Ultrafast Shape Recognition algorithm (USR) with extended mass-weighted descriptors proposed by Chen *et al.*¹⁷⁷ In this algorithm the similarity between a *i*-structure and a *j*-structure is quantified through the S_{ij} parameter, which takes a value close to 1.0 if the structures are similar and a value close to 0.0 in the opposite case. For the trial structures a tolerance criterion defined $S_{ij} \geq 0.70$ was established to discriminate by similarity. select the best candidates for the final optimization at higher level of theory.

Finally, the program provides the coordinates of the optimized molecular clusters ordered by energy relative (electronic with or without ZPE correction and according their free energy). Figure A-2.3 shows examples of clusters before and after optimization.

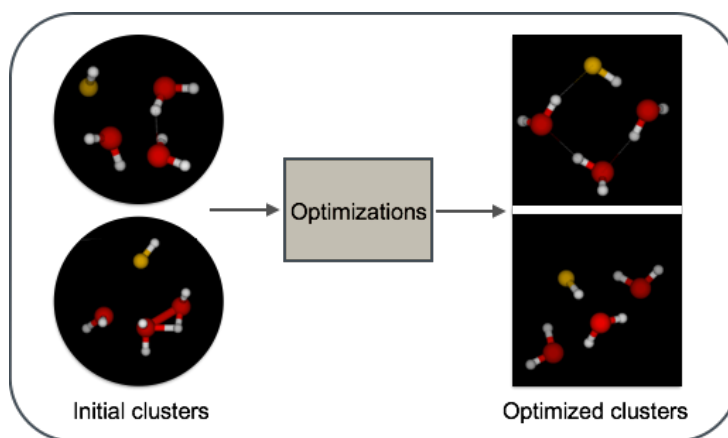


Figure A-2.3 Examples of initial and optimized clusters of hydrogen halide and water molecules.

Chapter 3

Ethanol dimers

Introduction

The ethanol dimer is a particularly interesting case of a hydrogen-bonded system; its relatively small size allows carrying out high-quality quantum mechanical computations^{159, 205-208} and its experimental detection is mainly through spectroscopic techniques as FTIR and Raman.^{159, 205-206, 209-213} In principle, ethanol dimers have contributions from three different rotamers, $g^+(\theta = 60^\circ)$, $t(\theta = 180^\circ)$, and $g^-(\theta = 300^\circ)$, created by variations in the CCOH dihedral angle (Fig. 3.1). The energetically preferred monomer is the *trans* conformation, separated from both *gauche* forms by rotational barriers of ≈ 1 kcal mol⁻¹.²¹⁴ Then, the relatively small rotational barrier allows the coexistence of the three isomers for the monomer at room temperature.²⁰⁶

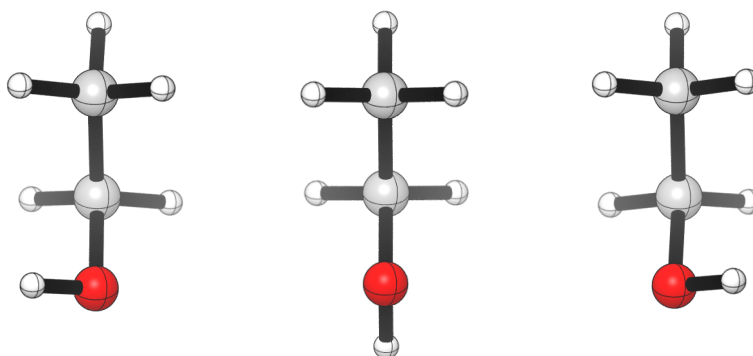


Figure 3.1 Three structural rotamers of ethanol: from left to right g^+ , t , g^-

González *et al.* identified a *tt* dimer as the most stable species.²⁰⁸ However, it has later become more accepted that the g^+g^+ form is the most stable one.^{159, 205-208} It must be stressed that due to the floppiness of this dimer, unequivocal identification of the global minimum is not possible. Provencal *et al.*²⁰⁵ have specifically addressed this issue. They used infrared cavity ring-

down laser absorption spectroscopy and concluded that “given the typically broad nature of these red-shifted bands and the floppy nature of these clusters, assigning the experimental spectrum features to individual conformers from the *ab initio* data is not feasible.”

Most studies attempting exhaustive characterization of the ethanol dimer potential energy surface focus on the construction of molecular geometries dictated by intermolecular O-H \cdots O hydrogen bonds. Using this approach, only nine distinct conformations are discerned (see for example the excellent works by Emmeluth *et al.*¹⁵⁹ and by Wassermann and Suhm²⁰⁶): *tt*, *tg*⁺, *tg*⁻, *g*⁺*t*, *g*⁺*g*⁺, *g*⁺*g*⁻, *g*⁻*t*, *g*⁻*g*⁺, and *g*⁻*g*⁻. In this notation, which we follow in this work, the monomer to the left acts as the proton donor to the hydrogen bond. However, a closer look at the structural possibilities reveals a number of other interactions able to contribute to the energies and geometrical patterns in the ethanol dimers; such interactions include in one hand secondary C-H \cdots O hydrogen bonds where an alkyl hydrogen interacts with an oxygen atom and, on the other hand, dispersive interactions from alkyl chains in two different ethanol molecules.

The array of weak interactions mentioned above is set to produce weakly bound dimers with possibly high energies relative to the global minimum. However, not taking them into account will leave a sizable portion of the PES unexplored. In intermolecular clusters, local minima far apart in energy from the lowest energy structure should not be overlooked, as it is well known that chemical and physical processes are not restricted to global minima; put in other words, high relative energy should not be mistaken for instability.

Computational details

As mentioned in the methodology chapter, GLOMOS code was used for the exploration of the PES.^{140, 173-174} The preliminary search was done at the PBE0²¹⁵/D95V²¹⁶ level, while for the final optimizations were selected the M06 functional²¹⁷ in conjunction with the def2-TZVP²¹⁸ basis set, using the tight and ultrafine options available in the G09 package.¹⁷⁵ These options enhance calculation accuracy at reasonable additional cost and are recommended for molecular systems with low frequency vibrational modes, such as methyl rotations, making the optimizations more reliable. All structures were characterized as true minima by harmonic vibrational frequencies analysis. Given that dispersive forces are crucial for the correct description of molecular clusters stabilized by weak interactions; we selected the M06 functional²¹⁷ from the Minnesota family of functionals, which carries sufficient dispersive corrections (the s_6 scaling factor on Grimme's long range dispersion is 0.25) as to make it an appropriate computational model for the ethanol dimer.¹¹⁶ Highly correlated CCSD(T)²¹⁹ energies were computed for all stationary points found at the M06 level. The binding energy (BE) was computed at the CCSD(T)/def2-TZVP//M06/def2-TZVP level and is defined as:

$$BE = (E_{monomer1} + E_{monomer2}) - E_{dimer}$$

where $E_{monomer1}$ and $E_{monomer2}$ are the energies of the two relaxed monomers and E_{dimer} is the dimer energy. Note that the relaxation energy is taking into account for BE. In order to study the nature of the interactions responsible for the stability of ethanol dimers, the energy decomposition analysis (EDA) proposed by Su and Li¹⁹³ as implemented in GAMESS¹⁹⁶ was used.

Results and discussions

Potential energy surface analysis

The stochastic search and further optimization of candidate structures afforded 77 local minima on the PES for the ethanol dimer in a range of 6.5 kcal mol⁻¹. This number is considerably higher than any other previous report^{159, 205-208} and is an evidence of the very rich and complex energy landscape of the ethanol dimer. The sampling of the PES produced 25 structures stabilized by traditional O–H···O hydrogen bonds, 44 structures stabilized by C–H···O hydrogen bonds, and 8 structures stabilized by purely dispersive interactions. Figures 3.3 and 3.4 summarize the first 45 different structures, removing the enantiomeric forms. The least stable forms (32 structures) are collected in figures A-3.1 and A-3.2 in the Appendix B at the end of this chapter.

Discriminating different forms with the naked eye is a very difficult task. Some useful parameters to differentiate isomers were the O–H···O distances, the C···C distances between the methyl groups, and pseudo-dihedral angle defined by the C–O···O–C atoms (Fig. 3.2). Additionally, each structure has an enantiomer (except one *tt* form). Then, strictly 153 different local minima were found in the range of 6.5 kcal mol⁻¹. Geometrical and energetic data are presented in Tables 3.1, 3.2, and Table A-3.1 (Appendix B).

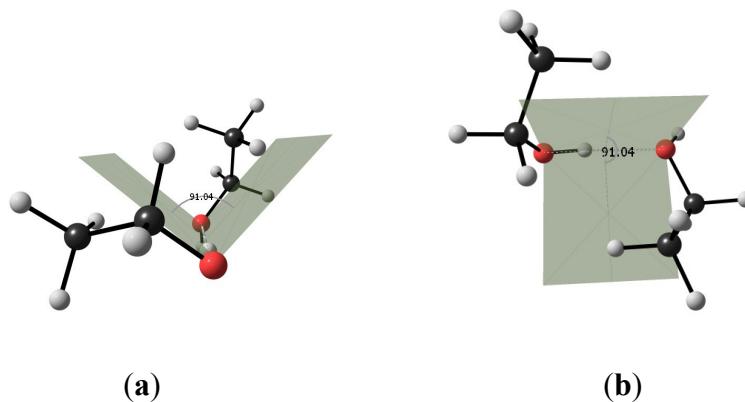


Figure 3.2 Definition of the pseudo-dihedral angle, **a** front view, and **b** side view.

The O–H···O interaction distances are closely packed in the 1.907–1.950 Å interval; the structures also show considerably weaker C–H···O hydrogen bonds spanning the 2.537–3.054 Å range, both ranges consistent with what is known about these types of interactions. On the other hand, out of the 44 structures stabilized by C–H···O interactions, 34 contain contacts where the donor is the methyl group and 10 arise from the CH₂ group. The range of distances of both C–H···O interactions (CH₂ or CH₃) is of 2.415–3.996 Å. In all cases, the structures of the constituent monomers are marginally affected by the stabilizing interaction that produces the dimers. It is important to emphasize that while the search produced a large number of stable dimers, this sample is by no means a complete characterization of the PES for the ethanol dimer. However, the sampling recovers the most important features of the title PES and that any missing structures could be safely classified into our three main groups; under these circumstances, and due to the very small energy differences among isomers, unequivocal identification of the global minimum is not possible.

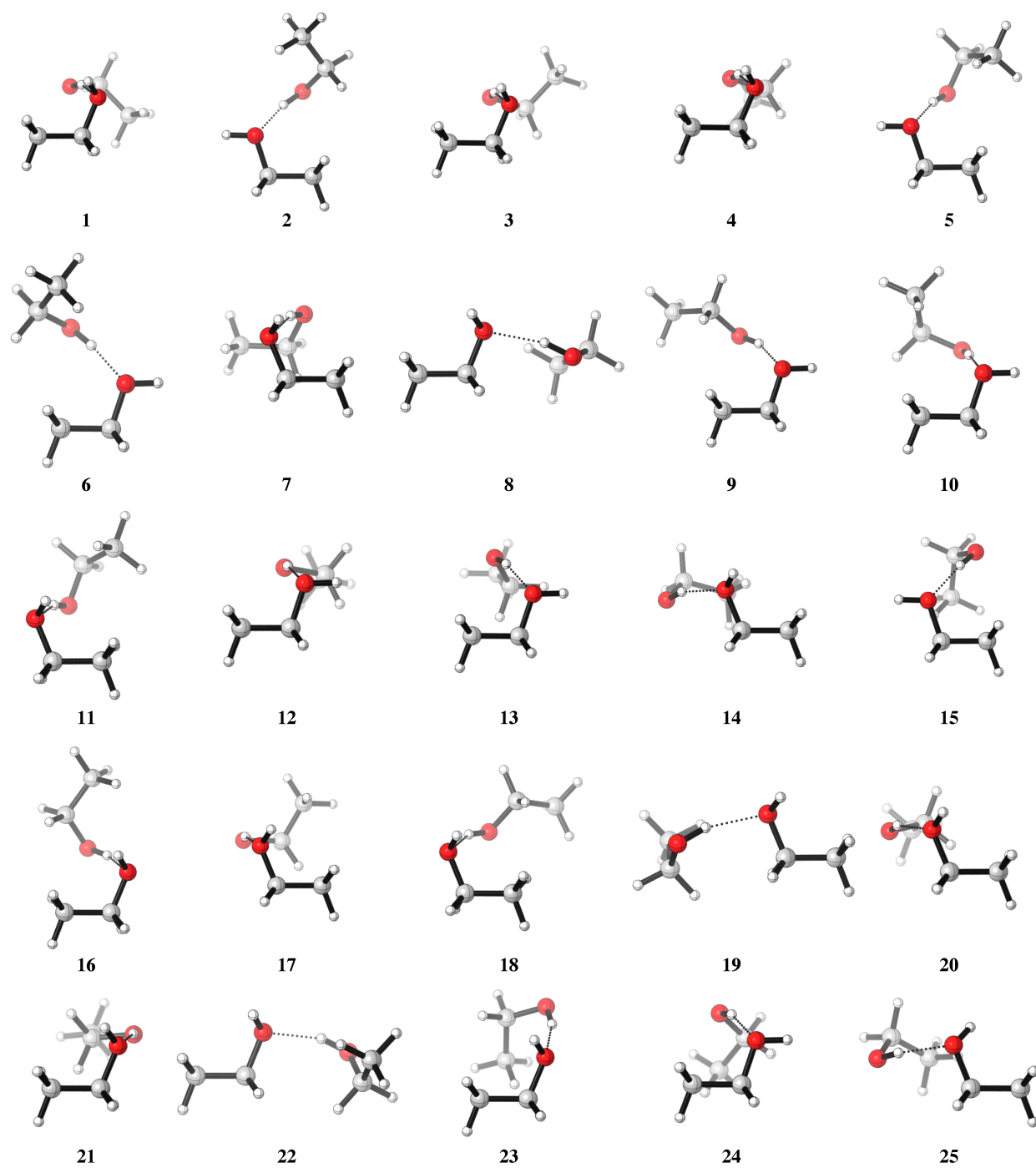


Figure 3.3 Local minima (ordered from lowest to highest relative energy) for the ethanol dimer with intermolecular O-H...O hydrogen bonds.

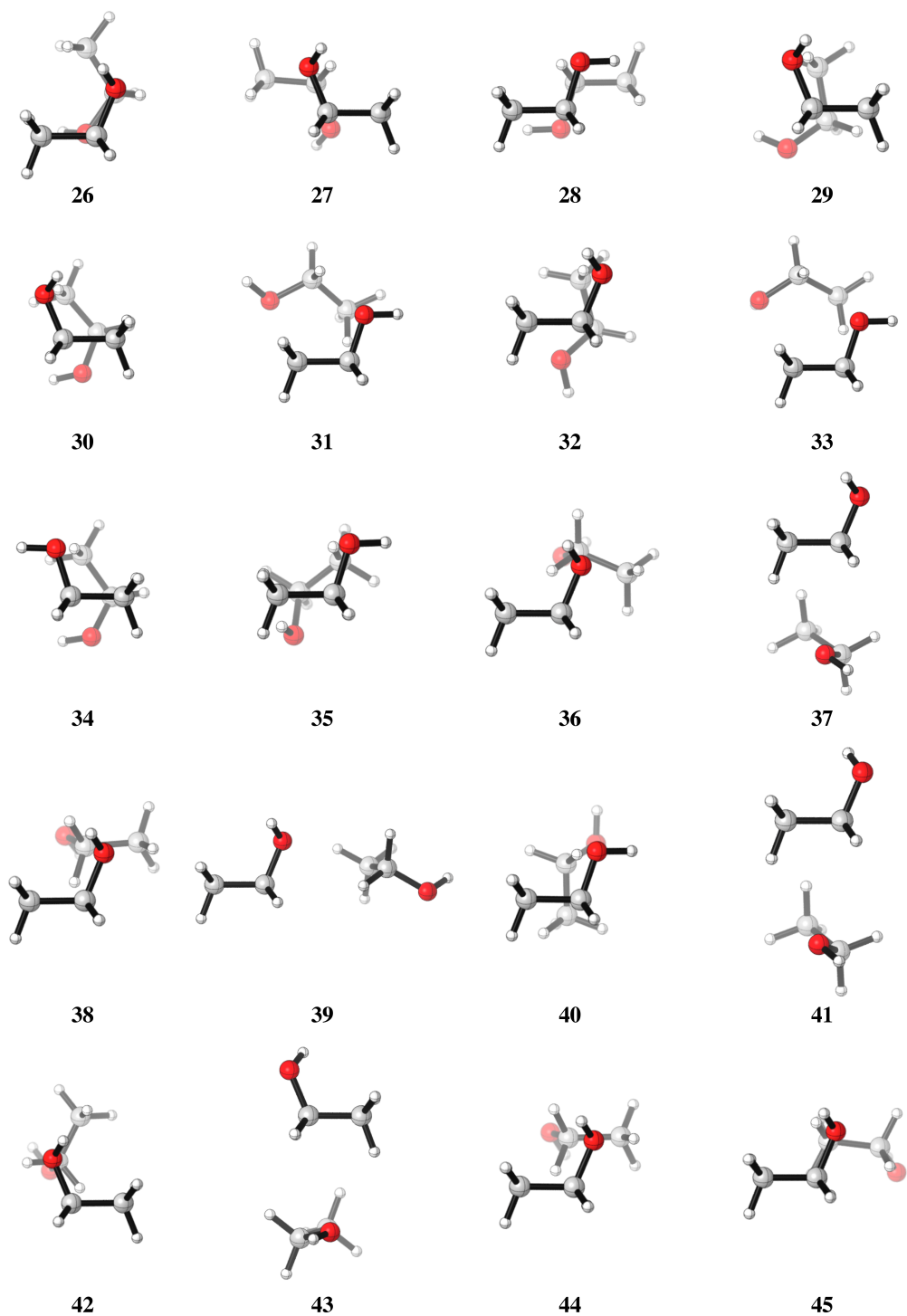


Figure 3.4 Local minima (ordered from lowest to highest relative energy) for the ethanol dimer with intermolecular C-H...O hydrogen bonds.

Molecular interactions lead to shifts in the vibrational frequencies of functional groups when compared to isolated species. Vibrational frequencies are commonly used among other things as hydration sensors^{46, 220} and as indicators of the strength of hydrogen bonding. For the ethanol dimer, previous reports^{205, 208} agree that vibrational frequencies of the acceptor O–H groups are not significantly affected by hydrogen bonding and our own results show the same behavior. On the other hand, down field shifts in the O–H stretching frequency of the donor monomer have been reported. Gonzalez *et al.*²⁰⁸ reported a 161 cm⁻¹ shift using B3LYP/6–311++G(*d,p*) approach, while Provencal *et al.*²⁰⁵ stated that from their IR measurements and MP2 computations a 150 cm⁻¹ shift is inferred. Our results, shown in Table 3.1, are in outstanding agreement with the experimental values, with our lowest energy structure exhibiting a red shift of the donor OH stretch of 178 cm⁻¹ (Table 3.1). The stretch harmonic vibrational frequency of the *trans* monomer is 3744 cm⁻¹ (computed at the M06 level with a scale factor of 0.9648).²²¹

Energetics

Tables 3.1, 3.2 and A-3.1 summarize energy and structural related quantities calculated for the ethanol dimers. A few important facts are immediately evident upon inspection:

1. Binding energies are quite small, not exceeding roughly 7.0 kcal mol⁻¹. These energies are sensibly smaller than the 19.0, 34.1, 37.5, 44.7 kcal mol⁻¹ binding energies calculated in related hydrogen-bonded clusters such as the carbonic acid dimers,²²² water hexamers,¹⁴⁵ methanol tetramers,²²³ and water heptamers,¹³⁸ respectively.
2. Isomers with an O–H···O are tightly packed in a narrow energy window (1 kcal mol⁻¹); this is

especially true for the first 20 isomers.

3. There is a clear separation in the binding energies for systems stabilized by primary and by secondary hydrogen bonds. A 2.0 kcal mol⁻¹ energy gap separates isomer 25 from 26.

4. Structures 70-77 (see Table A-3.1) do not exhibit hydrogen bonds and are stabilized by dispersive interactions between the alkyl chains.

5. Judging by the estimated Boltzmann distributions, several structures should have significant contributions to the properties of the ethanol dimer.

Table 3.1 Selected quantities calculated of the ethanol dimers with O-H...O bonds. r_1 is the C...C distance between methyl groups. r_2 is the distance of O-H...O bond. θ is the pseudo-dihedral angle. ΔE is the relative energy computed at the CCSD(T)/def2-TZVP//M06/def2-TZVP level. BE is the binding energy. ν_{\min} is the lowest frequency. $\Delta\nu$ is the O-H stretching frequency shift of the donor fragment. All energies are in kcal mol⁻¹, distances are in Å, θ are in degrees, and frequencies in cm⁻¹.

Dimer		r_1	r_2	θ	ΔE	BE	ν_{\min}	$\Delta\nu$
1	g^+g^+	4.845	1.910	247.7	0.0	7.20	35	-178
2	g^-t	4.707	1.925	252.9	0.26	6.94	29	-166
3	g^-g^+	5.503	1.917	263.0	0.28	6.92	20	-148
4	tg^+	5.507	1.907	262.2	0.29	6.91	35	-157
5	g^+t	3.877	1.922	225.4	0.30	6.89	22	-176
6	g^+t	4.279	1.929	91.0	0.41	6.78	55	-164
7	g^+g^-	4.739	1.943	57.3	0.43	6.77	61	-171

8	g^-g^+	5.055	1.922	108.8	0.61	6.59	36	-161
9	tt	4.405	1.919	108.6	0.66	6.52	31	-150
10	g^+t	4.173	1.926	91.8	0.67	6.52	49	-177
11	g^+g^-	4.079	1.927	218.1	0.69	6.51	44	-177
12	tt	5.587	1.937	262.9	0.72	6.46	30	-153
13	tt	5.105	1.938	303.0	0.73	6.45	35	-151
14	g^+g^-	4.204	1.918	253.8	0.74	6.46	32	-140
15	g^-t	3.985	1.937	91.2	0.77	6.43	37	-153
16	g^+g^+	4.885	1.950	118.8	0.78	6.42	45	-164
17	g^-g^-	4.186	1.919	292.8	0.83	6.37	45	-147
18	tg^-	4.420	1.937	247.3	0.92	6.28	51	-150
19	g^-g^-	5.450	1.939	297.0	0.92	6.28	43	-165
20	tg^-	5.641	1.908	278.3	0.97	6.23	30	-126
21	tg^+	5.198	1.912	61.8	1.03	6.16	52	-135
22	g^-g^+	5.440	1.929	304.8	1.11	6.09	56	-150
23	g^-g^+	3.850	1.936	39.2	1.12	6.08	39	-142
24	g^+t	4.156	1.929	291.2	1.51	5.69	63	-135
25	g^+g^+	4.508	1.943	252.3	1.73	5.47	35	-158

The computed lowest energy dimer (1) corresponds to a structure with both monomers in the gauche conformation, in agreement with recent reports^{159, 207} and in contrast with early studies where the global minimum was predicted to be tt ,²⁰⁸ gt , or tg .²⁰⁵ As pointed out by Provencal *et al.*,²⁰⁵ classifying structures according to their energies in the particular case of the ethanol dimer, where the energy differences are too small to be discerned by experimental or theoretical methods, is a futile exercise.

Table 3.2 Selected quantities calculated on the ethanol dimers with C-H...O bonds. r_1 is the C...C distance between methyl groups. r_2 is the distance of O-H...O bond. θ is the pseudo-dihedral angle. ΔE is the relative energy computed at the CCSD(T)/def2-TZVP//M06/def2-TZVP level. BE is the binding energy. ν_{\min} is the lowest frequency. All energies are in kcal mol⁻¹, distances are in Å, θ are in degrees, and frequencies in cm⁻¹.

Dimer		r_1	r_2	θ	ΔE	BE	ν_{\min}
26	g ⁺ g ⁺	4.225	4.305	193.6	3.79	3.42	41
27	g ⁺ g ⁻	4.821	4.531	184.9	3.79	3.41	27
28	tt	4.734	4.193	180.0	4.12	3.07	53
29	g ⁺ g ⁻	3.913	4.231	259.0	4.22	2.98	36
30	g ⁺ g ⁻	4.002	4.383	218.9	4.22	2.98	41
31	tt	4.002	4.426	214.7	4.27	2.91	41
32	g ⁺ t	4.001	4.719	203.6	4.34	2.85	33
33	g ⁻ t	4.035	4.815	203.8	4.36	2.83	43
34	g ⁺ t	3.910	4.502	219.3	4.51	2.69	36
35	g ⁺ t	4.046	3.756	178.7	4.71	2.48	25
36	g ⁺ g ⁻	4.695	5.177	213.3	4.91	2.29	24
37	g ⁺ t	3.842	4.945	150.7	4.93	2.27	45
38	g ⁺ g ⁺	4.777	5.182	279.3	5.00	2.20	26
39	g ⁺ g ⁺	5.094	5.195	145.4	5.03	2.18	20
40	tt	3.893	4.464	40.1	5.06	2.13	36
41	g ⁺ t	3.867	5.109	120.5	5.07	2.12	29
42	g ⁻ g ⁻	4.251	5.048	252.7	5.08	2.12	37
43	g ⁺ t	3.975	4.964	262.5	5.08	2.11	44
44	g ⁺ g ⁺	4.612	5.235	274.8	5.08	2.12	41
45	g ⁺ g ⁺	3.968	5.411	153.1	5.09	2.11	40
46	g ⁺ t	4.734	4.97	214.8	5.10	2.10	23
47	g ⁺ t	3.970	4.572	142.4	5.12	2.07	41

48	g^+g^+	3.775	5.800	277.3	5.13	2.07	40
49	tt	3.818	4.964	262.5	5.17	2.02	44
50	tt	3.921	4.439	326.4	5.19	2.0	31

Energy decomposition analysis

In this work, we use the scheme proposed by Su and Li,¹⁹³ which splits the interaction energy of a given cluster into electrostatic (ΔE^{ele}), exchange (ΔE^{ex}), repulsion (ΔE^{rep}), polarization + charge transfer (ΔE^{pol}), and dispersion (ΔE^{disp}) terms (Tables 3.4 and 3.5). The dispersion contribution is taken as the post-HF energy CCSD(T) in this case.¹⁹³ There are very good correlations between total interaction energy and all separate components (see Fig. 3.5), except for dispersion that is low; adjusted trends afford regression coefficients of 0.99, 0.91, and 0.98 for the electrostatic, exchange, and polarization + charge transfer terms, respectively.

Table 3.4 Results of the EDA at the CCSD(T)/def2-TZVP//M06/def2-TZVP level of the ethanol dimers with O-H...O bonds. The percentage values in parenthesis give the contribution to the total attractive interactions. All energies are in kcal mol⁻¹.

Dimer	ΔE^{ele}	ΔE^{ex}	ΔE^{rep}	ΔE^{pol}	ΔE^{disp}	ΔE^{total}
1	-10.43 (34.7)	-13.67 (45.5)	24.15	-3.17 (10.6)	-2.77 (9.2)	-5.90
2	-10.28 (34.3)	-13.87 (46.2)	24.34	-3.08 (10.3)	-2.78 (9.3)	-5.66
3	-9.99 (34.6)	-13.19 (45.6)	23.27	-3.01 (10.4)	-2.71 (9.4)	-5.63
4	-10.03 (35.5)	-12.77 (45.2)	22.69	-3.04 (10.8)	-2.43 (8.6)	-5.58
5	-10.40 (34.0)	-14.21 (46.5)	24.99	-3.14 (10.3)	-2.80 (9.2)	-5.56

6	-10.09 (33.2)	-14.24 (46.8)	24.85	-3.05 (10.0)	-3.03 (10.0)	-5.56
7	-9.89 (31.8)	-14.75 (47.4)	25.72	-3.06 (9.8)	-3.44 (11.0)	-5.43
8	-9.85 (34.7)	-13.02 (45.9)	22.97	-2.97 (10.5)	-2.52 (8.9)	-5.38
9	-10.62 (33.6)	-14.92 (47.2)	26.20	-3.13 (9.9)	-2.94 (9.3)	-5.41
10	-9.82 (32.5)	-14.17 (47.0)	24.86	-3.08 (10.2)	-3.11 (10.3)	-5.34
11	-9.77 (33.5)	-13.64 (46.7)	23.99	-2.99 (10.2)	-2.79 (9.6)	-5.19
12	-9.18 (33.7)	-12.60 (46.3)	22.26	-2.83 (10.4)	-2.61 (9.6)	-4.97
13	-9.46 (32.8)	-13.55 (46.9)	23.73	-2.89 (10.0)	-2.98 (10.3)	-5.15
14	-9.68 (33.7)	-13.40 (46.6)	23.41	-2.91 (10.1)	-2.77 (9.6)	-5.34
15	-9.71 (32.1)	-14.40 (47.6)	25.10	-2.99 (9.9)	-3.16 (10.4)	-5.16
16	-9.68 (32.9)	-13.91 (47.3)	24.31	-2.88 (9.8)	-2.94 (10.0)	-5.11
17	-9.17 (32.2)	-13.34 (46.8)	23.27	-2.86 (10.0)	-3.14 (11.0)	-5.23
18	-9.94 (32.7)	-14.48 (47.6)	25.32	-2.93 (9.6)	-3.05 (10.0)	-5.08
19	-9.13 (33.8)	-12.45 (46.0)	21.93	-2.80 (10.4)	-2.67 (9.9)	-5.12
20	-8.92 (35.4)	-11.31 (44.9)	19.98	-2.71 (10.8)	-2.25 (8.9)	-5.21
21	-9.14 (33.3)	-12.67 (46.2)	22.26	-2.86 (10.4)	-2.74 (10.0)	-5.14
22	-8.98 (33.0)	-12.68 (46.6)	22.23	-2.77 (10.2)	-2.77 (10.2)	-4.98
23	-9.33 (31.8)	-13.87 (47.2)	24.12	-2.89 (9.8)	-3.27 (11.1)	-5.23
24	-10.04 (31.6)	-15.17 (47.8)	26.48	-3.09 (9.7)	-3.45 (10.9)	-5.27
25	-8.98 (31.1)	-13.89 (48.1)	24.30	-2.90 (10.0)	-3.09 (10.7)	-4.56

Table 3.5 Results of the EDA at the CCSD(T)/def2-TZVP//M06/def2-TZVP level of the ethanol dimers with C-H...O bonds. The percentage values in parenthesis give the contribution to the total attractive interactions. All energies are in kcal mol⁻¹.

Dimer	ΔE^{ele}	ΔE^{ex}	ΔE^{rep}	ΔE^{pol}	ΔE^{disp}	ΔE^{total}
26	-3.49 (22.1)	-8.08 (51.3)	13.22	-0.94 (6.0)	-3.25 (20.6)	-2.55
27	-3.60 (22.8)	-8.05 (51.0)	13.24	-0.98 (6.2)	-3.16 (20.0)	-2.55

28	-2.68 (18.5)	-7.74 (53.5)	12.57	-0.78 (5.4)	-3.26 (22.5)	-1.88
29	-3.65 (21.1)	-9.25 (53.6)	15.25	-1.11 (6.4)	-3.25 (18.8)	-2.00
30	-3.27 (20.7)	-8.36 (53.0)	13.72	-0.97 (6.2)	-3.17 (20.1)	-2.03
31	-3.11 (19.8)	-8.51 (54.2)	13.88	-0.90 (5.7)	-3.19 (20.3)	-1.84
32	-3.31 (21.1)	-8.37 (53.4)	13.74	-0.96 (6.1)	-3.03 (19.3)	-1.94
33	-3.05 (19.4)	-8.49 (54.0)	13.87	-0.97 (6.2)	-3.22 (20.5)	-1.86
34	-2.91 (19.0)	-8.33 (54.3)	13.63	-0.87 (5.7)	-3.23 (21.1)	-1.71
35	-2.32 (16.4)	-7.69 (54.2)	12.69	-0.95 (6.7)	-3.22 (22.7)	-1.49
36	-2.23 (19.9)	-5.79 (51.7)	9.43	-0.62 (5.5)	-2.56 (22.9)	-1.77
37	-2.08 (18.6)	-5.89 (52.5)	9.55	-0.53 (4.7)	-2.71 (24.2)	-1.66
38	-1.98 (18.8)	-5.40 (51.4)	8.78	-0.56 (5.3)	-2.57 (24.5)	-1.73
39	-2.14 (21.2)	-5.17 (51.2)	8.42	-0.56 (5.5)	-2.23 (22.1)	-1.67
40	-2.06 (17.4)	-6.43 (54.3)	10.42	-0.52 (4.4)	-2.83 (23.9)	-1.42
41	-1.92 (18.1)	-5.57 (52.5)	9.02	-0.53 (5.0)	-2.58 (24.3)	-1.58
42	-1.92 (18.7)	-5.32 (51.9)	8.66	-0.52 (5.1)	-2.50 (24.4)	-1.61
43	-2.01 (17.4)	-6.18 (53.5)	10.05	-0.55 (4.8)	-2.82 (24.4)	-1.52
44	-2.14 (18.3)	-6.17 (52.7)	10.07	-0.64 (5.5)	-2.75 (23.5)	-1.63
45	-2.11 (18.7)	-5.91 (52.5)	9.65	-0.59 (5.2)	-2.65 (23.5)	-1.61
46	-1.89 (17.8)	-5.59 (52.5)	9.05	-0.57 (5.4)	-2.59 (24.3)	-1.59
47	-1.93 (16.8)	-6.19 (54.0)	10.10	-0.56 (4.9)	-2.78 (24.3)	-1.38
48	-2.18 (17.2)	-6.89 (54.4)	11.25	-0.65 (5.1)	-2.95 (23.3)	-1.43
49	-2.02 (18.0)	-6.04 (53.7)	9.77	-0.53 (4.7)	-2.66 (23.6)	-1.48
50	-1.99 (17.3)	-6.20 (54.0)	10.07	-0.57 (5.0)	-2.72 (23.7)	-1.42
51	-2.03 (19.5)	-5.46 (52.3)	8.92	-0.56 (5.4)	-2.38 (22.8)	-1.51
52	-1.76 (16.2)	-5.87 (54.1)	9.49	-0.55 (5.1)	-2.68 (24.7)	-1.36
53	-1.63 (15.6)	-5.58 (53.5)	9.03	-0.49 (4.7)	-2.73 (26.2)	-1.39
54	-1.68 (22.5)	-3.62 (48.5)	5.89	-0.44 (5.9)	-1.72 (23.1)	-1.59
55	-1.81 (15.0)	-6.72 (55.6)	10.88	-0.51 (4.2)	-3.04 (25.2)	-1.20
56	-1.65 (15.6)	-5.72 (54.0)	9.28	-0.49 (4.6)	-2.73 (25.8)	-1.31
57	-1.73 (16.3)	-5.71 (53.9)	9.24	-0.50 (4.7)	-2.65 (25.0)	-1.35
58	-1.58 (14.3)	-6.10 (55.1)	9.85	-0.48 (4.3)	-2.92 (26.4)	-1.22

59	-1.96 (18.4)	-5.76 (54.1)	9.39	-0.54 (5.1)	-2.39 (22.4)	-1.26
60	-1.77 (15.3)	-6.41 (55.3)	10.40	-0.53 (4.6)	-2.89 (24.9)	-1.19
61	-1.68 (17.4)	-5.10 (53.0)	8.27	-0.50 (5.2)	-2.35 (24.4)	-1.37
62	-1.96 (15.8)	-6.81 (55.1)	11.11	-0.63 (5.1)	-2.97 (24.0)	-1.26
63	-1.82 (20.3)	-4.67 (52.1)	7.61	-0.52 (5.8)	-1.96 (21.9)	-1.37
64	-1.54 (12.3)	-6.92 (55.1)	11.38	-0.71 (5.7)	-3.38 (26.9)	-1.18
65	-1.86 (17.0)	-5.93 (54.3)	9.64	-0.50 (4.6)	-2.64 (24.2)	-1.29
66	-1.54 (13.9)	-6.14 (55.5)	9.96	-0.53 (4.8)	-2.85 (25.8)	-1.10
67	-1.47 (25.7)	-2.60 (45.5)	4.23	-0.39 (6.8)	-1.26 (22.0)	-1.50
68	-1.78 (19.2)	-5.00 (53.9)	8.16	-0.46 (5.0)	-2.04 (22.0)	-1.12
69	-1.69 (22.7)	-3.77 (50.6)	6.18	-0.50 (6.7)	-1.49 (20.0)	-1.27
70	-0.90 (9.6)	-5.21 (55.3)	8.49	-0.41 (4.4)	-2.90 (30.8)	-0.94
71	-0.97 (8.4)	-6.56 (56.6)	10.78	-0.65 (5.6)	-3.40 (29.4)	-0.81
72	-0.66 (12.9)	-2.67 (52.4)	4.31	-0.14 (2.7)	-1.63 (32.0)	-0.80
73	-0.68 (8.6)	-4.51 (56.9)	7.27	-0.25 (3.2)	-2.49 (31.4)	-0.66
74	-0.44 (5.3)	-4.73 (57.3)	7.68	-0.33 (4.0)	-2.76 (33.4)	-0.57
75	-0.46 (7.9)	-3.21 (55.4)	5.17	-0.18 (3.1)	-1.94 (33.5)	-0.62
76	-0.35 (8.1)	-2.30 (53.4)	3.69	-0.11 (2.6)	-1.55 (36.0)	-0.63
77	-0.40 (8.6)	-2.53 (54.3)	4.07	-0.14 (3.0)	-1.59 (34.1)	-0.58

There is a clear gap (2.0 kcal mol⁻¹) for the interaction energies, which reflects the nature of the stabilizing interactions: Below -4.5 kcal mol⁻¹, structures are stabilized by a typical hydrogen bond, while above -2.6 kcal mol⁻¹, the dimers interact via secondary hydrogen bonds (C-H...O) and via dispersive interactions between the alkyl chains. For the O-H...O bonds, individual contributing terms are more clearly separated energy wise, while for secondary C-H...O bonds, the contributions from the energy components are closer to each other, suggesting that for the hydrogen bonds, there are dominant contributions to the interaction energy

(exchange, electrostatic), but for secondary hydrogen bonds, all interactions are comparatively as important.

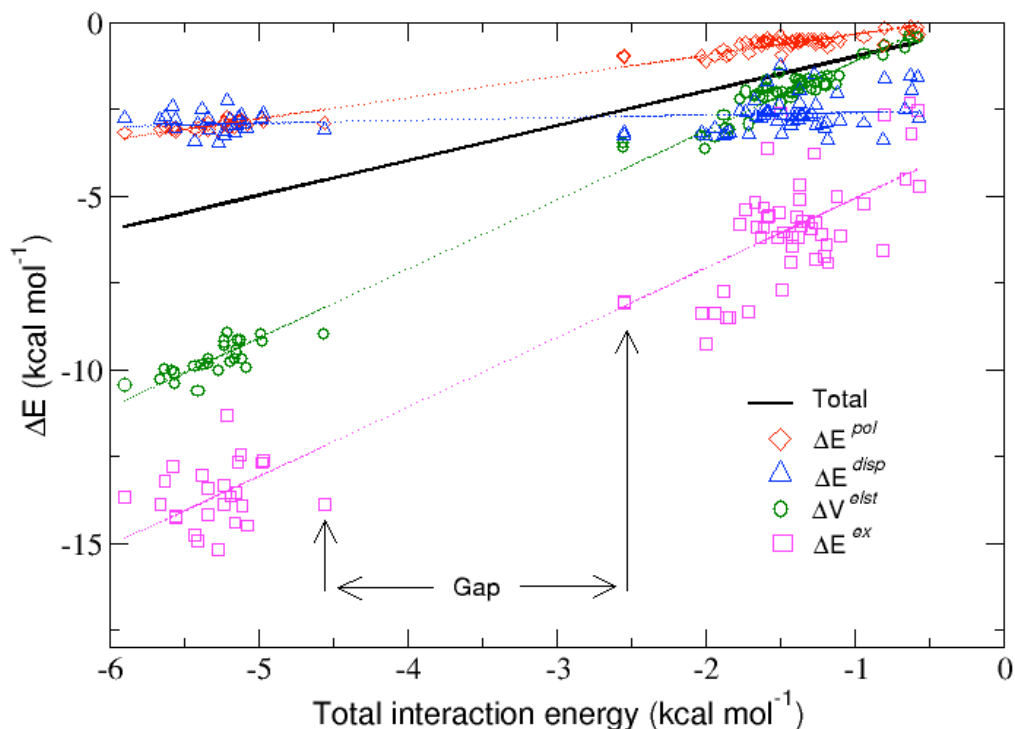


Figure 3.5 Correlation between the total interaction energy and its different contributions.

In all cases, exchange is the most stabilizing contribution, progressively reducing its dominant role as the interaction energy decreases. A very insightful observation is that the electrostatic term seems to run almost parallel to the interaction energies for primary hydrogen bonds, while for secondary C-H···O contacts, it is the dispersion contribution which seems to reproduce the trend of the interaction energies; thus, it can be argued that O-H···O bonds are predominantly stabilized by electrostatic (dipole–dipole) interactions and that secondary hydrogen bonds, despite having sizable contributions from all types of interactions, are predominantly stabilized by dispersive forces.

Conclusions

Clearly, the PES of the ethanol dimer is quite complicated. 153 different local minima in a range of 6.5 kcal mol⁻¹ were found. Three different types of interactions are at play stabilizing the dimers. On one hand, isomers with an O–H···O are tightly packed in a narrow energy window (1 kcal mol⁻¹) and are stabilized mostly by electrostatic interactions. A large number of structures show C–H···O hydrogen bonds, which are stabilized by charge transfer and dispersion. There is a clear division for the interaction energies: Below –4.5 kcal mol⁻¹, structures are stabilized by a typical hydrogen bond, while above –2.6 kcal mol⁻¹, the dimers interact via C–H···O contacts and via dispersive interactions between the alkyl chains.

This work has been cited in other studies about ethanol dimers and other systems with hydrogen bonds.²²⁴⁻²²⁶ For example, Umer *et al.*²²⁶ calculated the thermochemical properties of clusters of methanol, ethanol, and longer alcohols. The authors cited our results on EDA and reported entropies and energies of dimerization. In 2017, Loru *et al.*²²⁵ carried out an experimental work by chirped pulse Fourier transform microwave spectroscopy and theoretical calculations at MP2 and M062X level. They obtained the same lowest energy structure g⁺g⁺ and reported three new conformers. Both articles confirmed the complexity of the PES and the low energy differences between isomers for this system.

Appendix B

Ethanol dimers

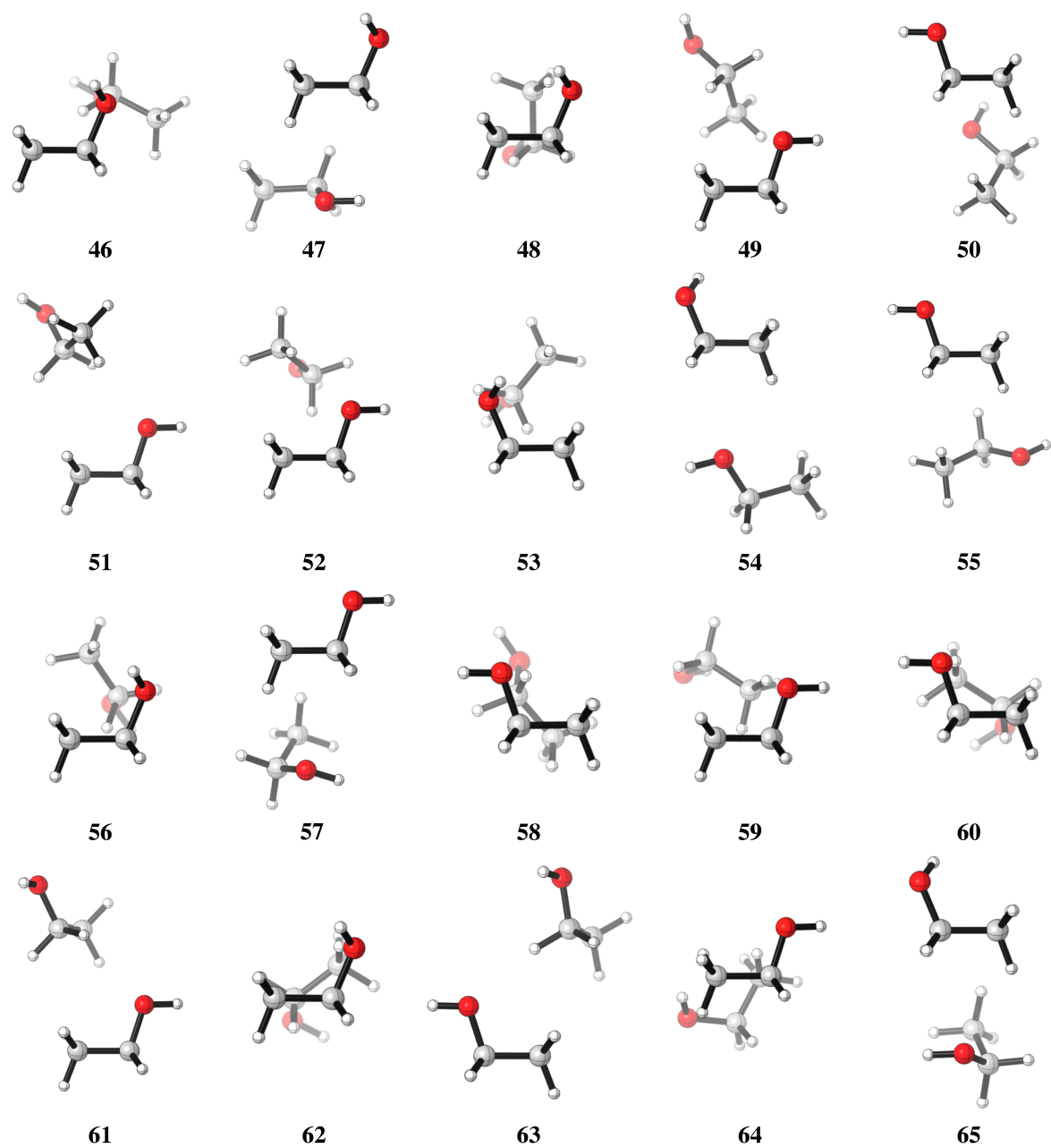


Figure B-3.1 Local minima (ordered from lowest to highest relative energy) for the ethanol dimer with intermolecular C-H...O hydrogen bonds and dispersion interactions

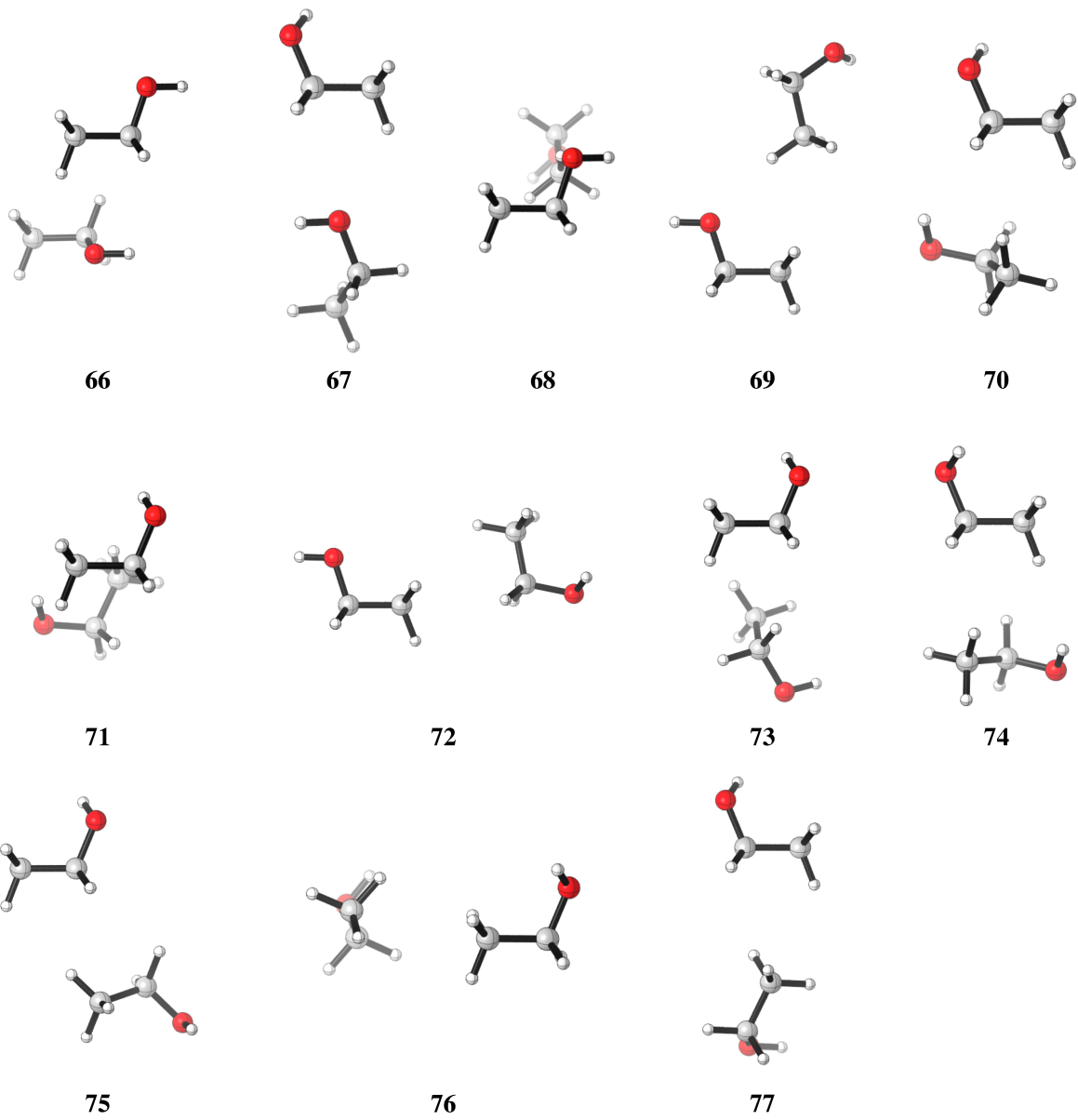


Figure B-3.2 Local minima (ordered from lowest to highest relative energy) for the ethanol dimer with intermolecular C-H...O hydrogen bonds and dispersion interactions.

Table B-3.1 Selected quantities calculated on the ethanol dimers with C-H...O bonds. r_1 is the C...C distance between methyl groups. r_2 is the distance of O-H...O bond. θ is the pseudo-dihedral angle. ΔE is the relative energy computed at the CCSD(T)/def2-TZVP//M06/def2-TZVP level. BE is the binding energy. ν_{\min} is the lowest frequency. All energies are in kcal mol⁻¹, distances are in Å, θ are in degrees, and frequencies in cm⁻¹.

Dimer		r_1	r_2	θ	ΔE	BE	ν_{\min}
51	g^-t	4.123	5.315	61.1	5.22	1.97	41
52	tt	3.795	5.092	151.4	5.25	1.93	33
53	g^-t	3.992	4.896	274.3	5.27	1.92	34
54	g^+t	4.266	4.816	321.3	5.29	1.90	14
55	tt	3.948	5.800	91.7	5.30	1.88	45
56	g^+t	3.913	5.182	124.5	5.34	1.85	34
57	g^-t	3.828	5.029	129.7	5.35	1.84	12
58	tt	3.780	4.499	16.6	5.36	1.82	40
59	g^-t	3.754	6.005	155.8	5.36	1.83	29
60	g^-t	3.950	5.714	270.3	5.37	1.82	41
61	tt	4.101	4.982	322.9	5.37	1.81	51
62	g^+g^+	3.967	5.602	86.4	5.37	1.83	43
63	tt	4.213	4.186	11.6	5.38	1.80	19
64	g^-t	3.870	4.301	275.8	5.39	1.80	28
65	g^+g^+	3.851	4.675	285.3	5.41	1.79	41
66	tt	3.960	4.656	158.8	5.42	1.76	32
67	g^+g^+	5.727	4.703	36.0	5.43	1.77	14
68	g^+t	3.920	6.034	149.7	5.51	1.68	32
69	g^+t	3.820	6.024	188.4	5.57	1.63	20
70	g^+g^+	3.942	3.928	346.5	5.82	1.38	46
71	g^-g^-	3.850	4.548	271.8	5.91	1.29	41

72	g^+t	3.876	7.213	115.6	6.25	0.94	16
73	g^-g^+	3.804	6.125	38.9	6.27	0.93	32
74	g^-g^-	3.967	5.595	72.7	6.27	0.93	31
75	g^-g^-	4.243	6.246	23.1	6.36	0.84	17
76	g^+g^+	3.649	6.053	30.6	6.42	0.79	26
77	g^+g^+	3.803	7.26	64.7	6.42	0.78	25

Chapter 4

Metallocene dimers

Introduction

In 1951, with the discovery and subsequent elucidation of the sandwich structure of ferrocene²²⁷⁻²³¹ an entire new branch, metallocene chemistry, emerged in organometallic chemistry. Gradually, the importance of metallocenes became tremendous due to their versatile applications in several fields such as biological chemistry,²³² medicinal chemistry,²³³⁻²³⁴ catalysis,²³⁵⁻²⁴⁴ and non-linear optics,²⁴⁵⁻²⁴⁹ among others. Promising new applications in the field of supramolecular chemistry were uncovered by studying several self-aggregated metallocene derivatives interacting through non-covalent interactions (mainly H-bonds).

Recently, Bogdanović and Novaković²⁵⁰ evaluated the frequency of occurrence of the ferrocene dimer in crystals reported in the Cambridge Structural Databank.²⁵¹ They found that 46.8% of ferrocene derivative crystals contain a dimer where both units are in a parallel orientation; with one of the ferrocene units shifted along the z-axis by half of the Cp-Fe bond length (see Figure 4.1).

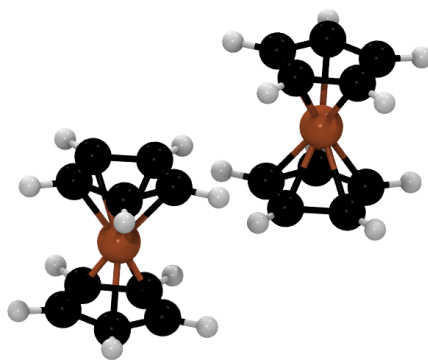


Figure 4.1 Building block identified by Bogdanović and Novaković in ferrocene derivative crystals.²⁵⁰

Keeping in mind the study of Bogdanović and Novaković, the potential energy surface (PESs) of the ferrocene dimers were explored. In addition, the search was extended to the PESs of ruthenocene and osmocene dimers.

4.2 Computational details

The computational procedure employed GLOMOS to systematically explore the potential energy surfaces (PESs) of molecular clusters.^{173-174, 176} Final equilibrium geometries are reported at the PBE²⁵²/def2-TZVP²¹⁸ and PBE-D2/def2-TZVP levels. To describe the scalar relativistic effects, an effective core potential was used for Ru and Os, describing the behavior of 28 and 60 core electrons, respectively. The latter approach included the D2 version of Grimme's dispersion corrections²⁵³ because in the D3 model there is one term that depends on the coordination number of the atoms involved and the analytical expression for the second derivative of such term is not numerically stable for large coordination numbers (~8 or higher), as the case of metallocenes, with coordination numbers around 10 for the transition metals. Therefore, D2 model was used to obtain the analytic frequency calculations; such model does not have a dependency on the coordination numbers. The energy differences discussed here include the harmonic zero point energy (ZPE) correction. In order to evaluate the thermal effects, the procedure described by Irikura²⁵⁴ was used as is implemented in thermo code,²⁵⁵ where the standard molar entropy and enthalpy changes are computed from the molecular partition function. All the quantities needed are taken from the harmonic vibrational frequency computations. All the computations are done using the *Gaussian 09* program.¹⁷⁵

The nature of the interactions is analyzed by the non-covalent interaction (NCI) index²⁰⁰ and EDA¹⁹⁸ at the revPBE-D3^{185, 256}/TZ2P//PBE-D2/def2-TZVP level using the ADF (2013.01) package.¹⁹⁷ We do not use the frozen core approximation; rather, an all-electron basis set is used. Scalar relativistic effects were considered using the zeroth-order regular approximation (ZORA).

Results and discussions

Structures and energetics

Our KS-DFT computations reveal a scarce diversity of structures within a range of 10 kcal·mol⁻¹. At higher energies, there are several arrangements with one or more covalent bonds between two cyclopentadienyl rings, which are irrelevant for this study. Without dispersion, we found five different forms for ferrocene, seven for ruthenocene, and four for osmocene dimers (see Figure C-4.1 in the Appendix C). The lowest-lying energy forms for Fe, Ru, and Os are **3**, **1**, and **2**, respectively (Figure 4.2). The inclusion of dispersion *via* Grimme's corrections induces the collapse of some of these isomers, resulting in only four dimers for each metallocene dimer (Figure 4.2). Remarkably, regardless of the conformation of the monomers in the initial guess (eclipsed or staggered), dimers have only eclipsed units. When dispersion is involved, structure **1**, in which two metallocenes are oriented perpendicular to each other, becomes the most stable one in all cases. Structure **2** is the one described by Bogdanović and Novaković and is the second most stable form.²⁵⁰ In the higher energy forms, one cyclopentadienyl ring of the first unit interacts perpendicularly (**3**) or in a parallel manner (**4**) to the second unit. In the case of ferrocene, while **1** is only 1.7 kcal·mol⁻¹ lower in energy than **2**, isomers **3** and **4** are 3.0 and 4.7 kcal·mol⁻¹ above the global minimum, respectively. The same energy order is noticed for the

ruthenocene and osmocene dimers, but the energy differences increase considerably (see Figure 4.2).

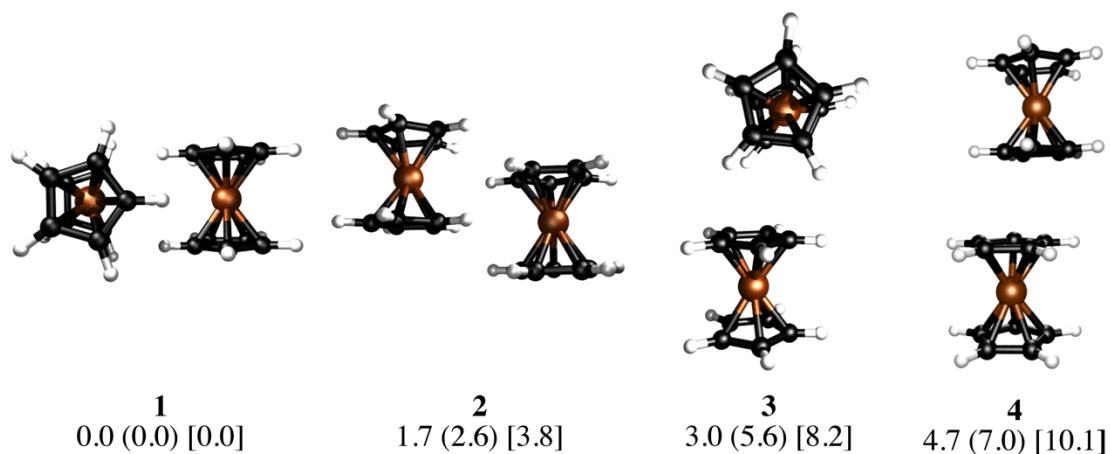


Figure 4.2 PBE-D2/def2-TZVP local minima on the potential energy surfaces of the MCp_2 dimers ($M = Fe, Ru, Os$; $Cp = \text{cyclopentadienyl}$). All relative energies (in $\text{kcal}\cdot\text{mol}^{-1}$) include the ZPE correction. The first value corresponds to the relative energy for the ferrocene dimer. In parentheses and brackets are relative energies for the ruthenocene and osmocene dimers, respectively.

Dispersion has strong effects on the geometrical parameters. The $M\cdots M$ distances without dispersion in isomer **1** are 5.80 (Fe), 5.56 (Ru), and 5.48 (Os) Å. These distances are reduced to 4.84 (Fe), 4.72 (Ru), and 4.64 (Os) Å by applying the D2 correction to PBE, *i.e.*, the intermolecular dispersion reduces the $M\cdots M$ distances by almost 1 Å. Note that a reduction in the $M\cdots M$ distance from Fe to Os is independent of the dispersion inclusion, indicating a stronger interaction for the osmocene dimer. A similar shortening of the $M\cdots M$ distance is perceived in

the other three isomers as a consequence of the dispersion inclusion. At the PBE-D2/def2-TZVP level, with inclusion of the ZPE correction, the computed bond dissociation energies (BDE) for **1** without dispersion are 0.7 (Fe), 1.3 (Ru), and 1.0 (Os) kcal·mol⁻¹. These values are remarkably increased to 7.5 (Fe), 10.0 (Ru), and 13.7 (Os) kcal·mol⁻¹, when dispersion is included.

Thermal effects

The previous discussion is based on the energies computed at 0 K. Our computations show that in the case of ferrocene, the relative free energy at room temperature between structures **1** and **2** is reduced only to 0.1 kcal·mol⁻¹ (at the PBE-D2/def2-TZVP level). Most interesting is that at this temperature structure **3** becomes the lowest lying isomer by 1.3 kcal·mol⁻¹ with respect to **1**. Single-crystal X-ray diffraction analysis at 298 K indicated that the crystal structure of ferrocene is monoclinic *P21/n* ($a = 5.9252 \text{ \AA}$, $b = 7.6035 \text{ \AA}$, $c = 9.0354 \text{ \AA}$, $\beta = 93.165^\circ$),²⁵⁷ with motifs similar to dimers **2** and **3**. Although **2** is a very common building block in crystal structures and **1** is the most stable in the gas phase at low temperatures, the other motifs (**3** and **4**) are stabilized by entropic factors. Figure 4.3a shows the dominant regions of each structure as a function of temperature for the ferrocene dimers.

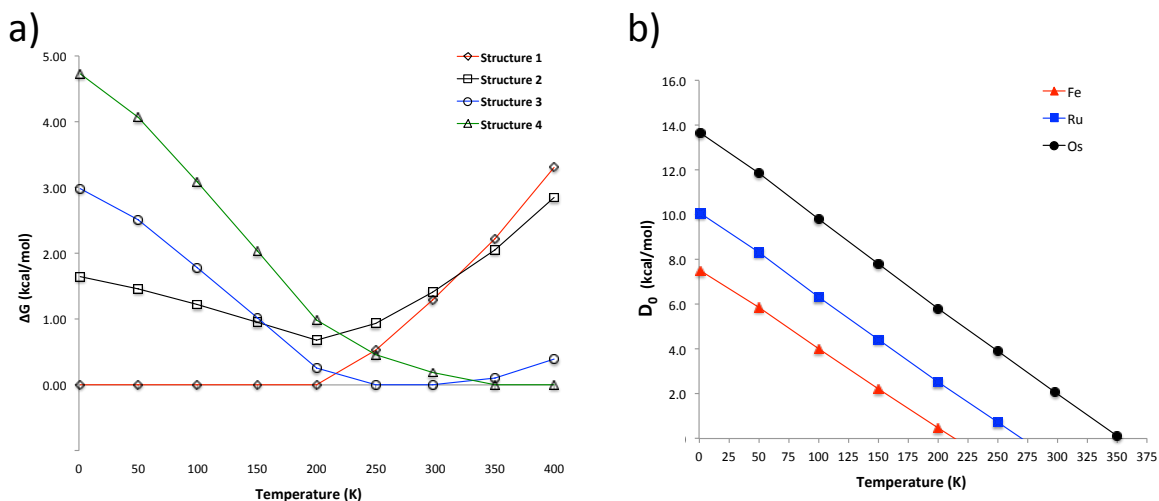


Figure 4.3 a) Thermal effects on the relative energies for the ferrocene dimer and b) thermal effects on the dissociation energies of structure **1** of the MCp_2 dimers ($M = Fe, Ru, Os$; $Cp =$ cyclopentadienyl). All energy differences are computed at the PBE-D2/def2-TZVP level.

For ruthenocene and osmocene, the energetic order computed at 0 K is maintained at room temperature, but it is also altered at higher temperatures (Figures 4.4 and C-4.2, Appendix C). It is also apparent from Fig. 4.3a and Figure 4.4 that isomer **1** will be dominant until 200, 320, and 400 K for Fe, Ru, and Os, respectively.

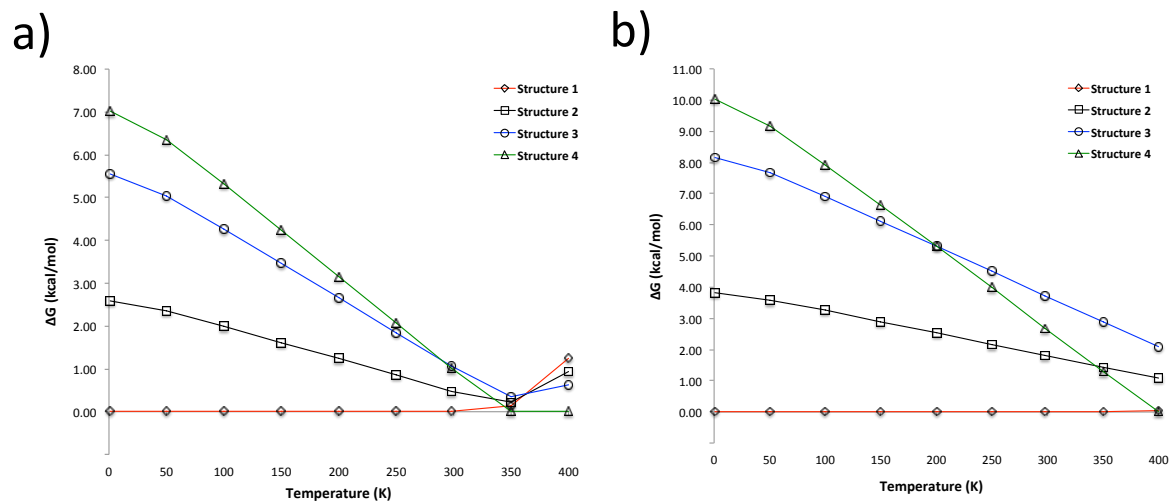


Figure 4.4 Thermal effects on the relative energies for the a) ruthenocene dimers and b) osmocene dimers. All energy differences are computed at the PBE-D2/def2-TZVP level.

Temperature also significantly affects the dissociation energies. Figure 4.3b indicates that while the ferrocene dimer is stable until 220 K, the ruthenocene and osmocene dimers are stable complexes until 270 and 350 K, respectively. The main reason is that at high temperatures, the contact area between the two units decreases and less compact clusters are obtained. In other words, the ideal gas behavior (no intermolecular interactions, thus no cluster formation) is recovered at high temperatures.

Bonding and EDA

What is nature of the interactions in a metallocene dimer? In principle, at low temperatures, dissociation energies are higher than the computed interaction energy of the water dimer ($4.8 \text{ kcal}\cdot\text{mol}^{-1}$), a system that exhibits a single hydrogen bond. There is a comprehensive literature dealing with the important problem of the nature and strength of interactions stabilizing the water and benzene dimers, this literature is too extensive to be reviewed here and this problem falls outside the scope of this work.²⁵⁸⁻²⁶³ Nonetheless, we point out that MP2 calculations overestimate deformation energies in the water monomer when compared to the highly sophisticated CCSD(T) methods²⁶⁴ and that experimentally measured dissociation energies for the benzene dimer²⁵⁸ are $2.4 \pm 0.4 \text{ kcal}\cdot\text{mol}^{-1}$ which are in outstanding agreement with our results in Table 4.1. Obviously, these interactions are of different nature since metallocenes lack a permanent dipole moment, thus the driving force behind the formation of metallocene dimers is of dispersive origin as discussed above. Additionally, it is important to remark that a ferrocene dimer has many more atoms than a water dimer, so the collective action of very small interaction energies of dispersive nature is responsible for the stabilization of the metallocene dimers. On the other hand, the ferrocene dimer has a quadrupole moment, and the quadrupole-quadrupole interaction decreases more slowly ($1/R^5$) at long distances than the dispersion interaction.

Bogdanović and Novaković found an electrostatic complementarity between the two ferrocene units in structure **2**.²⁵⁰ This complementarity occurs in a very large area, including the four “puzzle-like” regions of mutual compatibility and recognition. Figure 4.5 shows molecular electrostatic potential isosurfaces for the four local minima of ferrocene. It is apparent that this complementarity concept is also applicable to structure **1**. However, this does not apply to **3** and **4**, where the overlap of the negative regions interrupts the complementarity.

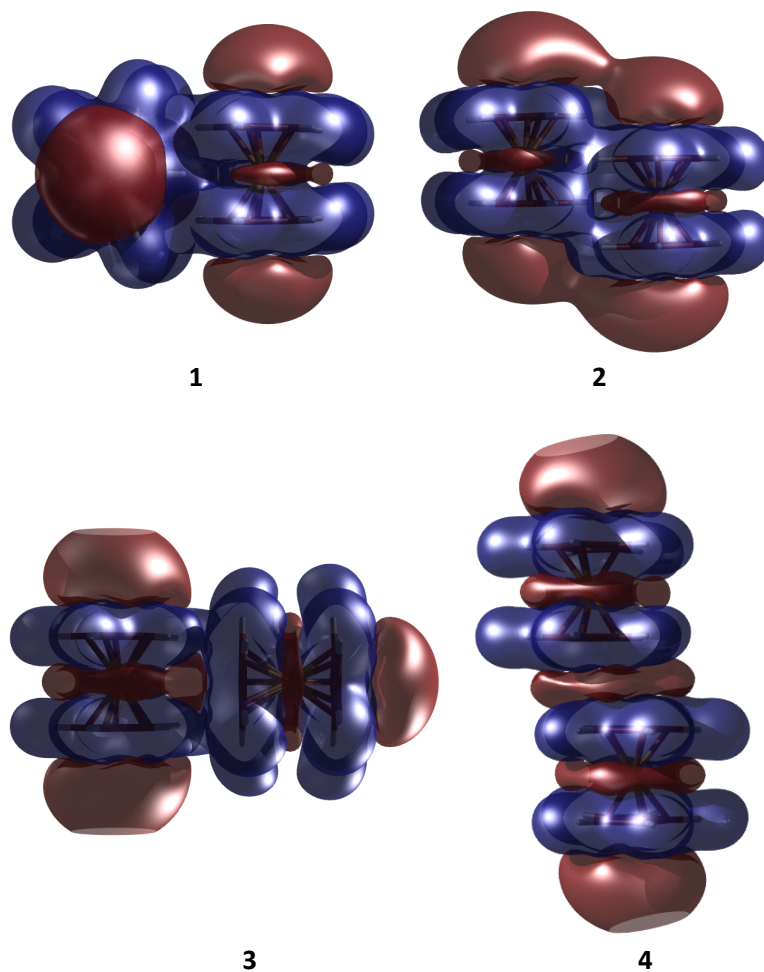


Figure 4.5 Molecular electrostatic potential maps of the ferrocene dimers. Isosurface are plotted with an isovalue of 0.01. Positive regions are in red and negative regions in blue.

Charge density difference plots give a precise representation of the electron redistribution upon dimer formation (Figure 4.6). Clearly, the electron redistribution in the three dimers is negligible. The most relevant changes are perceived in the density of the C-H bond involved in the contact. While the hydrogen atoms lose density, carbon atoms gain it. So, a very poor polarization contribution is expected (*vide infra*). Note that dispersion forces always will be attractive even without any charge transfer.

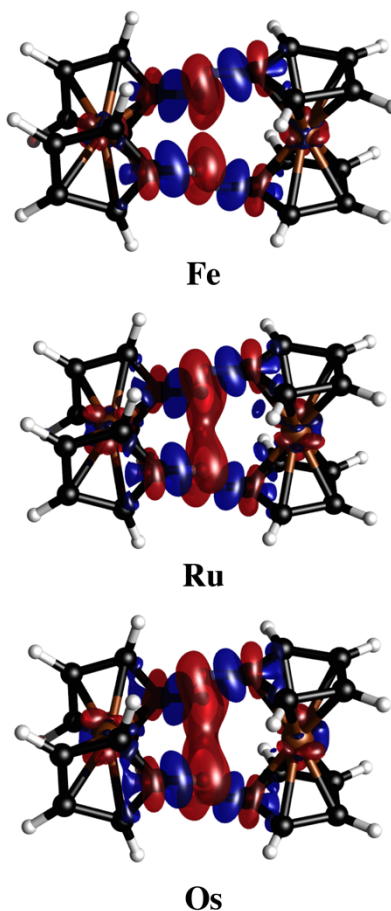


Figure 4.6 Electron density differences in isosurfaces ($\Delta\rho = 0.0005$ a.u.). Negative and positive regions are in red and blue, respectively.

The strength of the overall contributions of dispersion and electrostatic terms to the interactions can be quantitatively estimated by EDA. Table 4.1 gives the EDA values at the revPBE-D3/TZ2P//PBE-D2/def2-TZVP level calculated for the two most stable isomers. It becomes apparent that the electrostatic contribution is not the sole term stabilizing the dimers. It contributes *ca.* 28-32% towards the total attraction. ΔE^{disp} is found to be the major contributor towards the total attraction with $\approx 50\%$. The contribution from ΔE^{orb} is the least towards the total

attraction (less than 20%) as a consequence of negligible orbital overlapping between two monomers. Note that the interaction energy gradually increases on moving from Fe to Os. It is also important to mention that monomers do not suffer any significant structural variation, thus preparation energy is negligible. Clearly, EDA shows a delicate balance between dispersion and electrostatic contributions to stabilize a metallocene dimer.

Note that although the magnitude of the interaction energy between two metallocene units is quite close to typical H-bond energy, the nature of the bonding between them is quite different. As a reference point, water dimer is considered (see Table 4.1). In this H-bonded dimer, the ΔE^{ele} contribution is found to be the most significant (60 %), whereas the contributions from ΔE^{orb} and ΔE^{disp} terms to the total attractive interaction are 32 and 8.2%, respectively. Therefore, according to EDA, in the water dimer, as in most cases, the H-bonding is mainly electrostatic in nature.²⁶³ We have also compared the title cases with the parallel-displaced benzene dimer with C_{2h} symmetry. EDA indicates that the benzene dimer is stabilized mainly by dispersion (65%). So, the nature of bonding of metallocene dimers is similar to that of the benzene dimer, but the interaction energy is higher in the first cases.

Table 4.1 EDA results of the metallocene dimers computed at the revPBE-D3/TZ2P//PBE-D2/def2-TZVP level. Energies are in kcal·mol⁻¹.

M	Cluster	ΔE^{ele}	ΔE^{Pauli}	ΔE^{orb}	ΔE^{disp}	ΔE^{total}
Fe	1	-9.3 (30.0)	23.3	-5.3 (17.1)	-16.4 (52.9)	-7.7
	2	-6.2 (28.4)	16.1	-3.7 (17.0)	-11.9 (54.6)	-5.7
Ru	1	-11.1 (31.4)	26.5	-6.6 (18.6)	-17.7 (50.0)	-9.0
	2	-8.2 (32.2)	18.8	-4.6 (18.0)	-12.7 (49.8)	-6.7
Os	1	-13.4 (32.1)	30.2	-7.5 (17.9)	-20.9 (50.0)	-11.6
	2	-9.7 (32.7)	21.5	-5.2 (17.5)	-14.8 (49.8)	-8.2
	(H ₂ O) ₂	-8.8 (59.9)	9.9	-4.7 (32.0)	-1.2 (8.2)	-4.8
	(C ₆ H ₆) ₂	-2.5 (24.5)	7.3	-1.1 (10.8)	-6.6 (64.7)	-2.8

(The percentage values within the parenthesis show the contribution towards the total attractive interactions ($\Delta E^{\text{ele}} + \Delta E^{\text{orb}} + \Delta E^{\text{disp}}$))

Figure 4.7 depicts NCI isosurfaces for isomers **1** and **2** to illustrate the nature of the intermolecular interactions. As is mentioned above, a continuous color-coding scheme based on the second derivative of the electron density is used, where strong attractive interactions are represented in blue, weak attractive interactions in green, and strong repulsive interactions in red. The images of both isomers correspond to a typical dimer stabilized mainly by dispersion where attractive surfaces cover a very large area between both units. So, NCI analysis supports the fact that there is a collective action of small interaction energies of dispersive nature distributed in an ample area between both monomers.

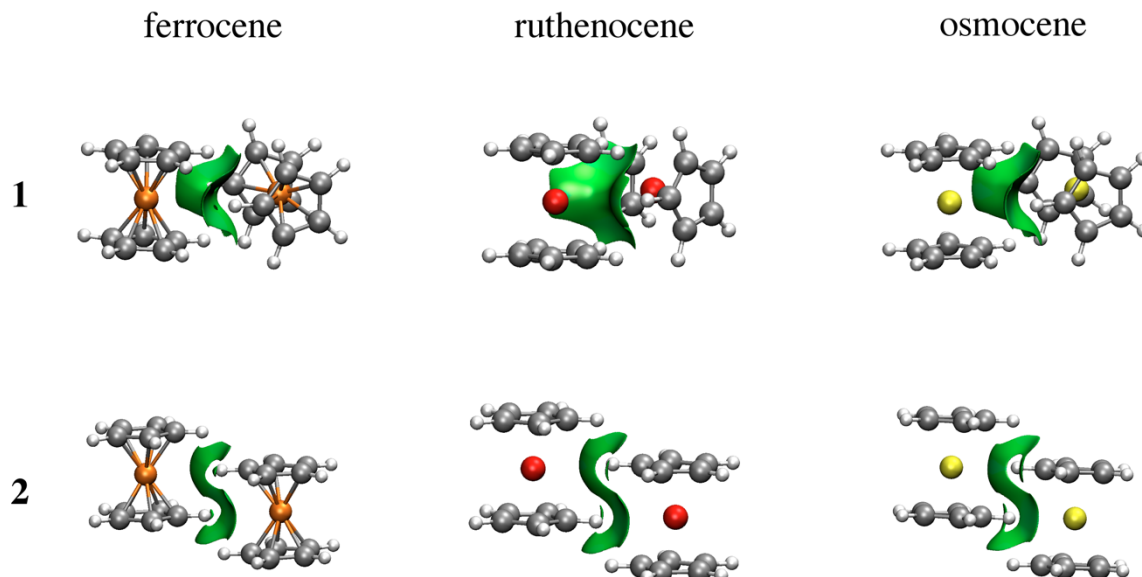


Figure 4.7 NCI plots of the MCp_2 dimers ($M = Fe, Ru, Os$). A density cutoff of $\rho=0.01$ a.u. was applied and the pictures were created for an isosurface value of $s=0.5$ and colored in the $[-0.03, 0.03]$ a.u. $\text{sign}(\lambda_2)\rho$ range.

Furthermore, the area of the green surface in **1** is larger than that in **2**. Integration of the volume of this surface for Fe (see Table C-4.1, Appendix C), gives 87.47 a.u. for the parallel conformer and 104.03 a.u. for the perpendicular one. The charges involved within these surfaces are also greater for the orthogonal conformation (1.78 lel in the parallel case *vs.* 1.90 lel for the orthogonal one). These values are in agreement with the relative weight of dispersive and electrostatic contributions in the EDA partition.

Conclusions

The results show that dispersion is the major contribution to stabilize a metallocene dimer. Dispersion has also strong effects on the geometrical parameters, reducing the M...M distances by almost 1 Å. The potential energy surface analysis, including dispersion, shows the presence of only four local minima for all cases. Calculations also reveal that inclusion of entropic factors modifies the relative stability of the complexes. At low temperatures, the lowest lying energy structure of (MCp₂)₂ (M=Fe, Ru, Os) is one in which the two fragments are oriented perpendicular to each other. At higher temperatures, relative and dissociation energies for the different isomers will be strongly affected. The interaction energy gradually increases on moving from Fe to Os. Our bonding analysis shows that the contribution from ΔE^{ele} term is important, but amounts to only about 30% of the total attraction energy. The most important attractive contribution is dispersion (almost 50%). The NCI analysis reveals the occurrence of attractive surfaces of dispersive nature between two metallocene units as the main factor responsible for the stability of the dimers. A larger area of the attractive surface in **1** indicates a larger dispersion interaction than in **2**. So, the collective action of very small interaction energies of dispersive nature is responsible for the stabilization of the metallocene dimers.

Relevant cites of this work are the experimental work on the synthesis of a covalente organic helical cage²⁶⁵ and the recent article of Pal *et al.*,²⁶⁶ they studied the bent gas-phase geometry of CaCp₂ in comparison with the linear sandwich structure of MgCp₂.

Appendix C

Metallocene dimers

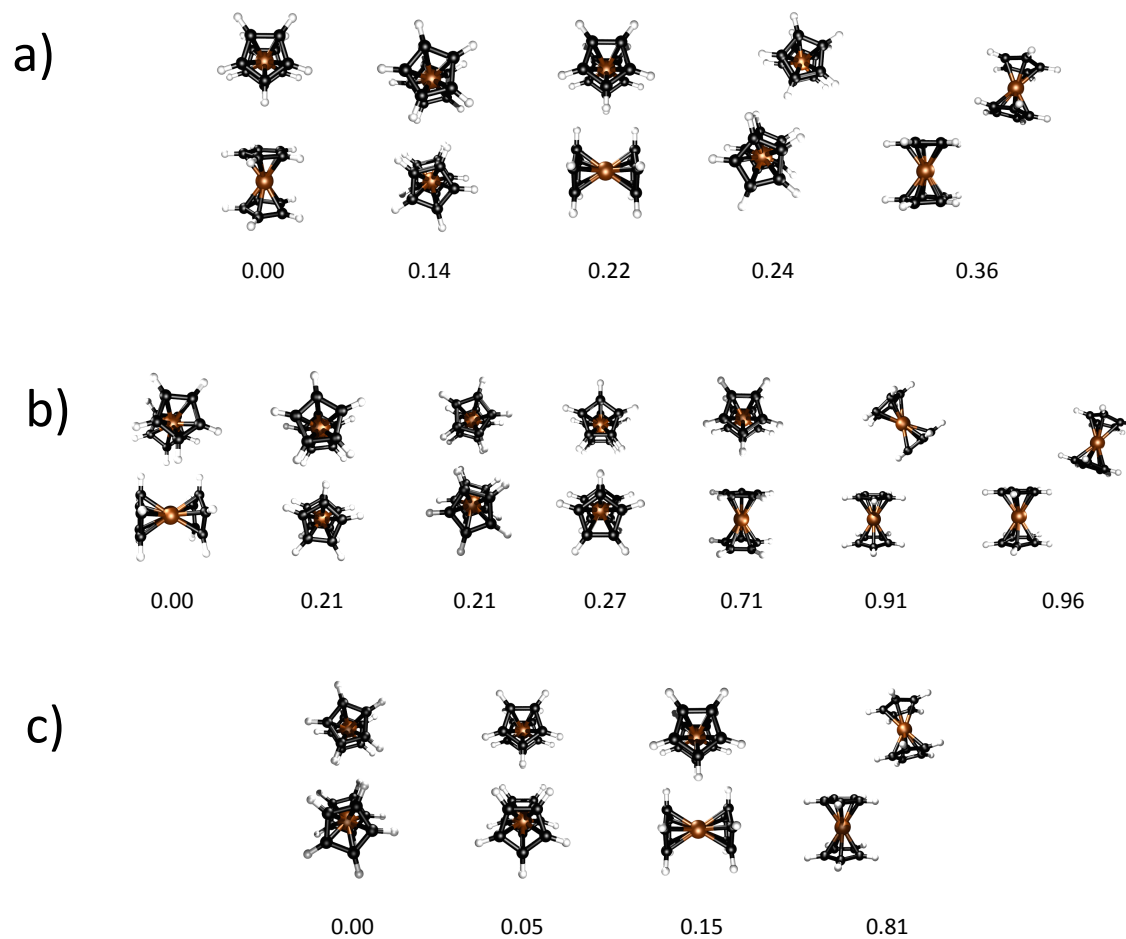


Figure C-4.1 PBE/def2-TZVP local minima on the potential energy surfaces of the MCp_2 dimers ($\text{M} = \text{Fe}, \text{Ru}, \text{Os}$; $\text{Cp} = \text{cyclopentadienyl}$). All relative energies in $\text{kcal}\cdot\text{mol}^{-1}$, including the ZPE correction. a) ferrocene dimers, b) ruthenocene dimers and c) osmocene dimers.

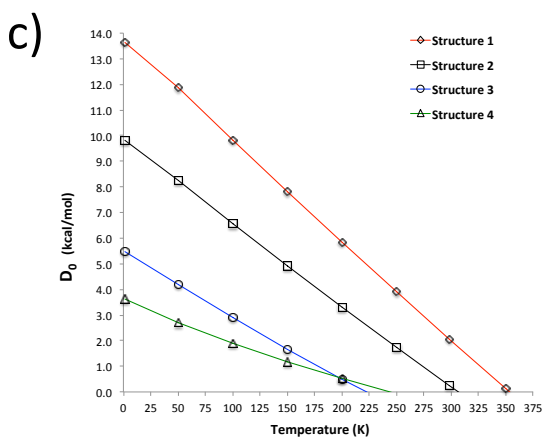
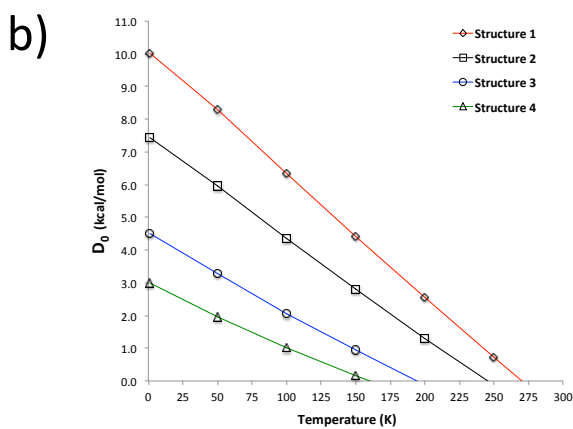
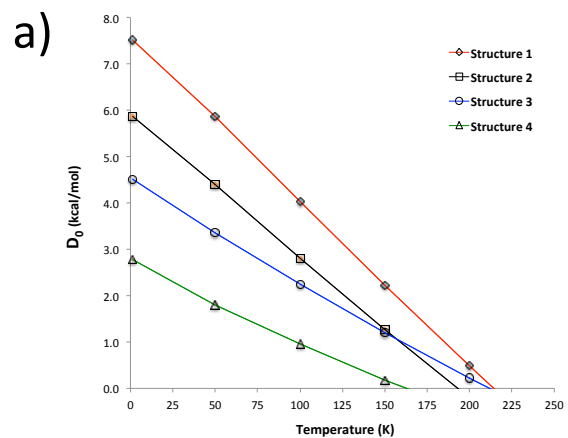


Figure C-4.2 Thermal effects on the dissociation energies for a) ferrocene dimers b) ruthenocene dimers, and c) osmocene dimers. All energy differences are computed at the PBE-D2/def2-TZVP level.

Table C-4.1. Value of integrals within NCI domain for ferrocene. Volumes in a.u. and charges (q) in lel. NCI images are provided as a guide to the eye.

	V_{NCI}	q_{NCI}
Parallel		
FeCp ₂	87.47	1.78
RuCp ₂	121.80	3.20
OsCp ₂	192.17	8.31
Orthogonal		
FeCp ₂	104.03	1.90
RuCp ₂	142.08	3.29
OsCp ₂	258.31	9.07

NCI computational data: Cubic grids with 0.1 a.u. increments. Cutoffs $\rho=0.2$ a.u., $s=2.0$



Chapter 5

Microsolvation of HCl

Introduction

The dissociation of HCl has been the focus of recent studies in ambient bulk water,^{51-52, 82, 90} as well as at low temperatures in confined geometries such as on amorphous ice surfaces, on ice nanocrystals, and in microsolvation environments, which are relevant to atmospheric or interstellar problems.^{87, 267-269} Very recently, after measuring the dipole moments of DCI-doped water clusters by the beam deflection method, Guggemos *et al.*⁷³ observed that “*the addition of a DCI molecule to a water cluster results in a strongly enhanced susceptibility. There is evidence for a noticeable rise in the dipole moment occurring at $n \approx 5-6$. This size is consistent with predictions for the onset of ionic dissociation*”. These results exceed by two the number of water molecules required to dissociate HCl reported in earlier experimental and theoretical works.^{76, 78} For instance, Gutberlet *et al.* reported the experimental observation of a nanoscopic aqueous droplet of acid formed within a superfluid helium cluster at 0.37 K. By using high-resolution mass-selective infrared laser spectroscopy, these authors found that successive aggregation of HCl with water molecules, $\text{HCl}(\text{H}_2\text{O})_n$, readily results in the formation of hydronium at $n = 4$.⁷⁴ The literature related to the dissociation of acids in aqueous environments and the microsolvation of the resulting anions and protons is extensive.^{65-66, 71, 73, 77, 80, 84, 90, 92, 94-95, 97, 100, 109, 160-161, 270-276}

In 2011, Leopold published a comprehensive review about this topic,⁷ in which Table 1 collected experimental and theoretical evidence about the number of water molecules needed to dissociate some simple acids, suggesting four water molecules for the case of HCl. A note accompanying Table 1 explicitly calls for the reader to “*note excellent agreement with the experimental work*”, making reference to papers by the groups of Maillard⁸⁰ and Suhm,^{71, 79} who used several IR spectroscopy techniques to draw their conclusions. As a generalization, Leopold summarized the results found in the literature in the following way: “*the overall picture is that*

*for acids that ultimately ionize in aqueous solution, three to five water molecules typically are needed to induce ionization in the lowest-energy isomer of a given cluster. This range is entirely consistent with available experimental evidence”.*⁷

Computations on interactions of water with HCl, dissociated or not, have been performed through intuitive construction of initial guesses for cluster structures with the aim of identifying the structural preferences for all possible combinations of interacting species that could be found in HCl/water mixtures.^{66, 92, 97, 144} In view of the preceding discussion, in this chapter the microsolvation process of HCl is examined, and specifically, to clarify why the number of water molecules needed to achieve dissociation may vary depending on the experimental technique employed.

Computational details

As the previous chapters, GLOMOS^{140, 173-174, 176} was employed to generate starting structures, establishing a hierarchical screening at the PBE0²¹⁵/D95V level, and the B2PLYPD3 dispersion-corrected double-hybrid functional^{184, 277} in conjunction with the def2-TZVP²¹⁸ basis set. Therefore, the geometrical and energetic discussion is based on the B2PLYPD3/def2-TZVP results. Each structure is characterized as a true minimum by harmonic vibrational frequency analysis. All computations are performed using the very-tight integral accuracy and ultrafine grid options available in the *Gaussian 09* (revision D.01) package.¹⁷⁵

To validate the methodology, the structures of the HCl-H₂O and HCl(H₂O)₂ clusters (one and seven local minima, respectively) were optimized and characterized at the CCSD(T)/def2-

TZVP level of theory, obtaining very similar structures and relative energies to those found at the B2PLYPD3 level, supporting the use of this approach.

Results and discussions

Structures and energetics

We uncovered minima on the PESs for the interactions of HCl with up to six water molecules of previously unnoticed complexity and structural diversity. A total of 431 different local minima were located, distributed as 1, 7, 22, 82, 148, and 171 isomers for $n=1, 2, 3, 4, 5,$ and $6,$ respectively (n is the number of water molecules). Despite the staggering number of structures found here, the PESs in question cannot be considered fully characterized; this is not an attainable goal with currently available experimental or computational methods because the number of possible local minima increases exponentially with the size of the system. Nonetheless, we are confident that our searches capture the most important structural features of the $\text{HCl}(\text{H}_2\text{O})_n$ clusters.

We found structures containing nondissociated, partially dissociated, and fully dissociated HCl. A wide variety of interactions stabilizing the clusters are at play: water–water and HCl–water hydrogen bonds (HBs) with the possibility of HCl acting as donor and as acceptor of one or two HBs, long-range $\text{Cl}\cdots\text{H}$ interactions, and microsolvation of the H_3O^+ cation in the form of Eigen cations (each proton interacting with a lone pair from a vicinal water molecule), and what we refer to as quasi–Eigen cations, in which Cl^- takes over the stabilizing role of one of the water molecules (in well-defined Eigen cations,^{7, 66} the H_3O^+ moiety is not in direct contact with the Cl^- anion). No Zundel ($\text{H}_2\text{O}\cdots\text{H}\cdots\text{OH}_2$)⁺ cations were located. However,

as in the case of the Eigen cations, a number of partially dissociated structures, in which the stabilizing role of the second water molecule is assumed by Cl^- , were identified ($\text{Cl}^- \cdots \text{H}^+ \cdots \text{OH}_2$). Figure 5.1A shows the global minimum structures of the $\text{HCl}(\text{H}_2\text{O})_n$ ($n=1-6$) clusters optimized using the B2PLYPD3 approach considering the zero-point energy (ZPE) corrections. In our nomenclature, $\text{HCl-}nx\text{-}y$, x indicates the number of water molecules, and y denotes the energetic relative ordering position with respect to the lowest free energy structures. The most noteworthy structural variation up to $n=3$ involves the key $\text{O} \cdots \text{H}$ interaction contracting rapidly (from 1.863 to 1.569 Å) until a hydrogen atom is transferred completely to form a hydronium ion for $n=4$ (structure $\text{HCl-}n4\text{-}36$). So, the overall picture provided by these computations is that for HCl, four water molecules are needed to induce full dissociation.

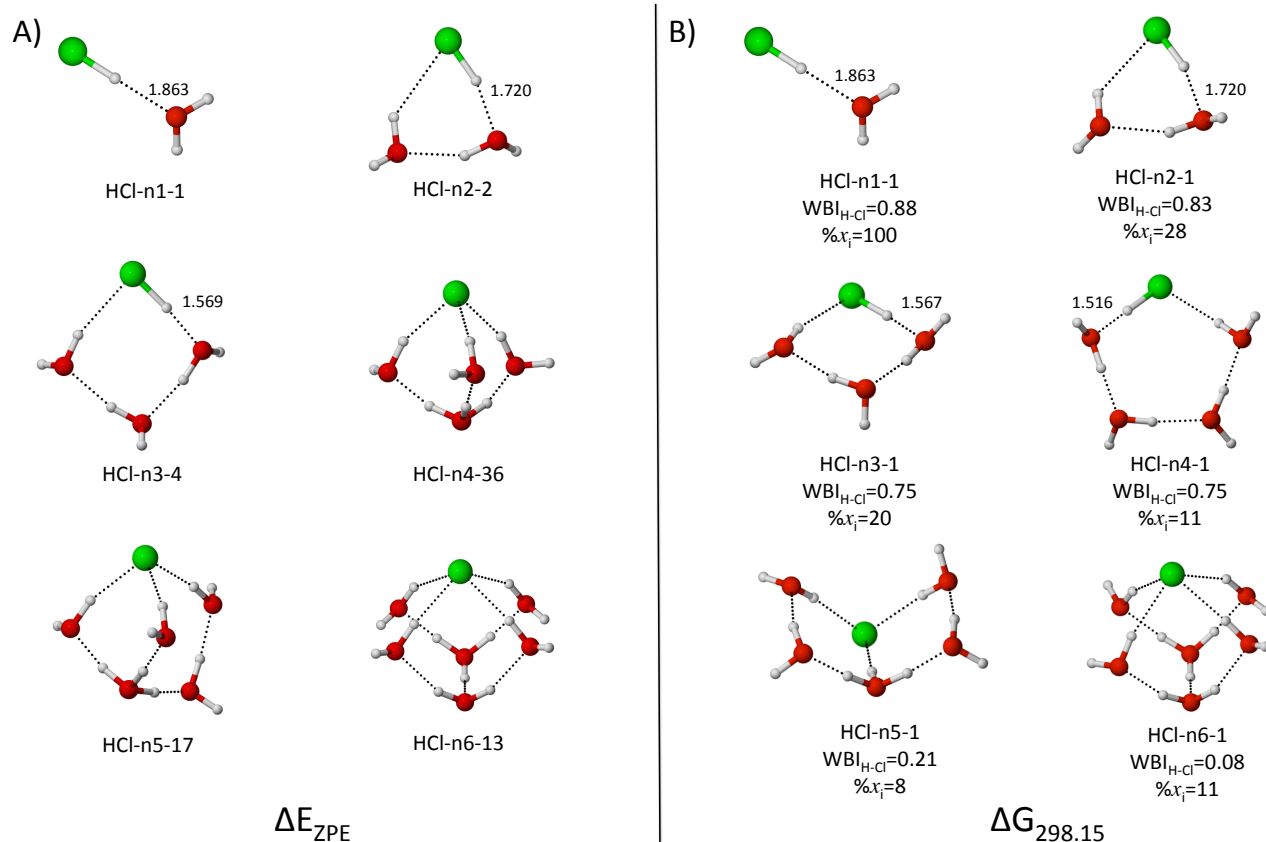


Figure 5.1 A) Lowest energy structures (ΔE_{ZPE}) and B) lowest free energy structures at 298.15 K and 1 atm ($\Delta G_{298.15}$) for $HCl(H_2O)_n$, $n=1-6$. Wiberg Bond Indices for the $H\cdots Cl$ interactions (WBI_{H-Cl}) are also shown. Isomer populations ($\%x_i$) were estimated from standard Boltzmann distributions using the Gibbs free energies (298 K, 1 atm). $ClH\cdots O$ distances in Å. Data taken from the B2PLYPD3/def2-TZVP optimized geometries.

Interestingly, our computations show that acid dissociation depends on the inclusion of the entropic factors. Figure 5.1 also collects the lowest free energy forms at 298.15 K and 1 atm. A comparison between the lowest energy and the lowest free energy structures reveals small structural differences for $n=2$ and $n=3$, in that the hydrogen atoms of the water molecules point in different directions. Strictly speaking, the structures are different, but the motif is the same.

The first notable change is perceived for $n=4$. At room temperature, the most stable structure is an associated pentameric form with an O \cdots H interaction distance of 1.516 Å (structure HCl- $n4$ -1). The dissociation is complete for the $n=5$ case (structure HCl- $n5$ -1), which is structurally closely related to the global minimum in the water pentamer.¹⁴⁹ It is clear that entropy factors are important for explaining the size evolution of these clusters.

Thus, temperature is a key variable in determining the equilibrium structure of a hydrated molecule. For $n=4$, isomer populations estimated through Boltzmann distributions suggest that at 298.15 K and 1 atm, the lowest energy form contributes only approximately 0.14% ($\Delta G = 2.6$ kcal mol⁻¹), whereas the lowest ΔG structure (see Figure 5.1B) contributes around 11%. There is no ambiguity about the fully dissociated character of the global minima and for $n= 5, 6$: the lowest ΔG structure for $n=5$ is a quasi-Eigen cation (structure HCl- $n5$ -1), and the structure for $n= 6$ contains an Eigen cation structure (HCl- $n6$ -1). The presence of Eigen and quasi-Eigen cations and the absence of Zundel cations are remarkable because it is known that Eigen cations are the dominant forms present in bulk samples of aqueous solutions of dissociated acids. In summary, dissociation of HCl occurs with four water molecules without correction for entropic effects and ZPE, as reported by Maillard⁸⁰ and Suhm,^{71, 79} but occurs with five water molecules when if such effects are included.

Guggemos *et al.*⁷³ reported the addition of a DCl (not HCl) molecule to a water cluster. In principle, this substitution could affect the energetics. Table 5.1 summarizes the free energy differences obtained for the $n= 2$ case upon substitution of the HCl unit by DCl. It is apparent that the substitution of HCl by DCl does not alter the relative energies.

Table 5.1 Comparison of free relative energies obtained with HCl and DCl for $n=2$.

Isomer	ΔG^{HCl}	ΔG^{DCl}
	[kcal mol ⁻¹]	[kcal mol ⁻¹]
1	0.00	0.00
2	0.00	0.00
3	0.16	0.14
4	0.16	0.14
5	4.35	4.10
6	5.07	5.04
7	5.07	5.04

Bonding analysis

Figure 5.2 shows the Stern-Limbach plot for HCl-water clusters.²⁰³ Cases as the lowest free energy form for $n=6$ are not included in this correlation. Reminding, for linear hydrogen bonds, q_1 , defined as $(r_1 - r_2)/2$, is the distance from the hydrogen atom to the center of the hydrogen bond, and q_2 is the distance between the Cl and O atoms (r_1 and r_2 are the Cl-H and O-H distances, respectively). High negative (positive) values of q_1 correspond to hydrogen atoms that are clearly attached to chlorine (oxygen) atom, $q_1 \approx 0$ indicates partially transferred protons, as the hydrogen atoms are equidistant from Cl and O. As in other proton transfer cases,²⁰⁴ a quadratic correlation is obtained regardless of the number of water molecules present. Figure 5.2 provides solid evidence for proton transfer beyond subjective visual inspection of the structures.

Clearly, the lowest free energy structures for $n \leq 4$ are into the attached region and complete transfer is evident for $n=5$.

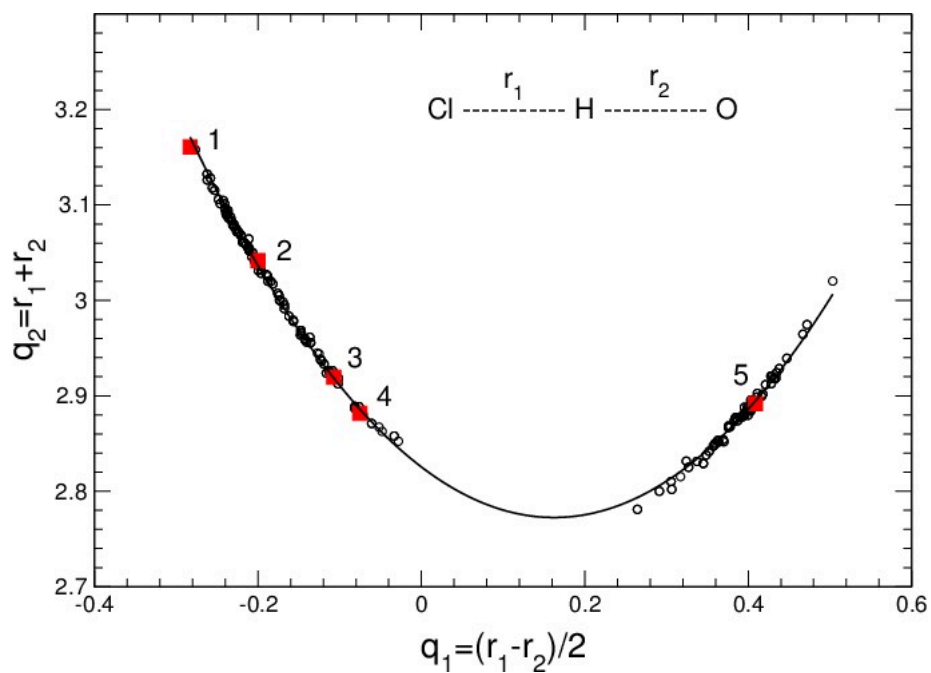


Figure 5.2 Correlation between q_2 and q_1 . The squares indicate the positions of the lowest free energy structures for each molecularity. q_2 and q_1 are in Å. Data taken from the B2PLYPD3/def2-TZVP optimized geometries.

Further evidence about the state of HCl dissociation in gas phase water clusters is provided in Figure 5.3; here, we analyze the Wiberg bond indices for the H–Cl interactions (as a reference, the computed bond index for isolated H–Cl is 0.94) for the same clusters as selected for Figure 2. Three distinct areas can be discerned. The undissociated region covers the [0.8-0.9] interval. There are two intervals of partial proton transfer: [0.65-0.75], corresponding to early to intermediate stages of the transfer process, and [0.25-0.45], corresponding to intermediate to late stages of proton transfer. Finally, the [0.1-0.2] interval encloses structures that all exhibit fully transferred protons. Figure 5.3 provides clear-cut evidence for proton transfer, which is consistent with the results discussed previously in Figure 5.2.

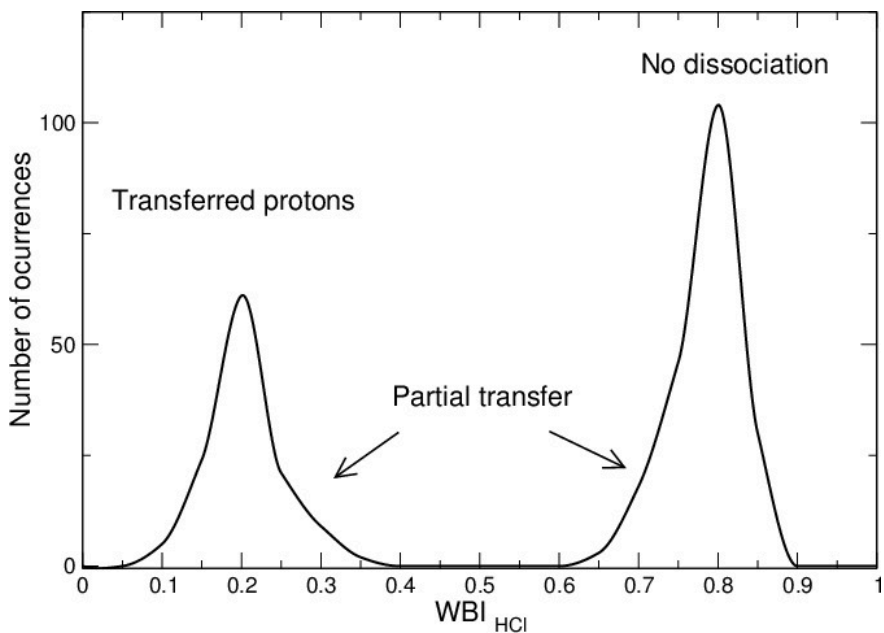


Figure 5.3 Wiberg bond indices (WBI) for the H–Cl interaction in clusters reported in this work. Partially transferred protons appear on two categories: the right peak shows those in the early stages of H–Cl dissociation, and the left peak comprises structures for advanced HCl dissociation. Data taken from the B2PLYPD3/def2-TZVP optimized geometries.

Dipole moment

Dipole moment is an observable, which contributes information about the microscopic structure of nanoscale solvation because is directly related to the charge distribution within a system. A strong shift in the magnitude of dipole moment in a doped water cluster can be due to one or both of the following mechanisms: either a significant increase in the separation between H^+ and X^- (i.e., dissociation of the molecule) and/or a strong shift in the rovibrational electric polarizability of the water cluster itself (i.e., a change in how effectively the water network screens the impurity).⁷³

Guggemos and coworkers⁷³ wrote “*we point out that the dynamically averaged dipole moment within a finite highly fluxional system can be qualitatively different from that computed for a static minimum–energy framework*”. We complement this statement by adding that the differences may also be quantitative. This issue is further complicated, because chemical and physical processes are not exclusive domains of the lowest energy structures in a given PES, and as mentioned above, many more structures may still be missing because no exploration of complex energy landscapes should be considered complete. This is particularly applicable to our case because of the large number of structural possibilities arising from the relative positions of hydrogen atoms not involved in the stabilizing hydrogen-bonding networks, which change the individual dipole moments significantly. Additionally, it is clear that the entropic effects play a key role in determining the equilibrium structure of the title clusters.

Using our calculated structures, we attempted to reproduce the dipole moment distributions reported by Guggemos *et al.*⁷³ Following the postulates of quantum mechanics, we computed the expected dipole, $\langle \mu_n \rangle$, as the average over dipole moments of all individual

structures in the given PES, μ_{in} , weighted by x_{in} , the estimated isomer populations on that surface obtained from standard Boltzmann distributions of the Gibbs free energies. The results at 298.15 K are plotted in Figure 5.4. Experimental points were taken directly from the work by Guggemos *et al.*⁷³

There is a perfect match between the expected dipole moment and the experimental value (Figure 5.4) only for $n=3$. For $n=4$ and 5 , there is no clear correlation between the two quantities. On the contrary, for $n=6$, the computed value for the dissociated forms is very close to that reported by Guggemos *et al.*

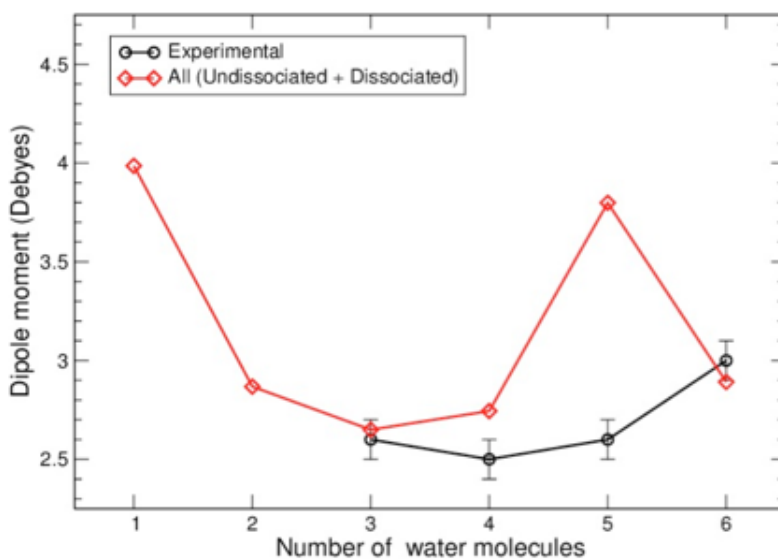


Figure 5.4 Expected dipole moments estimated from standard Boltzmann distributions of the Gibbs free energies at 298.15 K and 1 atm for the $\text{HCl}(\text{H}_2\text{O})_n$ clusters.

The $n=5$ case is interesting. Besides our stochastically located structures, we took the lowest ΔG isomer shown in Figure 5.1 and optimized the molecular geometries for all possible combinations of the “above” and “under” relative positions of the four peripheral protons (16 combinations in total). The resulting structures were energetically very close to the lowest ΔG isomer, with ΔG values no higher than $0.43 \text{ kcal mol}^{-1}$ relative to the reference structure. Without these additional structures, isomers had populations with higher values, with other geometries having smaller significance. Inclusion of the new structures complicates the population picture with 11 isomers now having contributions in the 3–6 % range. Individual dipole moments are also more susceptible to changes in the orientation of peripheral protons: amongst the new structures, expected dipole moments cover the 2.46–5.09 D range, (compared with 3.39 D for the reference structure). However, the expected averaged dipole moment only changed from 3.77 to 3.80 D. These results illustrate clearly the preceding discussion regarding contributions from individual structures to the properties of complex energy landscapes, and at the same time provide solid support for our approach to calculating expected properties as statistical averages weighted by isomer populations derived from Boltzmann distributions.

What about the temperature effect on the dipole moment distribution? Clearly, the isomer populations will change as a result of a temperature variation, and this could affect the expected dipole moment. In this sense, it has been shown that the number of water molecules needed to dissociate NaCl, for example, is sensitive to temperature.²⁷⁸ It is apparent from Figure 5.5 that changes in temperature induce very strong changes in the dipole moments. At very low temperatures, the variation is almost negligible (except for $n=6$).

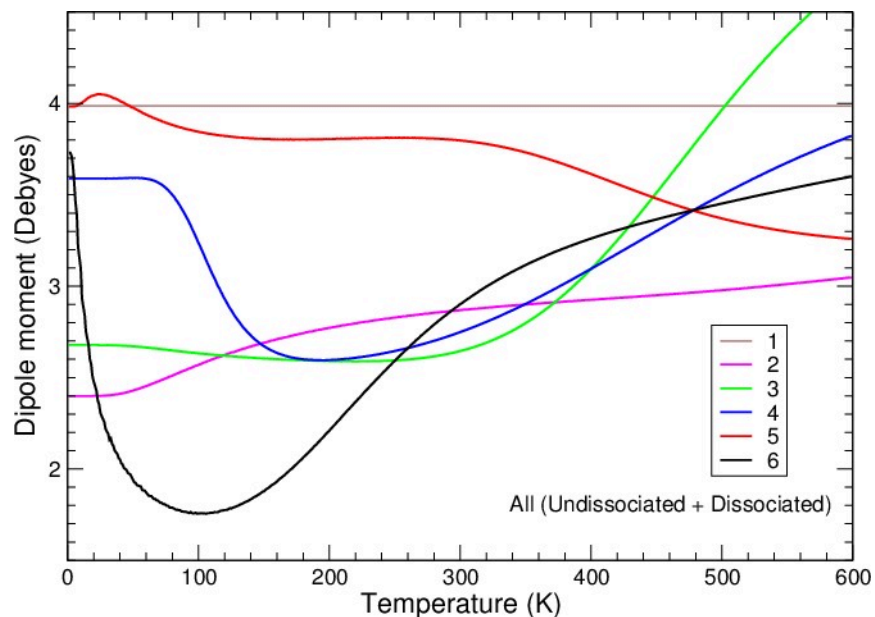


Figure 5.5 Variation in the expected dipole moments as a function of temperature for the $\text{HCl}(\text{H}_2\text{O})_n$ clusters. The expected dipoles moments are estimated from standard Boltzmann distributions of the Gibbs free energies at 1 atm.

Therefore, if the temperature is not controlled during the experiment, the values obtained for the dipole moments are susceptible to change, providing a different picture of the number of water molecules needed for HCl dissociation in water. The main reason is that at high temperatures, the number of hydrogen bonds decreases and less compact clusters are obtained. In other words, we recover the ideal gas behavior (no intermolecular interactions, thus no cluster formation) at high temperatures. Discrepancy between the experimental and calculated dipole moments can be explained by fluctuation effects and temperature. Quantum chemistry approaches based on normal modes analysis of optimized equilibrium structures are limited if species become unstable.⁹⁸

Conclusions

On the basis of electronic energies, the number of water molecules needed for HCl dissociation is four as reported by the groups of Maillard,⁸⁰ Suhm,^{71, 79} and others. However, based on Gibbs free energies, this number is 5. For $n=4$, the lowest ΔG structure is also partially dissociated. The nondissociated, partially dissociated and fully dissociated character of the H–Cl bond can be characterized unambiguously by Wiberg bond indices, and supported by quadratic correlations between the distance between Cl and O atoms and the distance from the proton to the center of the corresponding Cl \cdots H \cdots O interaction. Very narrow energy windows for the partially and fully dissociated structures in the corresponding PES preclude the assignment of macroscopic experimental observables to individual cluster structures. Although our search is comprehensive and exhaustive, it is by no means complete because of the large number of structural possibilities arising from the relative positions of peripheral hydrogen atoms in the clusters. Paraphrasing Guggemos *et al.*, we point out that *the dynamically averaged dipole moment within a finite highly fluxional system can be qualitatively and quantitatively different from that computed for a static minimum–energy framework.* Our computations show that if temperature is not controlled during the experiment, the values obtained for the dipole moment (or for any measurable property) are susceptible to change, providing a different picture of the number of water molecules needed for the HCl dissociation in water.

This work has been cited by several research groups, for example in studies on dissociation of HCl and HBr, and microsolvation of oxalic or benzoic acids.²⁷⁹⁻²⁸⁵

Chapter 6

Microsolvation of hydrogen halides HX

(X=F, Cl, Br, and I)

Introduction

The importance of acids in nature is undeniable. They take part in many physicochemical and biochemical processes and have a key role in the pH-balances.^{53, 286-291} In the aqueous phase, acidic strength is dictated by the pKa of the species in question. The hydrogen halide series covers a spectrum from the weak to the very strong acidity, as it is clear from Table 6.1. Moreover, the involved processes, such as proton transfer, acid dissociation, and the interactions that stabilize HX-water complexes, epitomizes some central questions in chemistry. The nature of the interactions escapes descriptions in simple terms, rather it is necessary to invoke a complex mixture of electrostatic, covalent, induction, and dispersion contributions, varying in relative weights. On the whole, all hydrogen bonds can be considered as incipient proton transfer reactions, and for strong hydrogen bonds, this reaction is in a very advanced state.^{163, 292}

Table 6.1. Acidic power and properties of the H-X bond in the hydrogen halide series. pKas for dissociation in aqueous environments, bond lengths in Å, and dipole moments in Debyes.^{103, 293-}

294

Property	HF	HCl	HBr	HI
pKa	3.2	-7.0	-9.5	-10.0
Bond lengths	0.92	1.27	1.41	1.60
Dipole moment	1.8	1.1	0.8	0.4

An approach to obtain a solid knowledge of the acid dissociation mechanism involves the analysis of the potential energy surface (PES) of clusters formed by the acid and a certain number of water molecules. The key question is: how many water molecules are needed to

dissociate an acid? As was previously mentioned, the review of Leopold⁷ published in 2011 provided a comprehensive summary of the number of water molecules required to dissociate some simple acids. Hydrogen halides are first in Leopold's list. These acids are excellent prototypes for a systematic study of dissociation in aqueous solution, in principle because of their "simplicity".²⁹³

It is well known that hydrogen fluoride is the weakest one of this set of acids (HAt is not considered here).^{83, 91, 295} Re¹⁰¹ reported that while the most stable arrangements of the HF(H₂O)_n clusters for n=2-4 are monocyclic non-proton-transferred structures, bicyclic forms are favored for clusters up to n=7. The author attributed the stability of the non-proton-transferred clusters to the strong H-F bond as well as the high ability of F to form hydrogen bonds. Odde *et al.*⁹⁶ extended this study up to n=10 and concluded that "the undissociated structures are found to be more stable than the dissociated structures until n=10...it is likely that HF would not be dissociated at 0 K because the HF···H bond is stronger than the HO···H bond, while the dissociation would occur probabilistically according to the Boltzmann distribution at finite temperatures". The relative energies and vibrational spectra of these HF-water clusters could be affected by the basis set selection. In fact, small basis sets favor hydrofluoric acid dissociation.¹¹⁰ Another reason for the relative weakness of HF towards dissociation may be inferred from the recent work of Florez and coworkers,⁹ where it was shown that the effective charge in F⁻ is so strong that it induces partial dissociation of surrounding water molecules to recover the HF character.

Microsolvation of HCl has also been extensively studied.^{66, 80, 84, 87, 92-93, 97, 100, 107-109} Let us only stated some of the most recent results. On the experimental side, Guggemos *et al.*⁷³ measured the dipole moments of DCl-H₂O clusters by the beam deflection method and observed

a noteworthy rise in the dipole moment occurring at $n=5-6$. In a subsequent work,¹⁰⁷ we explored the potential energy surfaces of the $\text{HCl}(\text{H}_2\text{O})_n$ clusters. We found that based on ZPE-corrected electronic energies, the number of water molecules needed for HCl dissociation is four, but at room temperature and including the entropic factors, this number is five. Given that the acid dissociation processes show significant quantum and thermal fluctuations, which may shift equilibria, several studies using *ab initio* molecular dynamics have been also performed.^{98, 105, 108-}
¹⁰⁹ The group of Marx⁹⁸ reported large-scale *ab initio* path integral simulations to include the nuclear quantum effects at finite temperatures for studying the HCl dissociation in water. Particularly, they computed the dipole moments to try to find a possible correlation between this observable and the dissociation process. However, the authors concluded that the impact of quantum fluctuations is determinant because the quantum averages deviate strongly the dipole moments from equilibrium.

The heavier analogs have been less studied.^{56, 62, 75, 84-85, 88, 97} In 2002, Hurley *et al.*⁵⁶ found that the onset of spontaneous ionic dissociation of HBr occurs with five water molecules. Only a couple of studies^{84, 97} included HI in their dissociation studies of hydrogen halides. Odde and co-workers⁹⁷ concluded that the dissociated structures of both HBr and HI can be realized for $n \geq 3$. Cabaleiro-Lago *et al.*⁸⁴ also concluded that the HI dissociation occurs for $n > 2$.

In this chapter, the water induced dissociation of the series of hydrogen halides was studied following the same systematic exploration as in HCl-water clusters. Questions as are there periodic trends? or what are the most stable structures? can be answered if we systematically explore the PES for the whole group. As additional water molecules are successively incorporated, the X-H distance in the acid increases gradually up to a given cluster size where fully dissociated forms were found.⁷

Computational details

In order to systematically explore the potential energy surfaces of the $\text{HX}(\text{H}_2\text{O})_n$ clusters, we used a modified kick algorithm implemented in GLOMOS.^{140, 173, 176} So, a hierarchical screening was established: obtaining cluster geometries at the PBE0²¹⁵/D95V level and refine the resulting structures using the B2PLYPD3 dispersion corrected double-hybrid functional^{116, 184} in conjunction with the def2-TZVP basis set.²¹⁸ Each structure was characterized as a true minimum by harmonic vibrational frequency analysis. All computations were done using the *Gaussian 09* (revision D.01) package.¹⁷⁵ Properties for such populations of structures were calculated, including average dipole moments, an analysis of bonding based on Wiberg Index, and $\text{O}\cdots\text{HX}$ and H-X distances collected in Stern-Limbach plots.²⁰³⁻²⁰⁴

Results and discussions

Energetics and Structures

Given the complexity and structural diversity, we thoroughly explored the PESs of the $\text{HX}(\text{H}_2\text{O})$ clusters up to 6 water molecules, except for HF where the search was extended up to $n=7$. We located a total of 3778 different minima (including enantiomers) in a range of 22 kcal mol⁻¹ from the corresponding global minima (see Table 6.2), with a staggering variety of structural options of non-, partially-, and fully-dissociated H-X moieties (see clusters in Appendix D). Of course, these PESs cannot be considered fully characterized; this is not an attainable goal with currently available experimental or computational methods because as discussed above, the number of

local minima increases exponentially with the size of the systems. Nonetheless, we are confident that our search captures the most important structural features of the $\text{HX}(\text{H}_2\text{O})_n$ clusters.

Table 6.2. Number of structures and energy ranges (in kcal mol^{-1}) of $\text{HX}(\text{H}_2\text{O})_n$ clusters. Ranges of ΔE_{ZPE} and ΔG (298.15 K and 1 atm) inside parenthesis and brackets, respectively.

Water molecules	HF	HCl	HBr	HI
n=1	1	1	2 (0 - 2.7) [0 - 2.1]	2 (0 - 0.8) [0 - 0.7]
n=2	4 (0 - 0.3) [0 - 0.2]	7 (0 - 7.3) [0 - 5.1]	7 (0 - 4.2) [0 - 4.0]	7 (0 - 1.6) [0 - 1.4]
n=3	19 (0 - 7.3) [0 - 5.1]	22 (0 - 13.2) [0 - 10.3]	32 (0 - 8.6) [0 - 9.1]	28 (0 - 5.9) [0 - 4.9]
n=4	70 (0 - 9.7) [0 - 8.0]	82 (0 - 12.6) [0 - 9.5]	91 (0 - 14.7) [0 - 14.5]	77 (0 - 12.9) [0 - 11.0]
n=5	327 (0 - 14.1) [0 - 12.8]	148 (0 - 11.8) [0 - 10.0]	232 (0 - 20.7) [0 - 17.4]	263 (0 - 15.9) [0 - 14.9]
n=6	622 (0 - 12.7) [0 - 10.4]	171 (0 - 14.5) [0 - 11.1]	359 (0 - 21.9) [0 - 21.2]	502 (0 - 21.6) [0 - 20.6]
n=7	702 (0 - 15.2) [0 - 12.9]			
Total	1745	431	723	879

Figure 6.1 shows the lowest free energy structures at room conditions for the $\text{HX}(\text{H}_2\text{O})_n$ ($n=1-7$) clusters. It is apparent that diverse interactions stabilize the clusters: traditional and charge assisted water to water and acid to water hydrogen bonds (HBs), microsolvation of the H_3O^+ cation mostly in the form of Eigen cations as well as a reduced number of quasi-Eigen structures, finally, there are also ionic and long-range $\text{X}\cdots\text{H}$ interactions. Interestingly, a few quasi Zundel structures are found where one proton is equally shared ($\text{X}\cdots\text{H}\cdots\text{O}$) as shown by the bond indices.

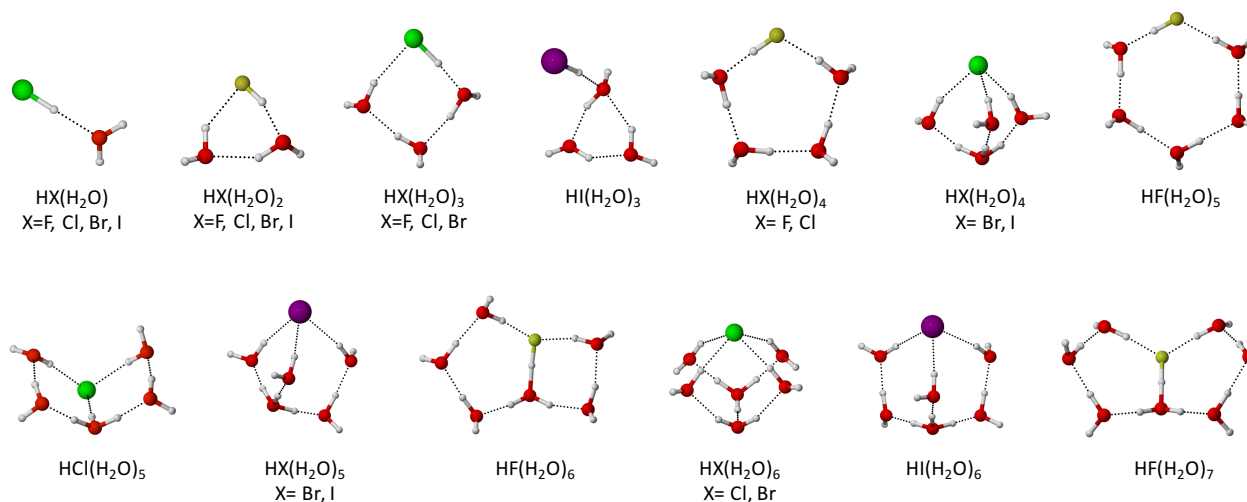


Figure 6.1 The B2PLYPD3/def2-TVZP lowest free energy structures (298.15 K and 1 atm) for the $\text{HX}(\text{H}_2\text{O})_n$, $n=1-7$ clusters.

Interestingly, our computations show that only for the smallest cases ($n = 1,2$), the lowest Gibbs free energy structures coincide with the energy global minimum (Figure 6.1 and Appendix D), independently of the identity of the halogen, therefore, not accounting for entropy and

temperature leads to wrong conclusions regarding acid dissociation as inferred from energetic preferences of the larger clusters. As a rule, besides temperature and entropy, the identity of the halogen determines not only structural preferences but also the number of water molecules needed to induce dissociation. We now discuss structural preferences on a case by case basis.

HF(H₂O)_n. A number of structures are in advanced stages of the proton transfer process, with full dissociation taking place in very few high-energy cases and only for the high molecularities. Interestingly, for this (and only for this!), the weakest acid in the group, a smooth transition from the undissociated to the dissociated forms is observed as the number of water molecules increases (see Figures 6.1 and Appendix D), thus, by the time 6 or 7 water molecules are present, a quasi-Zundel F \cdots H \cdots O structure, where the proton from HF is equally shared between the F and O atoms (both H \cdots O and F \cdots H interactions sport 0.35 bond indices for n=7), has the lowest free energy (Figure 6.1). Note that cage-like structures (prisms and cubes) are favored when the entropic factor is not considered (Appendix D). This is remarkable because, to the best of our knowledge, in proton dissociation from acids, the general norm is a sharp transition, there are no previous cases of such smooth dissociations as a function of *n* reported in the literature. Only for the larger clusters, where the H-X bond is in an advanced stage of dissociation and the H-O bond is in an advanced stage of formation, the global minima do not coincide with the lowest Gibbs free energy structures. All structures are packed within relatively narrow energy windows (Table 1), going above 10 kcal mol⁻¹ of the corresponding global minimum only for the larger molecularities.

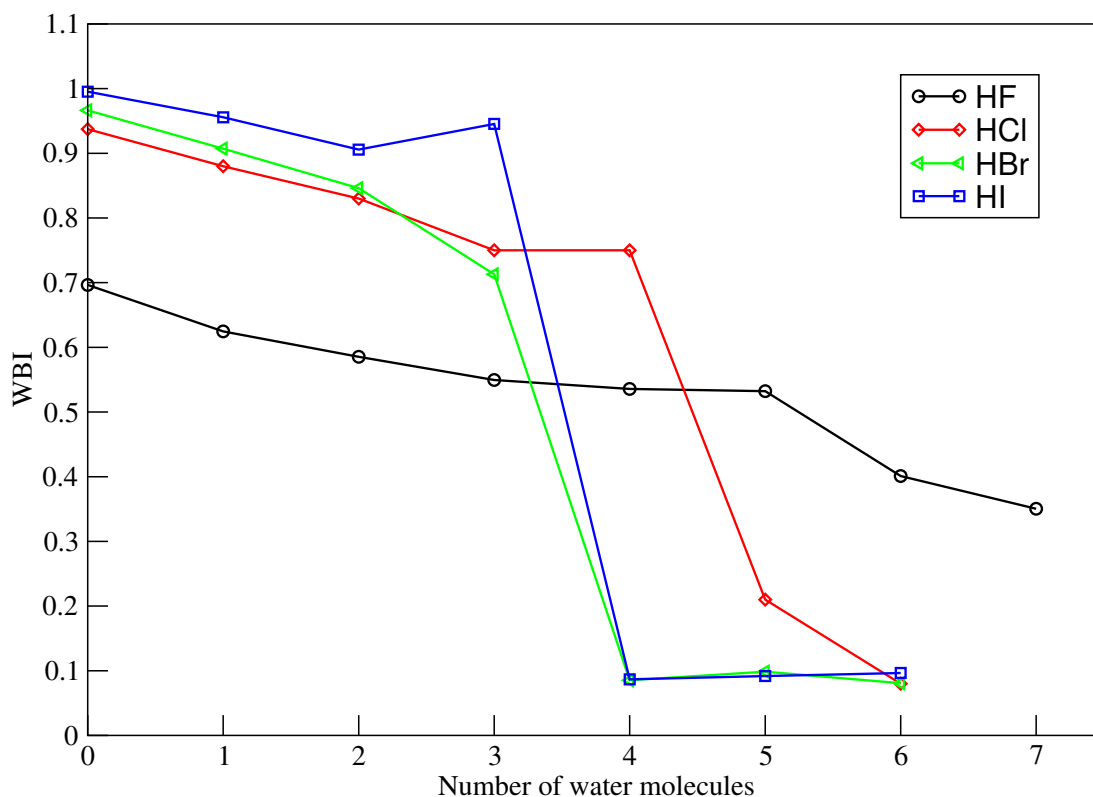


Figure 6.2 Evolution of the H-X Wiberg bond index (WBI) for lowest free energy structures as a function of the number of water molecules. An unexpected smooth decay for HF is seen while for all other acids, a sharp transition is observed.

HCl(H₂O)_n. The results obtained in this work for the dissociation of HCl are consistent with our previous work¹⁰⁷ and are only included here for completeness. The required number of water molecules needed to dissociate HCl on the grounds of ZPE-corrected electronic energies is four. $n=5$ is the corresponding number if temperature and entropy are accounted for in the computations. A multitude of partially dissociated structures are characterized as true minima. Energy ranges for HCl(H₂O)_n clusters are as tight as for the HF case, however, structures below 10 kcal mol⁻¹ are seen for as little as two water molecules (Table 1).

HBr(H₂O)_n and HI(H₂O)_n. For HBr, only minute differences related to the orientations of hydrogen atoms not taking part in the stabilizing HB network are seen between the global minima and the lowest Gibbs free energy structures. Four water molecules are needed to induce dissociation. Wider energy ranges are allowed for the HBr case, with structures lying up to 22 kcal mol⁻¹ above the corresponding global minimum, however, for up to $n=3$, all structures are very close in energy (Table 1).

In the case of HI, full dissociation of HI molecules occurs in the presence of just three water molecules (Appendix D). Interestingly, this structure contains a rare quasi-Zundel cation. Only four molecules are needed for a dissociated structure to become the global minimum considering both ZPE corrected electronic and Gibbs free energies. As in the case of HBr, the structures are very close in energy up to $n=3$, with larger energy windows for larger clusters.

So, in general, our computations indicate that for the hydrogen halides, an accurate description of acid dissociation in the presence of water molecules in the gas phase requires careful consideration of temperature (Appendix D). The influence of temperature is critical in determining structural preferences: on a fundamental level, at high temperatures and low pressures, gaseous mixtures approach the conditions for an ideal gas, thus disfavoring intermolecular interactions and favoring open structures over compact ones to the point that at sufficiently high temperatures, clusters cease to exist. This behavior is very well documented for molecular clusters held together by networks of hydrogen bonds.^{107, 138, 145, 296-297} In the present case, as a general norm, the structures with the lowest Gibbs energies (298.15 K and 1 atm) have little weight on the ZPE-corrected corresponding potential energy surface (Appendix D).

Bonding Analysis

A convenient way to structurally analyze proton transfer is provided by the so-called Stern-Limbach plots,²⁰³ that correlate the distances between the atoms involved in the hydrogen bond ($X\cdots H\cdots O$). For linear hydrogen bonds, two variables are defined (see Figure 6.3 for details): q_1 is related to the symmetry of the interaction, measuring the distance from the proton to the center of the hydrogen bond, while q_2 is connected to the size of the interacting region. Very nice quadratic correlations are obtained for all cases studied in this work.

Besides the generalized quadratic correlation, the plots in Figure 6.3 provide valuable insight on the nature of the dissociation process as a function of the identity of the halogen. For HF, some structures are in advanced stages of the proton transfer process and only a few among them should be considered as fully dissociated: many structures are found in the negative q_1 region, indicating that for those cases the proton is still well attached to F, similarly, a smaller number of structures are found in the positive regions of q_1 , denoting that the proton is closer to the oxygen atom. The smooth transition from undissociated to dissociated structures discussed above is evident from the facts that all regions of q_1 are populated and that there is a considerable amount of structures in the vicinities of $q_1 \approx 0$, indicating that for those cases, the proton is equally shared between F and O. Well defined gaps in q_1 values are seen for all other acids. Interestingly, the second gap in q_1 is clearly visible for HBr and for HI, these gaps separate undissociated structures from partially and fully dissociated structures, thus for the stronger acids, the dissociation process seems to occur as a sharp discontinuity. The second gap (roughly between -0.4 and -1.2 for q_1) is associated with the presence of structures with halogen bonds.

These structures containing halogen bonds are higher in energy than those with typical hydrogen bonds, so their contribution is small.

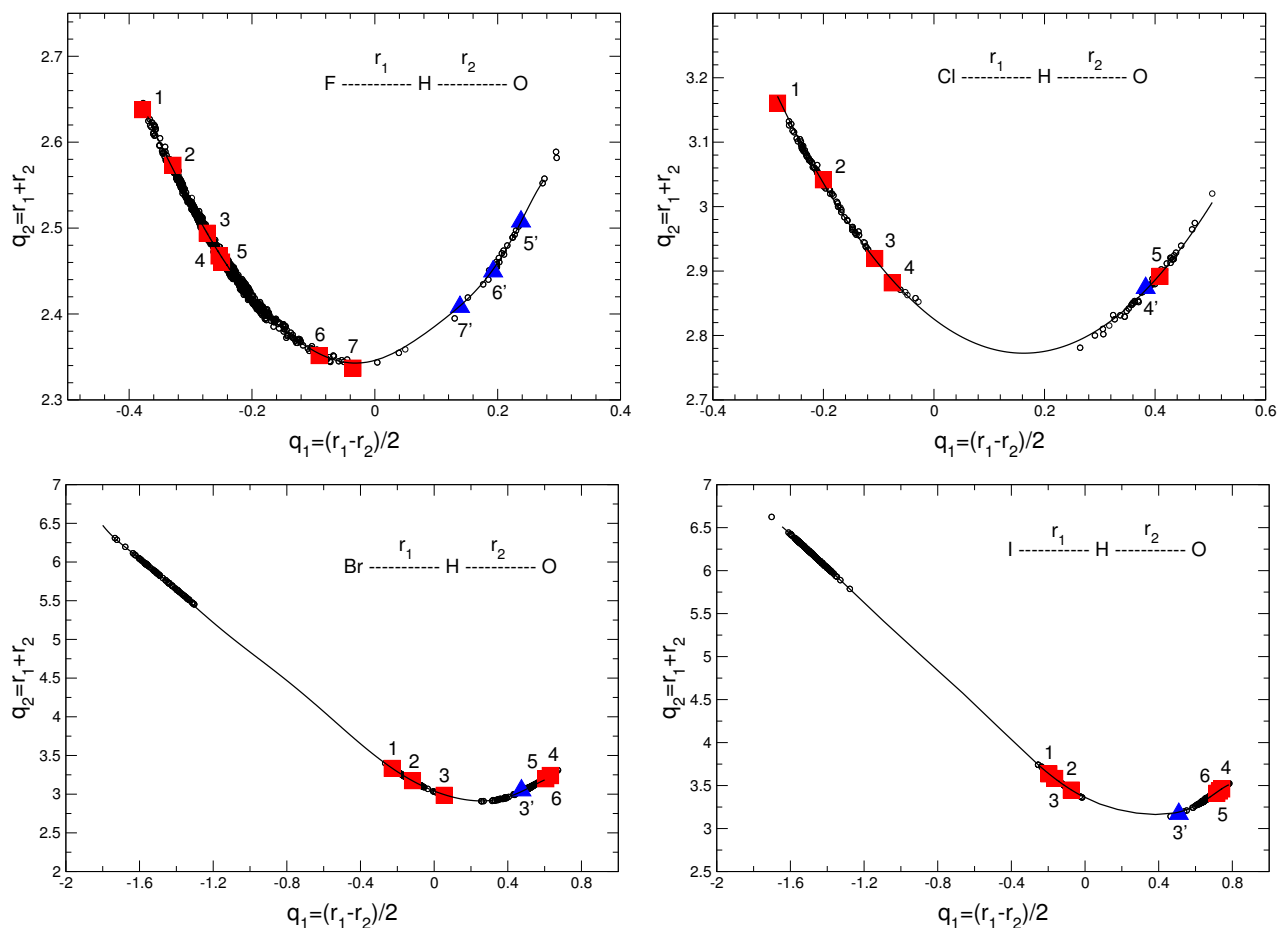


Figure 6.3 Correlation between q_2 and q_1 . Data taken from the B2PLYPD3/def2-TVZP optimized geometries. The square points indicate the position of the lowest free energy structures for each molecularity and the triangle points indicate the position of the first dissociated structure.

Bond orders for the bare acids are 0.69, 0.94, 0.97, and 0.99 for HF, HCl, HBr, and HI, respectively. Figure 6.4 shows a very interesting trend, fully consistent with the information gathered from the Stern-Limbach plots. For HF, a well-defined curve resembling a Gaussian distribution centered at 0.5 is obtained with a couple of small shoulders located at the region of small H-F bond orders, reserved for dissociated structures, thus, further supporting the smooth transition from undissociated to dissociated character. For all other cases, there are evident gaps in the bond orders clearly separating dissociated from undissociated structures with apparent complexity (peak splitting) in both regions. The peaks to the right of 0.5 include non-dissociated structures and structures in early stages of the dissociation process; the peaks to the left indicate structures in the late stages of dissociation and fully dissociated structures. From the molecular structure perspective, the existence of multitude of structures with bonds that are partially formed/broken (bond orders in ranges away from 0 or 1) and that are well characterized minima on the corresponding PES (in some cases, the global minimum) is truly fascinating and imposes new challenges to current views of chemical bonding.

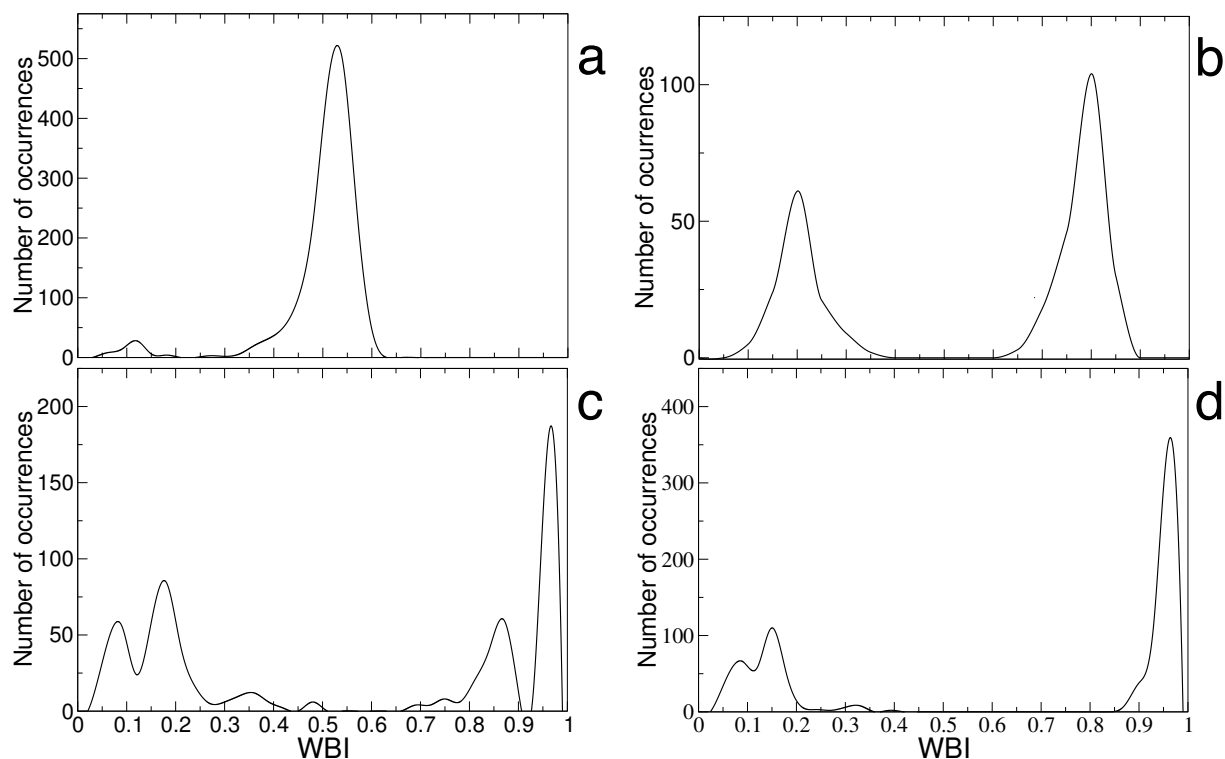


Figure 6.4 Wiberg bond indices (WBI) for the H–X interaction in clusters reported in this work. Data taken from the B2PLYPD3/def2-TVZP optimized geometries. Subfigures a, b, c, and d correspond to HF, HCl, HBr, HI, respectively.

Dipole moment distribution

Guggemos and co-workers⁷³ wrote “*we point out that the dynamically averaged dipole moment within a finite highly fluxional system can be qualitatively different from that computed for a static minimum–energy framework*”. This issue is further complicated since chemical and physical processes are not exclusive domains of the lowest energy structures in each PES, and because as mentioned, many more structures may still be missing because no exploration of

complex energy landscapes should be considered complete. This is particularly applicable to our case due to the large number of structural possibilities arising from the relative positions of hydrogen atoms not involved in the stabilizing hydrogen bonding networks, which significantly change individual dipole moments. Additionally, the entropic effects play a key role in determining the equilibrium structure of the title clusters. In any case, Table 1 lists very narrow energy windows calculated for the collection of dissociated and partially dissociated structures located in this work. Obviously, as n grows, it is increasingly harder and impractical to consider the global minimum or the lowest ΔG structures as the main contributors to the properties of the clusters. Under these circumstances, we computed the dipole moment distributions using the expected dipole, $\langle \mu_n \rangle = \sum_i x_{in} \mu_{in}$ as the average over dipole moments of all individual structures, μ_{in} , weighted by x_{in} , the estimated isomer populations on that surface obtained from standard Boltzmann distributions of the Gibbs free energies. The results at 298.15 K are plotted in Figure 6.5.

In the case of HCl, there is a perfect match between the expected dipole moment and the experimental value just for $n=3$ (see Figure 6.5), but for $n=4$ and 5 , there is no clear correlation between both two quantities. For $n=6$, the computed dipole moment is again very close to that reported by Guggemos *et al.*⁷³ In few words, there is not a correlation between the predicted values and the experimental results because, as is discussed by Marx and co-workers, dipole moments are susceptible to fluctuations effects.^{98, 108-109} Figure 6.5 also summarizes the average dipole moment results of the other $\text{HX}(\text{H}_2\text{O})_n$ clusters. There is not an experimental counterpart for the rest of the acids, but it is evident that there is not a correlation between the number of the water molecules required to dissociate the acid and the drastic changes in the dipole moments as

was suggested for HCl. For instance, in HBr the dipole moment variation is perceived for $n=2$, but the dissociation is complete for $n=4$.

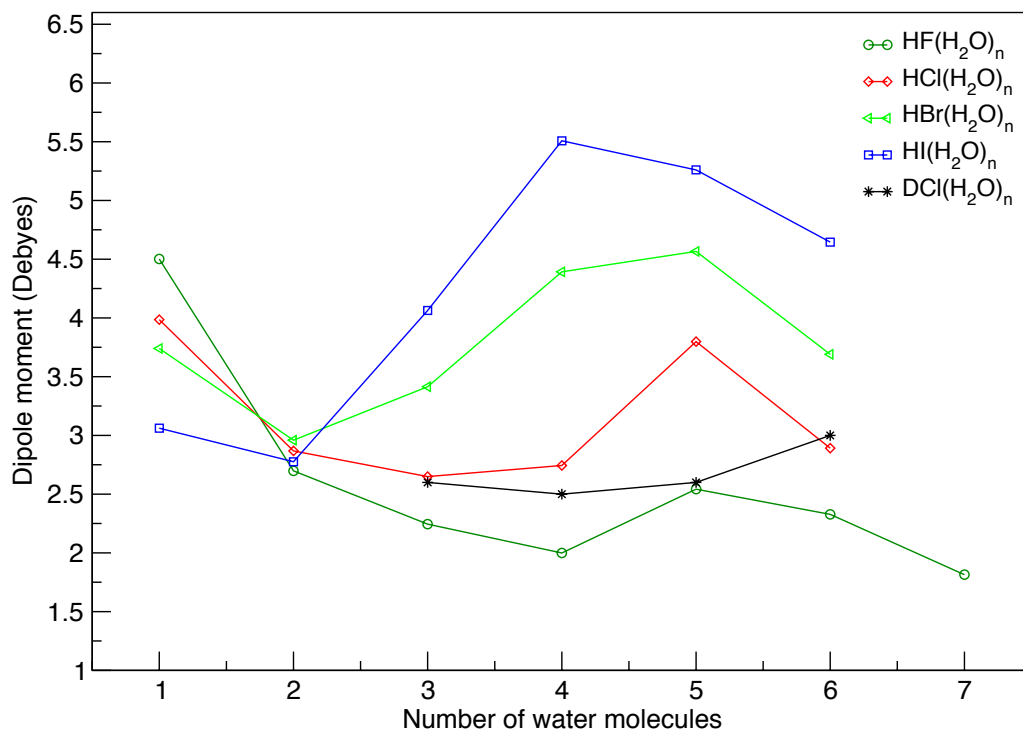


Figure 6.5 Dipole moments for the $HX(H_2O)_n$ clusters. Expected dipole moments for all structures in a given PES. The expected dipole moments are estimated via standard Boltzmann distributions of the Gibbs free energies at 298.15 K, 1 atm. Experimental points for DCI were directly taken from the work by Guggemos *et al.*⁷³

Conclusions

Our results reveal that it is possible to dissociate partially hydrogen fluoride with seven water molecules. Based on electronic energies, HCl is dissociated with four water molecules, but when the entropic factors are considered, five water molecules are required for dissociation. In the cases of HBr and HI acids, dissociation is carried out with four and three water molecules, respectively. This decrease in the number of water molecules is related to the electronegativity values of the halogens ($F > Cl > Br > I$). The non-, partially- and fully-dissociated character of the H-X bond can be characterized unambiguously by Wiberg bond indices and supported by quadratic correlations between the distance between the halogen and O atoms and the distance from the proton to the center of the corresponding $X\cdots H\cdots O$ interaction. The interactions that stabilize the clusters are hydrogen bonds between water molecules and HX-water, $X\cdots H$ long-range interactions, as well as the microsolvation of hydronium ions H_3O^+ (Eigen and quasi Eigen cations).

Appendix D

Microsolvation of hydrogen halides HX

(X=F, Cl, Br, and I)

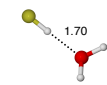
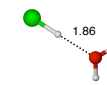
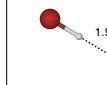
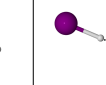
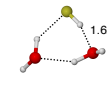
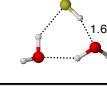
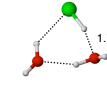
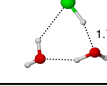
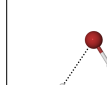

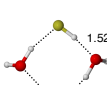
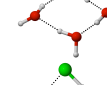
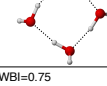
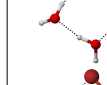
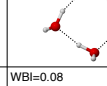

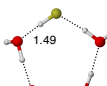
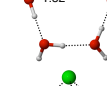
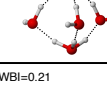
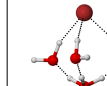
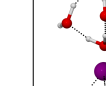

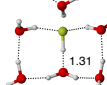
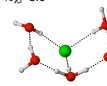
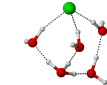
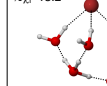
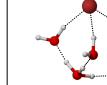
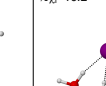
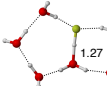
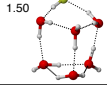
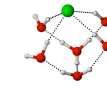
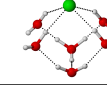
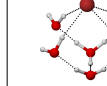
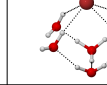
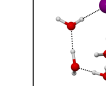
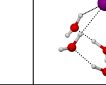
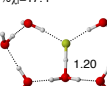
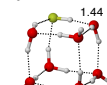
n	HF	HCl	HBr	HI
1	WBI=0.62 % χ_i =100 	WBI=0.88 % χ_i =100 	WBI=0.91 % χ_i =97.2 	WBI=0.96 % χ_i =76.1 
2	WBI=0.58 % χ_i =28.7  	WBI=0.83 % χ_i =28.0  	WBI=0.85 % χ_i =28.5 	WBI=0.91 % χ_i =25.0 
3	WBI=0.55 % χ_i =18.7 	WBI=0.75 % χ_i =20.0  	WBI=0.71 % χ_i =17.5  	WBI=0.94 % χ_i =16.6 
4	WBI=0.54 % χ_i =17.9 	WBI=0.75 % χ_i =11.0  	WBI=0.08 % χ_i =18.2 	WBI=0.09 % χ_i =38.9 
5	WBI=0.53 % χ_i =6.8  	WBI=0.21 % χ_i =8.0  	WBI=0.10 % χ_i =13.2  	WBI=0.09 % χ_i =10.2 
6	WBI=0.40 % χ_i =6.1  	WBI=0.08 % χ_i =11.0  	WBI=0.08 % χ_i =6.4  	WBI=0.10 % χ_i =4.7  
7	WBI=0.35 % χ_i =17.4  			

Figure D-6.1 The B2PLYPD3/def2-TVZP lowest free energy structures (298.15 K and 1 atm) and the corrected ZPE lowest energy structures for the $\text{HX}(\text{H}_2\text{O})_n$, $n=1-7$ clusters.

Chapter 7

Acid dissociation in $(\text{HX})_n(\text{H}_2\text{O})_n$ clusters

(X = F, Cl, Br, I; n = 2, 3)

Introduction

Studies dealing with microsolvation of a single acid molecule with one or more water molecules have expanded our understanding of acid dissociation and, in some cases, have pinpointed the number of solvent molecules needed to achieve the formation of the ion pair.^{62, 74-75, 82, 84-85, 87-90, 92, 97, 107, 274} These studies correspond to ideal situations and they do not account for crucial factors such as increasing acid concentration via the explicit addition of new molecules. Indeed, there are few reports about microsolvation of clusters with more than one acid molecule compared with those for a single molecule, and many of them are focused on HCl. For instance, Morrison *et al.*²⁷² reported an infrared spectroscopy study of mixed $(\text{HCl})_m(\text{H}_2\text{O})_n$ clusters ($m:n = 1:1, 2:1, 2:2, \text{ and } 3:1$) immersed in helium nanodroplets. They discussed infrared spectra in the HCl stretch region ($2600\text{-}2900\text{ cm}^{-1}$) and determined that the 2:2 cluster has a nonalternating cyclic arrangement (Figure 7.1a). Chaban *et al.*¹⁵⁸ analyzed the $(\text{HCl})_2(\text{H}_2\text{O})_2$ and $(\text{HCl})_4(\text{H}_2\text{O})_4$ complexes during the discussion on the transition from hydrogen bonding to ionization, including anharmonicity corrections. The hydrogen-bonded isomer of $(\text{HCl})_2(\text{H}_2\text{O})_2$ (see Figure 7.1b) is 6.9 kcal mol^{-1} lower in energy than the ionic one (Figure 7.1c), both with an alternating cyclic structure. Conversely, the 4:4 complex adopts a cubic form, where the full-dissociated isomer is almost 16 kcal mol^{-1} more stable than the hydrogen-bonded one. The authors consider that the incorporation of anharmonic effects is a crucial factor for the prediction of reliable vibrational spectra and that cooperative effects in the solvation of hydrogen halides are extremely important.

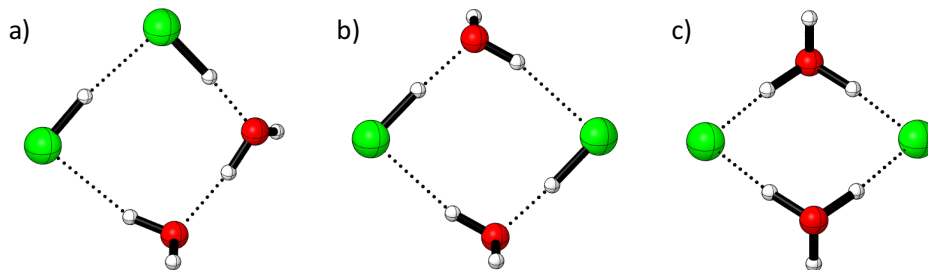


Figure 7.1. Geometrical motifs for $(\text{HCl})_2(\text{H}_2\text{O})_2$ clusters: a) H-bonded nonalternating cyclic form, b) H-bonded alternating structure, and c) ionic arrangement.

Recently, Zakai *et al.*²⁹⁸ performed classical molecular dynamics simulations to illustrate the transitions between the H-bonded and ionic isomers of $(\text{HCl})_2(\text{H}_2\text{O})_2$ (Figure 7.1b and 7.1c) and of $(\text{HF})_4(\text{H}_2\text{O})_4$. They reported that proton transfers were fully concerted in all trajectories for $[\text{Cl}^-\cdots\text{H}_3\text{O}^+]_2$, whereas for $[\text{F}\cdots\text{H}_3\text{O}^+]_4$, the fully concerted mechanism is dominant but partially concerted transfers of two or three protons at the same time also occur. The authors remarked that the high symmetry of the ionic and the H-bonded structures plays a key role in the collective propagation of the protons and cooperative effects.

In order to reply some important questions such as how many water molecules are required to onset dissociation and underline the cooperativity in hydrogen-bonded systems, we systematically explore the potential energy surfaces (PES) of $(\text{HX})_n(\text{H}_2\text{O})_n$ clusters, with $X = \text{F}, \text{Cl}, \text{Br}, \text{I}$ and $n = 2, 3$. We intend to provide new insights into the process of microsolvation of acids supported by a large variety of structures and interactions, ranging from hydrogen bonds of different strengths to halogen interactions. We hope that the spontaneous formation of hydrogen-

bridged bihalide anions and the increasing relevance of the X··H··X interactions in the heavier halogens stimulate new perspectives on the general subject of acid microsolvation.

Computational details

To systematically explore the PES of the (HX)_n(H₂O)_n clusters (with X= F, Cl, Br, I and n= 2, 3), the GLOMOS code was used.^{173-174, 176} A hierarchical screening was established, the initial structures were optimized at the PBE0/D95V level and refine them at the PBE0-D3/def2-TZVP level.^{116, 218, 253} Each structure was characterized as a true minimum by harmonic vibrational frequency analysis. All computations were done using the Gaussian 09 (revision D.01) package.¹⁷⁵ To analyze the interactions, Wiberg bond indices (WBI)¹⁹⁰ were computed and Stern-Limbach²⁰³ plots were used to correlate the symmetry and hydrogen bond lengths.

Results and discussions

Structures and Energetics

Table 7.1 contains the energy ranges and the number of structures obtained, which are 155 for the 2:2 systems and 817 for the 3:3 clusters, including enantiomers. As other systems interacting with water molecules, energy ranges are small if we consider the number of structures involved.^{84, 97, 107, 138, 148-149} The variety and complexity of these clusters increase because every

structure can be made up of different combinations of dissociated and non-dissociated hydrogen halides.

Table 7.1. Number of structures (N) and ZPE corrected electronic and Gibbs free energies (298.15 K and 1 atm) ranges in kcal mol⁻¹ of the (HX)_n(H₂O)_n clusters.

Energy	(HF) _n (H ₂ O) _n	(HCl) _n (H ₂ O) _n	(HBr) _n (H ₂ O) _n	(HI) _n (H ₂ O) _n
n= 2				
N	18	24	45	68
ΔE _{ZPE}	0 – 12.3	0 – 13.8	0 – 13.6	0 – 12.2
ΔG _{298.15} (1 atm)	0 – 9.5	0 – 10.8	0 – 9.1	0 – 8.1
n= 3				
N	255	192	162	208
ΔE _{ZPE}	0 – 12.8	0 – 12.3	0 – 26.4	0 – 25.4
ΔG _{298.15} (1 atm)	0 – 13.5	0 – 8.4	0 – 19.7	0 – 20.1

The structures with the lowest ZPE-corrected energy and with the lowest free energy for each molecularity are presented in Figure 7.2. Clearly, the global minimum is the same by both energy criteria for 2:2 complexes. Conversely, for 3:3 clusters, entropy effects for HF and HCl complexes afford a different global minimum: the lowest free energy structures are cyclic or

bicyclic forms, while the lowest ZPE corrected energy clusters adopt cage-like arrays. Then, as expected, at low temperatures intermolecular interactions are favored, while at high temperatures an approximate ideal gas behavior with less compact structures (fewer intermolecular contacts) is preferred.

Remarkably, our computations indicate dissociation with just two (for HBr and HI) and three (for HCl) water molecules. This is, on one hand, consistent with the pKas listed in Table 6.1, and on the other hand, it is a strong indicator of cooperative effects, which is a particularly relevant aspect in the theory of hydrogen bonding. Two hydrogen bonds may strengthen or weaken each other, because of charge delocalization among X-H sigma network.^{163, 292, 299-300} Cooperativity implies that the sum of at least two interactions is larger than the simple addition of the individual interactions. Several methods attempt to get a quantitative account of the cooperative effects by decomposing the interaction energy of a system of n bodies and by the inclusion of the many-body terms in the analysis.^{33, 300-302} Cooperativity has been reported as an important effect in studies about acid ionization and hydration of ions.^{47, 298}

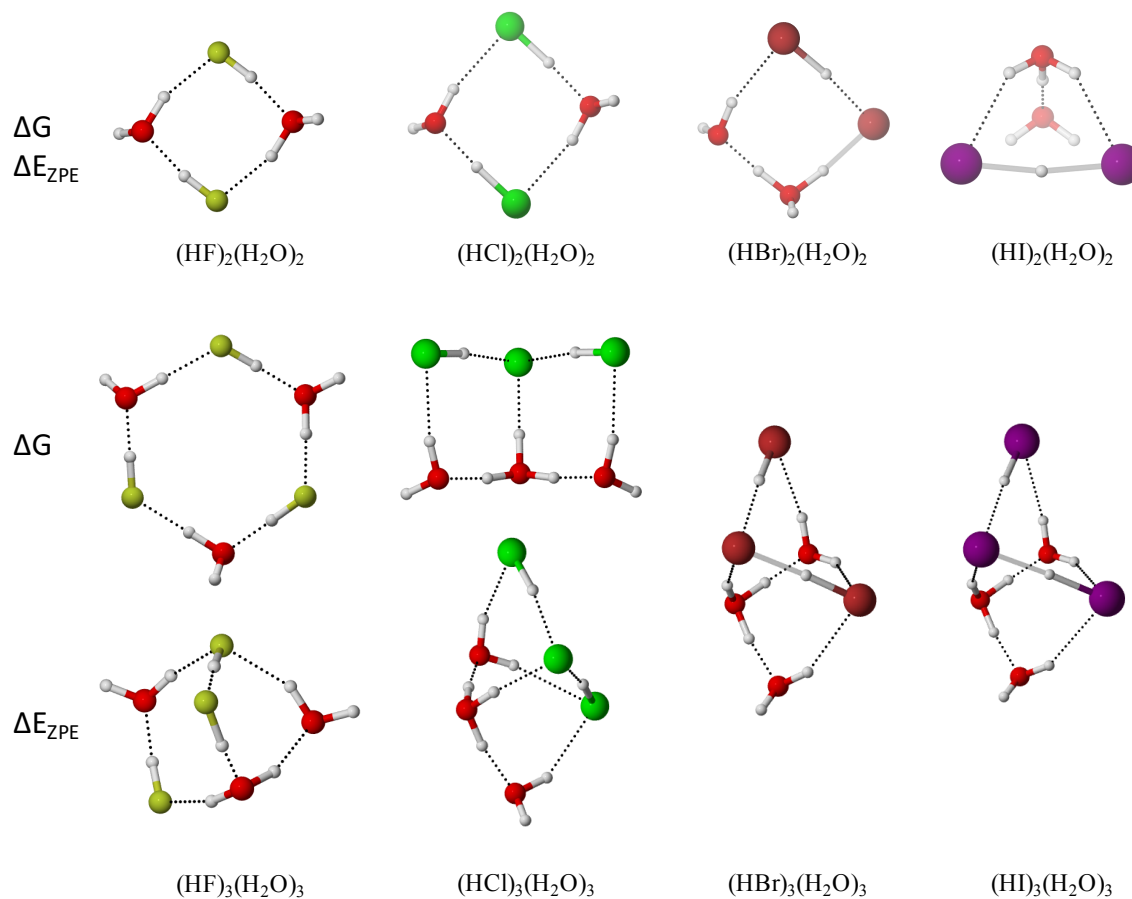


Figure 7.2. PBE0-D3/def2-TZVP lowest energy and lowest free energy structures for the $(\text{HX})_2(\text{H}_2\text{O})_2$ and the $(\text{HX})_3(\text{H}_2\text{O})_3$ clusters.

Interestingly, the relative weakness of HF and HCl exposed in Table 6.1 is manifested in the absence of the $\text{F}\cdots\text{H}\cdots\text{F}$ and $\text{Cl}\cdots\text{H}\cdots\text{Cl}$ bihalides, while for the stronger HBr and HI acids, the spontaneous formation of hydrogen bihalide anions is found. These anions are linear with a hydrogen atom placed between two halide atoms and form strong intramolecular hydrogen bonds.³⁰³⁻³⁰⁷ Kemp and Gordon³⁰³ conducted a study of $\text{BrHBr}^-(\text{H}_2\text{O})_n$ and $\text{IHI}^-(\text{H}_2\text{O})_n$ clusters with $n=1$ to 6 water molecules in order to determine the preferred solvated structures. They found that for $n=1,2$, water molecules prefer to donate their hydrogen atoms for hydrogen

bonding. Conversely, we started with neutral HX and H₂O and found the spontaneous formation of hydrogen bihalide anions! A beautiful example is the global minimum of (HI)₂(H₂O)₂ (see Figure 7.2), in which coexists the IHI⁻ anion and the hydronium cation. For the case of bromine, this structure is a transition state, and it is not viable for clusters with fluorine and chlorine. Other cases of global minimum structures with bihalide anions are the 3:3 complexes with Br and I (Figure 7.2).

Grabowski *et al.*³⁰⁶ studied the XHX⁻ anions as a way to compare the similarity between hydrogen and gold. Their electron density analysis suggested a significant covalent character for the hydrogen to halogen bonds. They also concluded, via an energy decomposition analysis, that FHF⁻ has dative bonds while the heavier homologs exhibit electron sharing through three-center two-electron bonds. Although their bonding analysis was based exclusively on the anions and our clusters include anions, hydronium and water molecules, it seems plausible to compare their computed X-H bond lengths (1.70 and 1.90 Å for Br-H and I-H, respectively) against our results. Thus, while the IHI⁻ anion in the (HI)₂(H₂O)₂ global minimum has an I-H bond length of 1.93 Å and it is symmetric, in 3:3 complexes there are differences between the X...H distances in transient symmetry, with ranges between 1.65-1.78 and 1.87-1.97 Å for BrHBr⁻ and IHI⁻, respectively. These asymmetries are due to the interactions with the solvent molecules.³⁰⁸

Most of the global minima have at least one dissociated HX molecule, except for systems with HF and for the (HCl)₂(H₂O)₂ cluster (Figure 7.3). Interestingly, the lowest energy fully dissociated (HCl)₂(H₂O)₂ arrangement, located 3.8 kcal mol⁻¹ above Gibbs global minimum, exhibits two chloride and two hydronium ions. This arrangement was also obtained for complexes with Br and I (see Figures E-7.1 and E-7.2 in Appendix E). The lowest energy dissociated structure with fluorine coincides with a book-like motif of the lowest free energy for

chlorine. The global minima for 3:3 clusters with bromine and iodine adopt cage-like forms, however, the dissociated book-like geometries are the second lowest free energy structures, located just 0.5 and 0.2 kcal mol⁻¹ above for (HBr)₃(H₂O)₃ and (HI)₃(H₂O)₃, respectively (see Figure E-7.3).

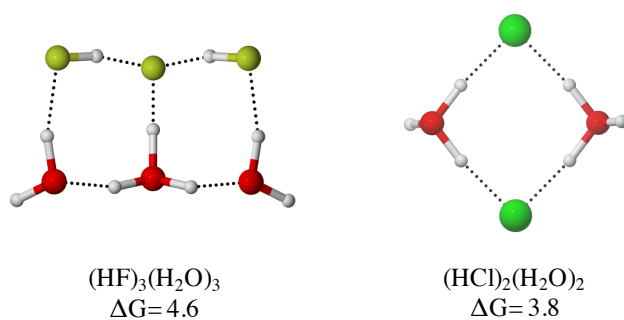


Figure 7.3. Lowest energy dissociated structures in (HF)₃(H₂O)₃ and (HCl)₂(H₂O)₂ clusters. Free energies relative to the global minimum in Figure 7.2 are listed in kcal mol⁻¹.

Bonding analysis

Wiberg bond index is a parameter related to the electron density shared between atoms, providing a reasonable quantification of bond order.^{187, 190} We provide in Figures 7.4a and 7.4b the distributions of the WBIs for H···X contacts for 2:2 and for 3:3 clusters, respectively. For both molecularities, most HF clusters fall in the 0.45-0.65 range, which denotes partial dissociation, there are a few dissociated clusters for n=3 (Figure 7.4b). For all the other acids, a clear separation between dissociated and undissociated complexes is noted. Dissociated/undissociated gaps are more defined for n=2 than for n=3. This is consistent with a greater variety of

geometries and more advanced dissociation stages as n grows. The halogen atom also plays an important role because the difference between the number of dissociated and undissociated groups is more evident in going from chlorine to iodine.

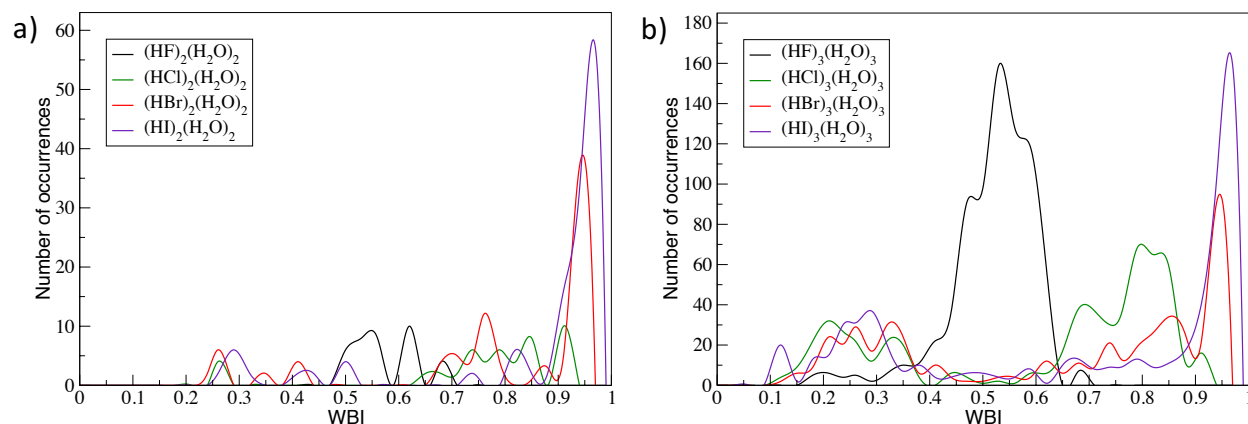


Figure 7.4. Wiberger bond indices (WBI) for the H–X interaction in a) $(HX)_2(H_2O)_2$, and b) $(HX)_3(H_2O)_3$ clusters. Data were taken from the PBE0-D3/def2-TVZP optimized geometries.

The Stern-Limbach plots for the $(HX)_2(H_2O)_2$ and $(HX)_3(H_2O)_3$ clusters provide valuable complementary information about the interactions (see Figures 7.5 and 7.6). In general, the clusters exhibit two types of interactions between the hydrogen halide and water molecules, one by means of hydrogen bonds and the other through halogen bonds (see Figures E-7.1 to E-7.4).

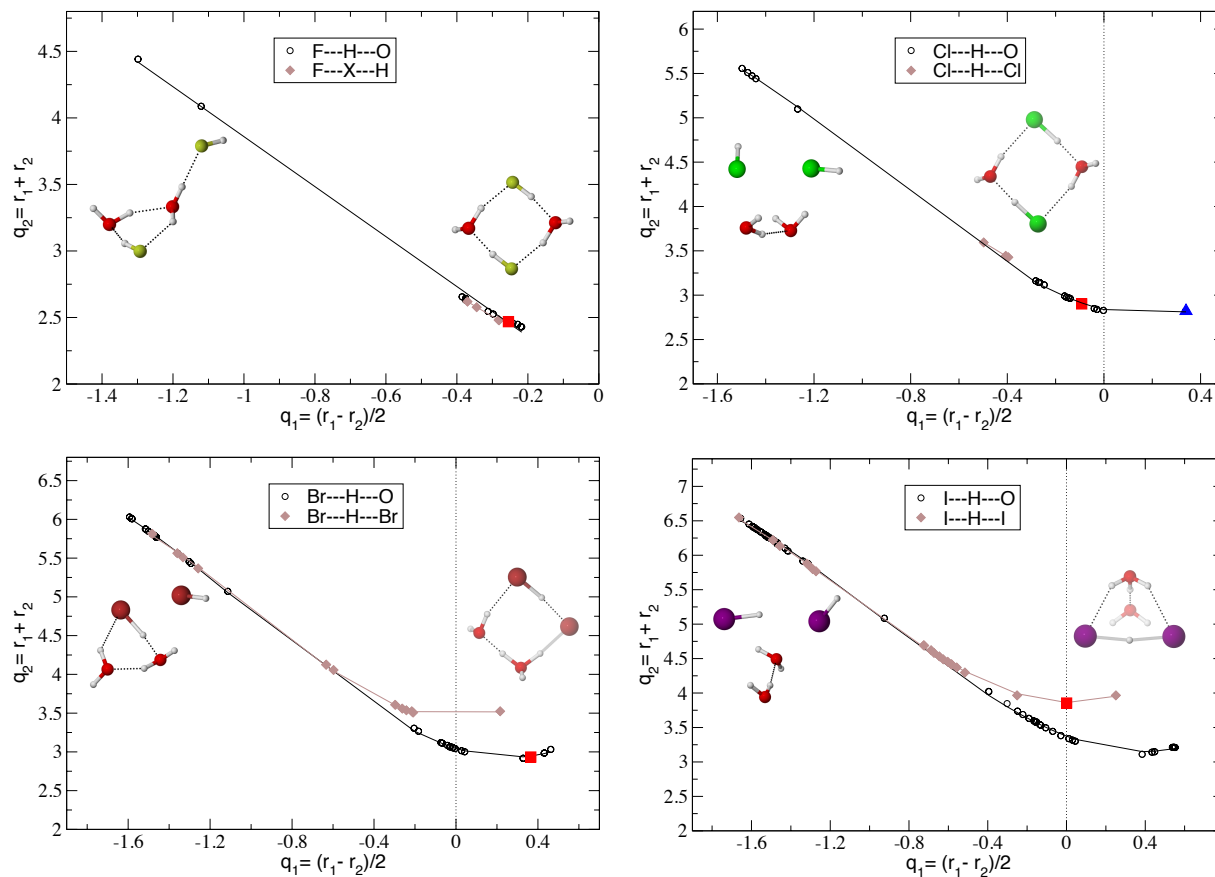


Figure 7.5. Correlation between q_2 and q_1 (See Figure 2.4 for definition of variables). Data taken from the PBE0-D3/def2-TVZP optimized geometries for the $(\text{HX})_2(\text{H}_2\text{O})_2$ clusters. Red squares indicate the lowest free energy structure; the blue triangle indicates the first dissociated structure in $(\text{HCl})_2(\text{H}_2\text{O})_2$. Distances are in Å.

The definition of q_1 and q_2 (Figure 2.4) corresponds to hydrogen bonding, however, large negative values of q_1 combined large values of q_2 denote undissociated species with long A··B distances. These combinations of q_1 and q_2 are due to clusters with halogen interactions (see some examples on the left side of the Figures 7.5 and 7.6 for Cl, Br, and I) or to cases where the hydrogen atom of an undissociated HX molecule does not interact with another molecule, such as the examples on the left side of the Figures 7.5 and 7.6 for HF. In fact, no halogen bonds were

formed for clusters with hydrogen fluoride, while the HCl, HBr and HI clusters with halogen interactions had higher relative energies with respect to the global minima.

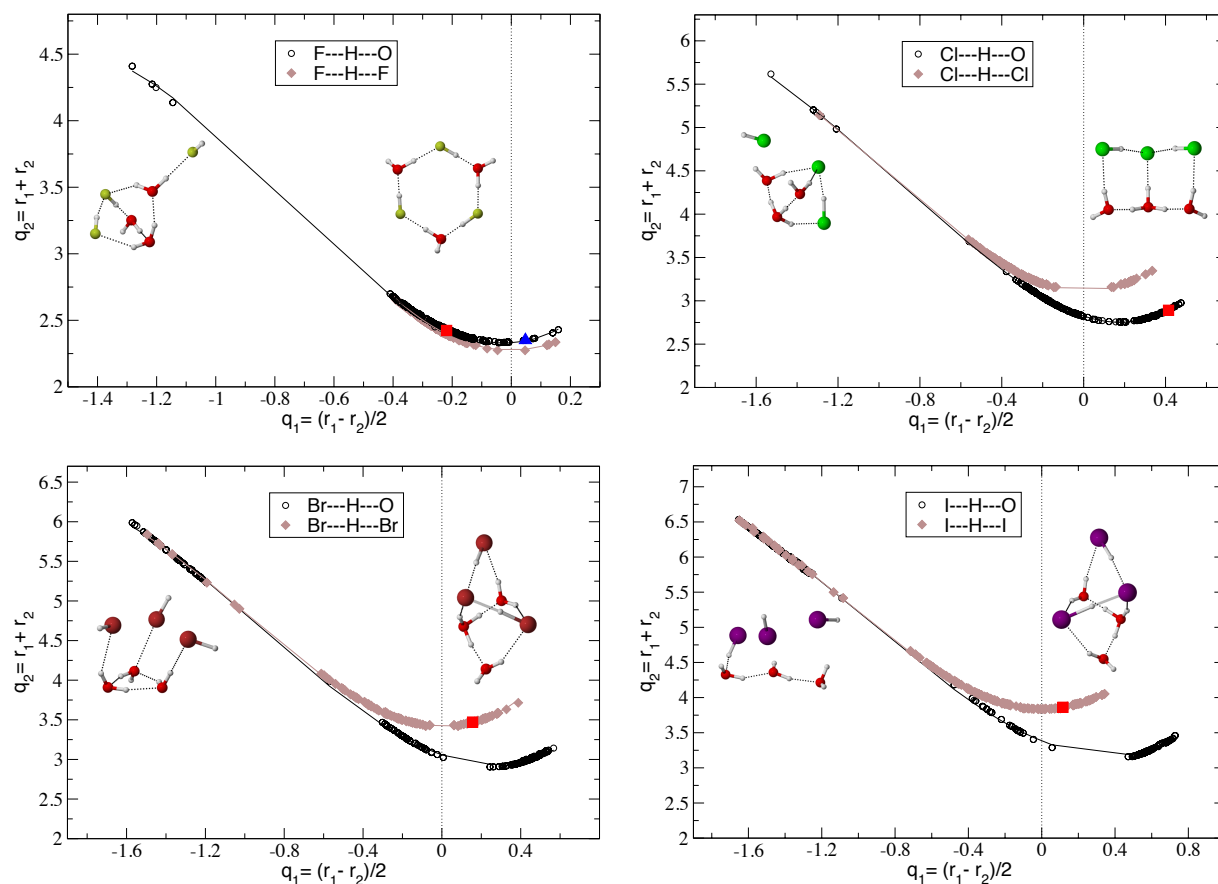


Figure 7.6. Correlation between q_2 and q_1 (see Figure 2.4 for definition of variables). Data were taken from the PBE0-D3/def2-TVZP optimized geometries for the $(\text{HX})_3(\text{H}_2\text{O})_3$ clusters. Red squares indicate the lowest free energy structure; the blue triangle indicates the first dissociated structure in $(\text{HF})_3(\text{H}_2\text{O})_3$. Distances are in Å.

We now focus in the clusters with HX molecules exhibiting some degree of dissociation, say, those for which $q_1 > -0.8$ (see Figures 7.5 and 7.6). Unlike the plots of q_1 vs q_2 reported

previously,^{107, 204} there are now two curves according to the type of interaction, $X\cdots H\cdots O$ or $X\cdots H\cdots X$, the latter becoming increasingly important for the heavier elements (Br and I) and three water molecules. The global minima are included in the plots to notice the type of interaction and are highlighted with red squares on the curves.

A detailed classification of the interactions and their percentages are given in Figures E-7.5 to E-7.7 in Appendix E. The assignment of interactions is based strictly on geometrical criteria. For $(HF)_2(H_2O)_2$, all the computed structures have hydrogen bonds as dominant interactions and do not present dissociated structures. The situation changes a little bit in $(HCl)_2(H_2O)_2$, where dissociated structures and XB interactions arising with $\sim 8\%$ each one (see Figure E-7.6). For the $(HBr)_2(H_2O)_2$ clusters, the separation of curves corresponding to $Br\cdots H\cdots O$, $Br\cdots H\cdots Br$ is evident. Concomitantly, the number of structures with hydrogen bonds decreases ($\sim 73\%$ for water-water and HX-water interactions), while those with dissociated forms and halogen bonds increase ($\sim 13\%$ and 40% , respectively). The global minimum is located on the curve of $Br\cdots H\cdots O$ interactions and possesses a cyclic ion-pair geometry, which belongs to the Zundel-like form ($X\cdots H\cdots O$), which represent $\sim 13\%$ of population (see Figure E-7.6). For the iodine analogs, the percentages of water-water and HX-water interactions decrease to roughly 60% and the $I\cdots H\cdots I$ interactions become the most important since the global minimum belongs to this Zundel-type (notice that it is the only one structure of this category in Figure E-7.6), with the formation of a hydrogen bihalide anion (Zundel-like structure), supported by the fact that the global minimum is located at $q_1 = 0$, corresponding to the central-symmetric anion. Structures with halogen bond interactions increase considerably (almost 74%), while the Zundel-like $I\cdots H\cdots O$ structures decreases at $\sim 9\%$ compared with HBr-water clusters.

The assortment of forms found for the $(\text{HX})_3(\text{H}_2\text{O})_3$ clusters is more diverse. The plot for HF (Figure 7.6) shows that the $\text{F}\cdots\text{H}\cdots\text{O}$ and $\text{F}\cdots\text{H}\cdots\text{F}$ curves are closer to each other. Hydrogen bonds of the $\text{F}\cdots\text{H}\cdots\text{O}$ type are longer than $\text{F}\cdots\text{H}\cdots\text{F}$. The global minimum is undissociated (an alternating six-membered ring) and belongs to the type of HF-water hydrogen bonds, the dominant interaction ($\sim 95\%$, Figure E-7.7). The lowest energy dissociated form is a quasi-Eigen cation and has a relative free energy of $4.6 \text{ kcal mol}^{-1}$ (see Figure 7.3). There are no structures with halogen bonds, but some examples of dissociated (2.8%) and quasi-Eigen forms (2%) were found (Figure E-7.6). F-H-O Zundel-type structures are 22.4% of total (see Figure E-7.3). The gap between curves is more evident for the HCl species (Figure 7.6). Again, a reduction of hydrogen bond interactions (about 77% and 45% for HX-water and water-water interactions, respectively) and a significant increment of the dissociated complexes ($\sim 57\%$, Figure E-7.7) are noted. The quasi-Eigen cations represent almost 10% of population (including the global minimum) and the structures containing Zundel cations is now present (about 5%), while Zundel-like Cl-H-O type and XB interactions contribute with ~ 5 and 1% , respectively. For the $(\text{HBr})_3(\text{H}_2\text{O})_3$ clusters, the highest percentages belong to HX-water interactions ($\sim 77\%$) and dissociated complexes (66% , see Figure E-7.7). Although the Zundel-type X-H-X interactions have a low percentage of occurrence (about 6%), leading to the same motif for the global minima, a cage-like geometry. Contributions increased in structures with halogen bond (about 12%), Zundel X-H-O type ($\sim 14\%$), Zundel (10%), and quasi-Eigen ($\sim 14\%$) cations. Finally, in $(\text{HI})_3(\text{H}_2\text{O})_3$ clusters, water \cdots water and HX \cdots water interactions decreased (about 29 and 62% , respectively). The percentage of dissociated structures is slightly lower ($\sim 61\%$) than those with bromine, but this is compensated by the increase of the special dissociated forms: quasi-Eigen ($\sim 18\%$), Zundel (11.5%), and Zundel I-H-I type ($\sim 9\%$). In this case, there are no Zundel I-H-O

type structures and the XB interactions represent ~59% of population. Another important remark is that the gap around $q_1=0$ in Figure 7.6 is decreasing from clusters with Cl to I, and for the latter, there are structures populating the whole range, including zero, which accounts for structures with bihalide ions being more symmetrical than those with bromine.

Conclusions

The exploration of the PES for the microsolvation of hydrogen halides with more than one HX ($X = \text{F}, \text{Cl}, \text{Br}, \text{I}$) molecule reveals that it is viable to dissociate the hydrogen halides with few water molecules. Particularly, HCl is dissociated with three water molecules while HBr and HI only needed two. Since two water molecules may not be sufficient to dissociate a single hydrogen halide molecule, and the same number of water molecules does that in the presence of two HX molecules, strong cooperative effects are suggested. Intriguingly, for the stronger acids, bihalide anions (BrHBr^- and IHI^-) are formed spontaneously.

A diverse set of interactions and forms is found for $(\text{HX})_3(\text{H}_2\text{O})_3$ clusters, such water \cdots water, HX \cdots water, and HX \cdots HX hydrogen bonds, halogen bonds, ionic and long-range X \cdots H contacts, as well as quasi-Eigen, Zundel, and Zundel-like-type structures. The first three types are dominant in HF-water complexes and in going from F to I, these decrease to make way for the other types of interactions, so that the dissociated forms, although smaller in percentage, can become very important because they contain the global minimum, as is the case of Zundel-type structures.

Appendix E

Acid dissociation in $(\text{HX})_n(\text{H}_2\text{O})_n$ clusters

(X = F, Cl, Br, I; n = 2, 3)

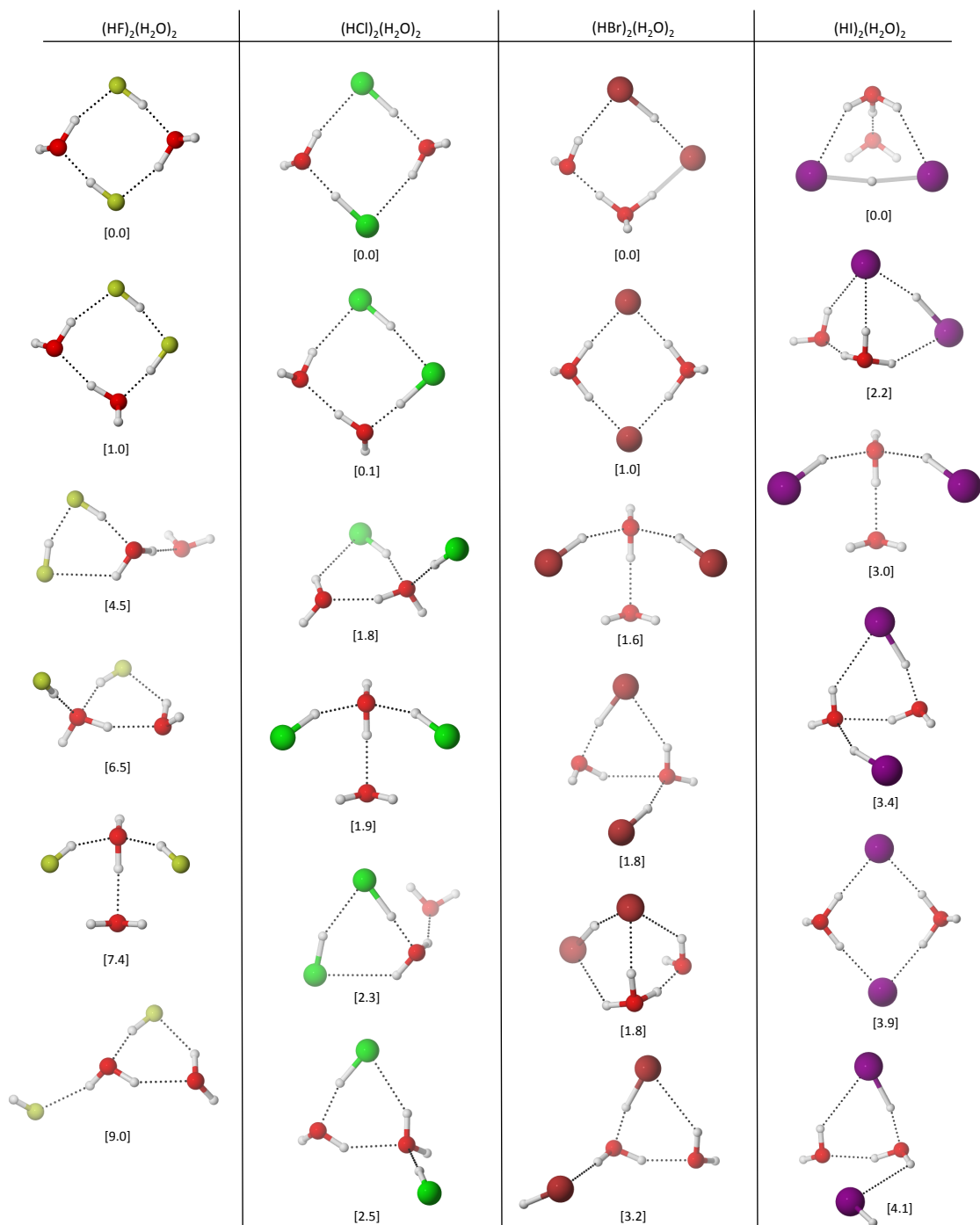


Figure E-7.1 Selected optimized structures of $(\text{HX})_2(\text{H}_2\text{O})_2$ clusters for $\text{X} = \text{F}, \text{Cl}, \text{Br},$ and I , at PBE0-D3/def2-TZVP level of theory. Relative stabilities of the isomers are shown with respect to the most stable free energy structures. Energies in kcal mol^{-1} .

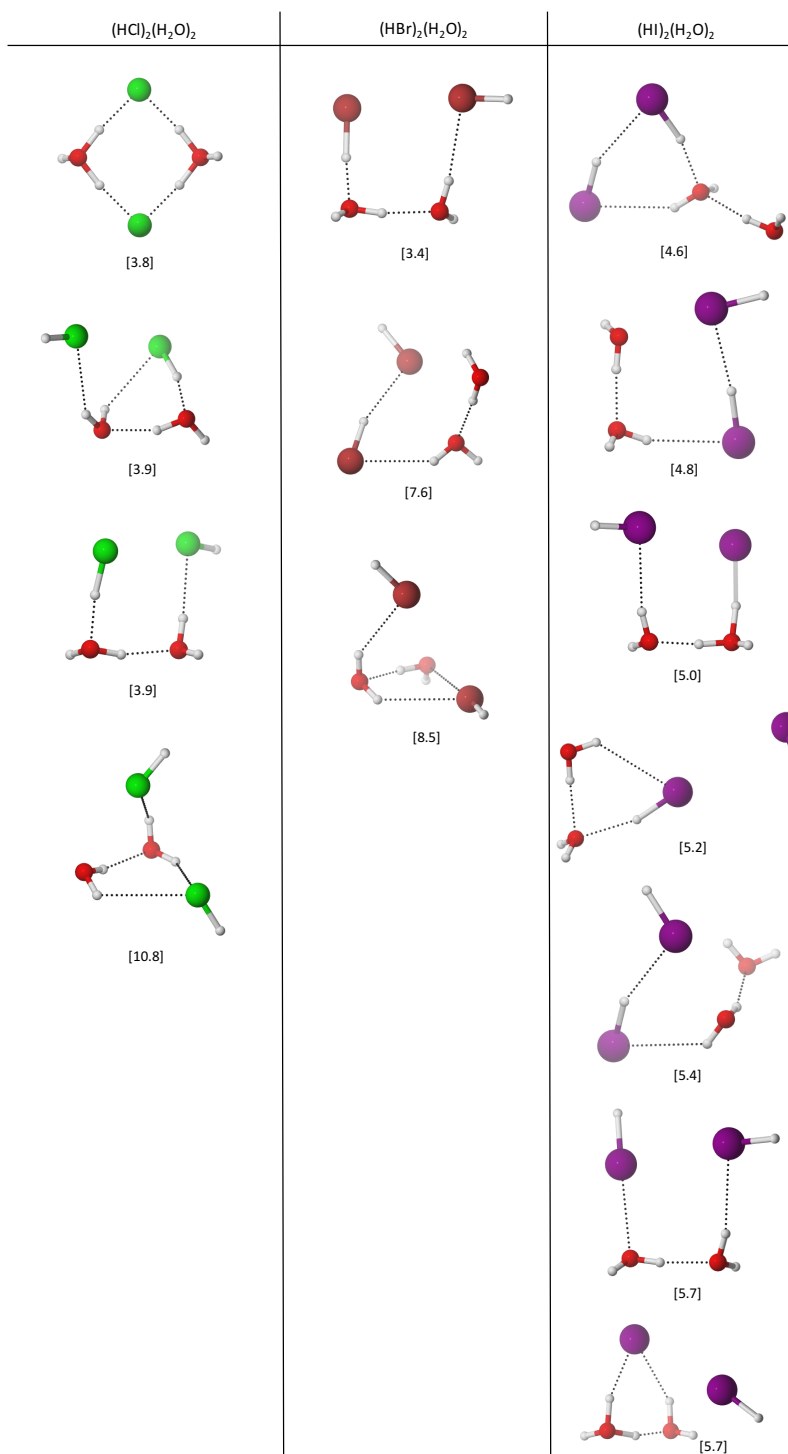


Figure E-7.2 Selected optimized structures of $(\text{HX})_2(\text{H}_2\text{O})_2$ clusters for $X = \text{Cl}, \text{Br},$ and I , at PBE0-D3/def2-TZVP level of theory. Relative stabilities of the isomers are shown with respect to the most stable free energy structures. Energies in kcal mol^{-1} .

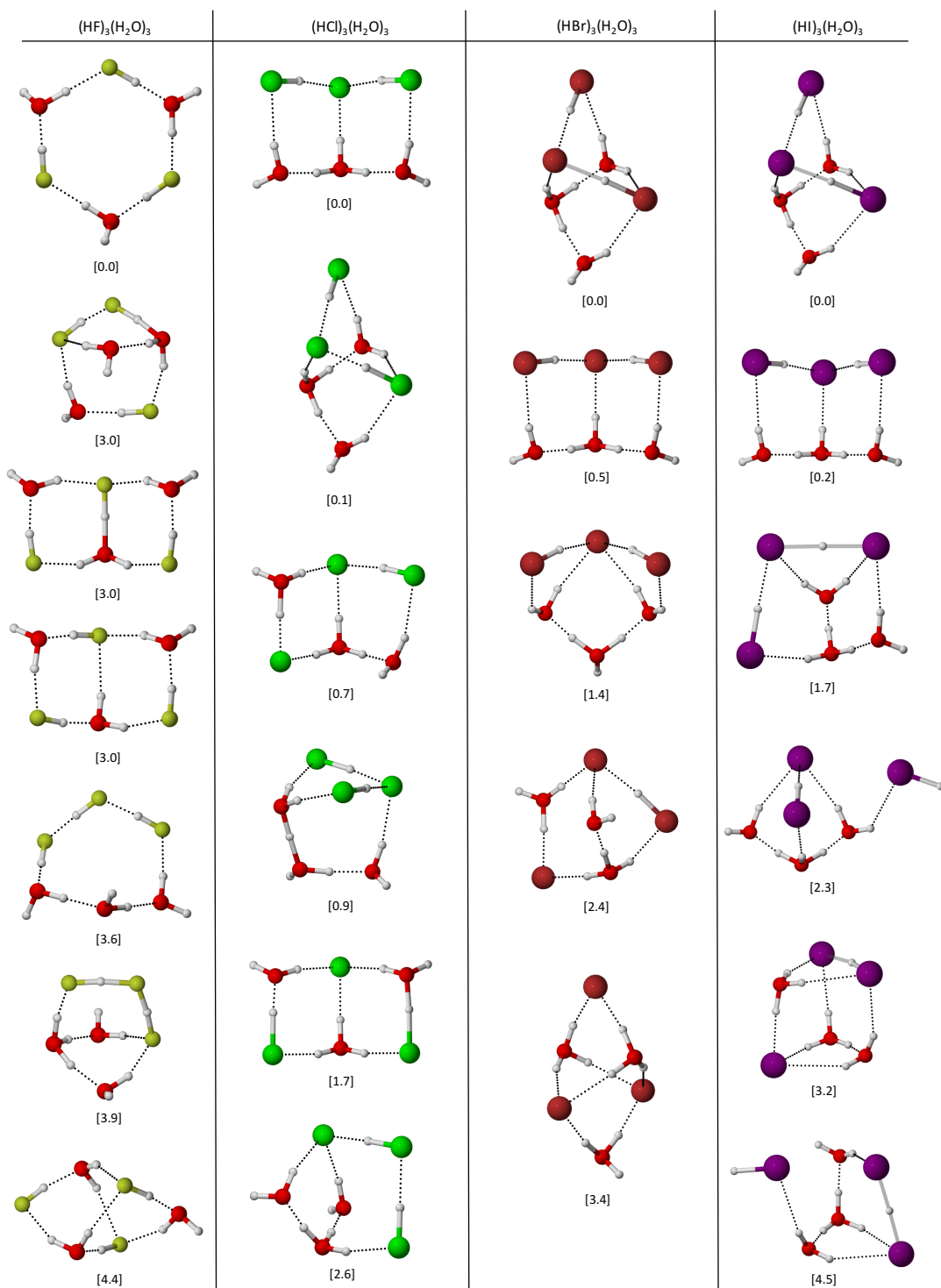


Figure E-7.3 Selected optimized structures of $(\text{HX})_3(\text{H}_2\text{O})_3$ clusters for $\text{X} = \text{F}, \text{Cl}, \text{Br},$ and I , at PBE0-D3/def2-TZVP level of theory. Relative stabilities of the isomers are shown with respect to the most stable free energy structures. Energies in kcal mol^{-1} .

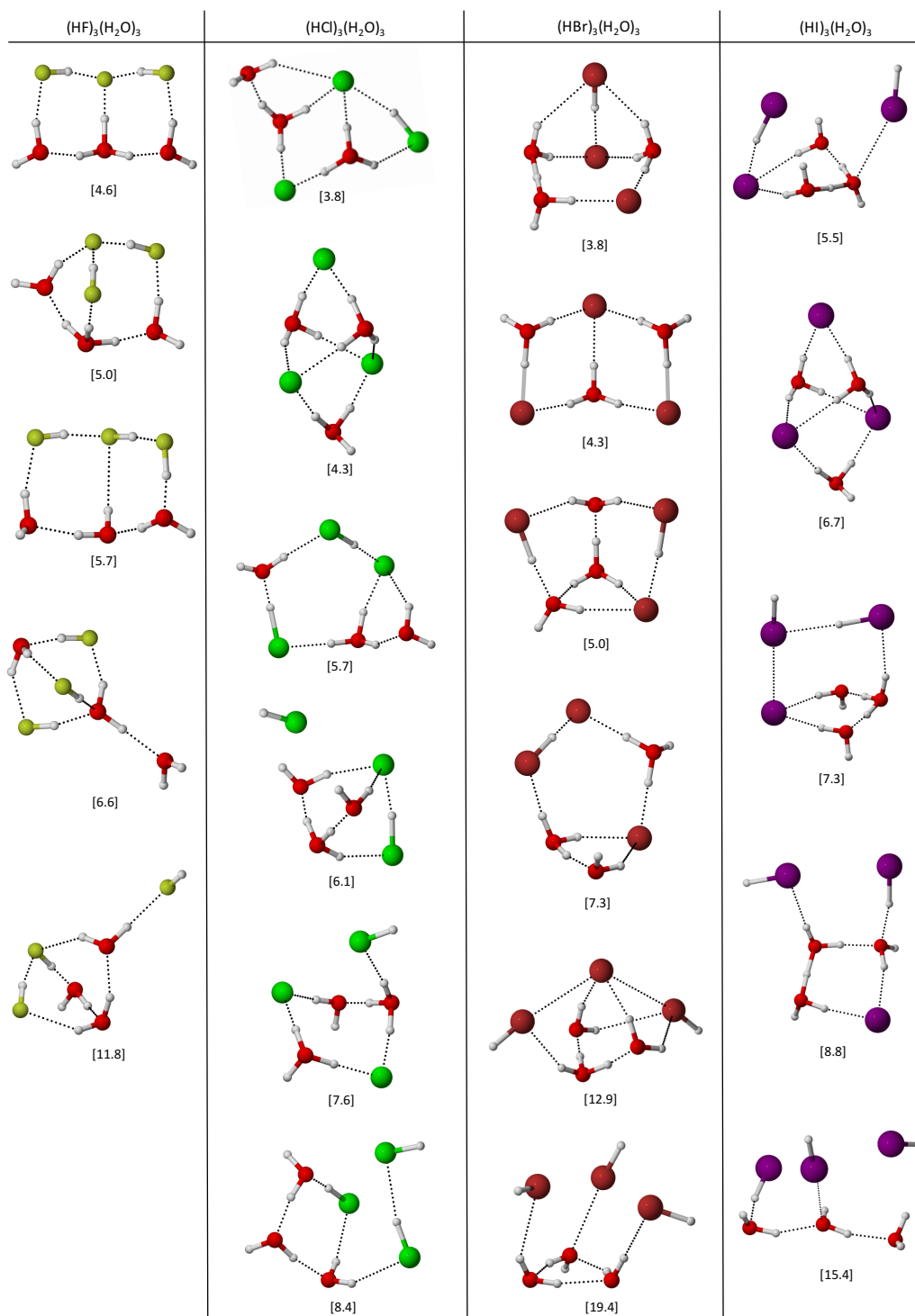


Figure E-7.4 Selected optimized structures of $(\text{HX})_3(\text{H}_2\text{O})_3$ clusters for $\text{X} = \text{F}, \text{Cl}, \text{Br},$ and I , at PBE0-D3/def2-TZVP level of theory. Relative stabilities of the isomers are shown with respect to the most stable free energy structures. Energies in kcal mol^{-1} .

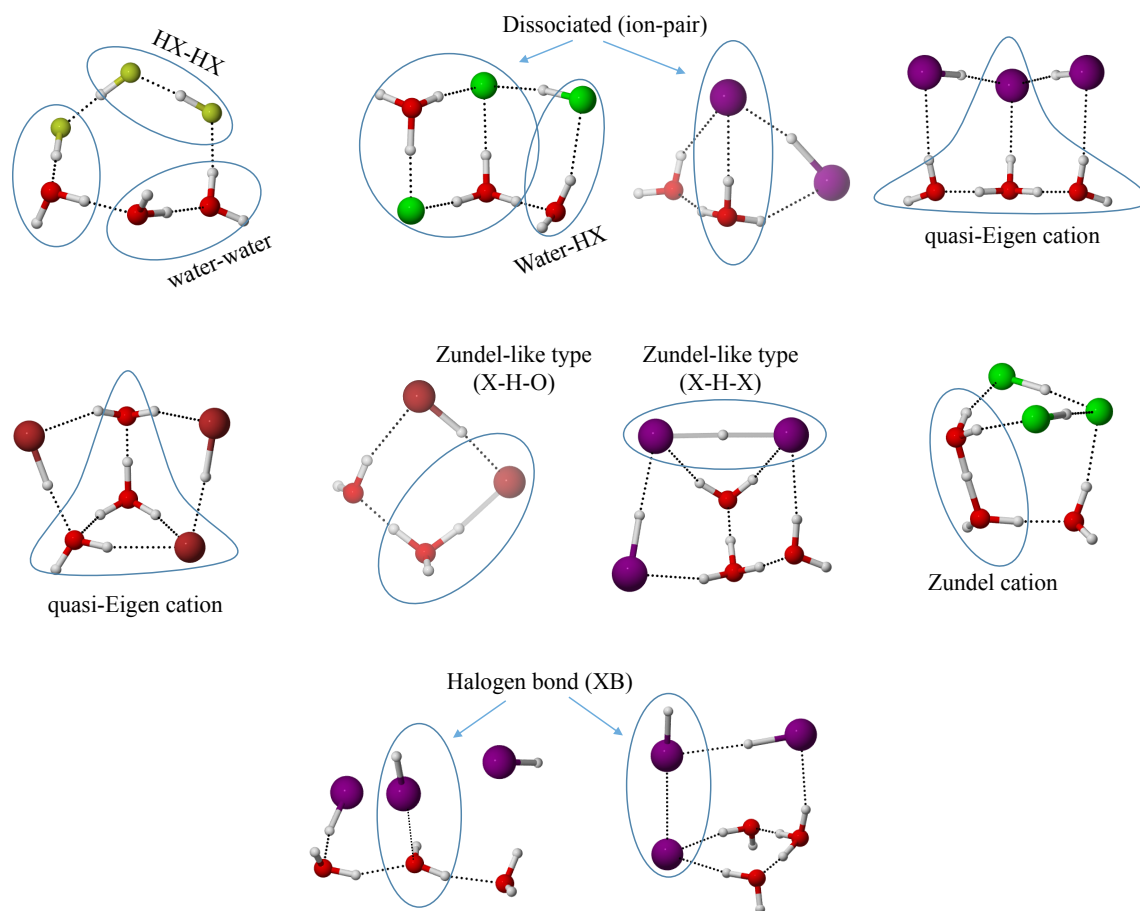


Figure E-7.5 Examples of interactions in $(\text{HX})_n(\text{H}_2\text{O})_n$ clusters for $\text{X} = \text{F}, \text{Cl}, \text{Br}, \text{and I}$, with $n=2,3$ at PBE0-D3/def2-TZVP level.

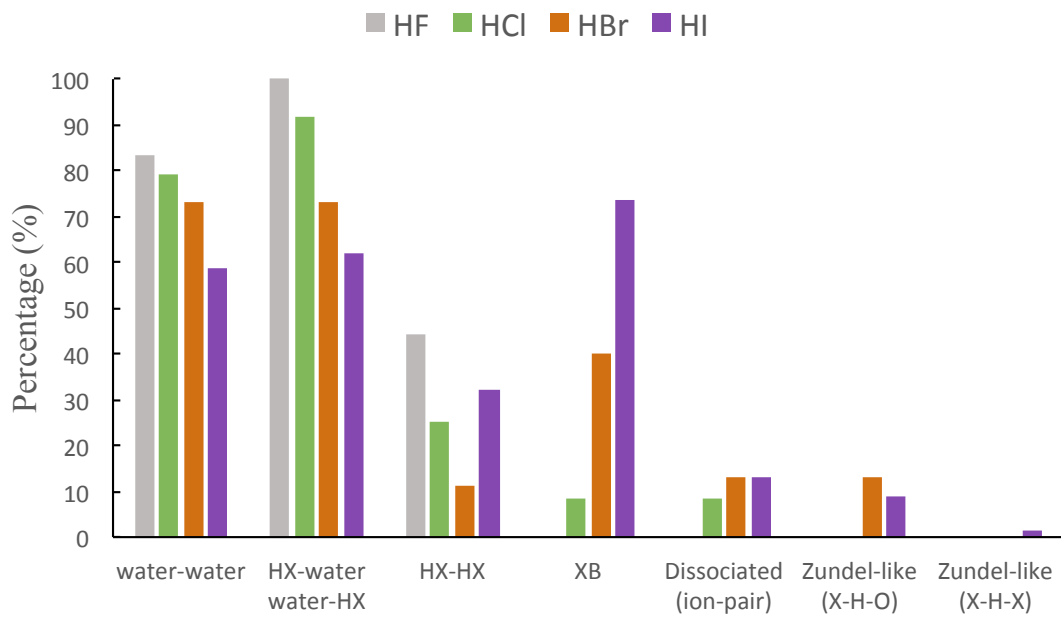


Figure E-7.6 Percentage of interactions in optimized structures of $(HX)_2(H_2O)_2$ clusters for X= F, Cl, Br, and I, at PBE0-D3/def2-TZVP level.

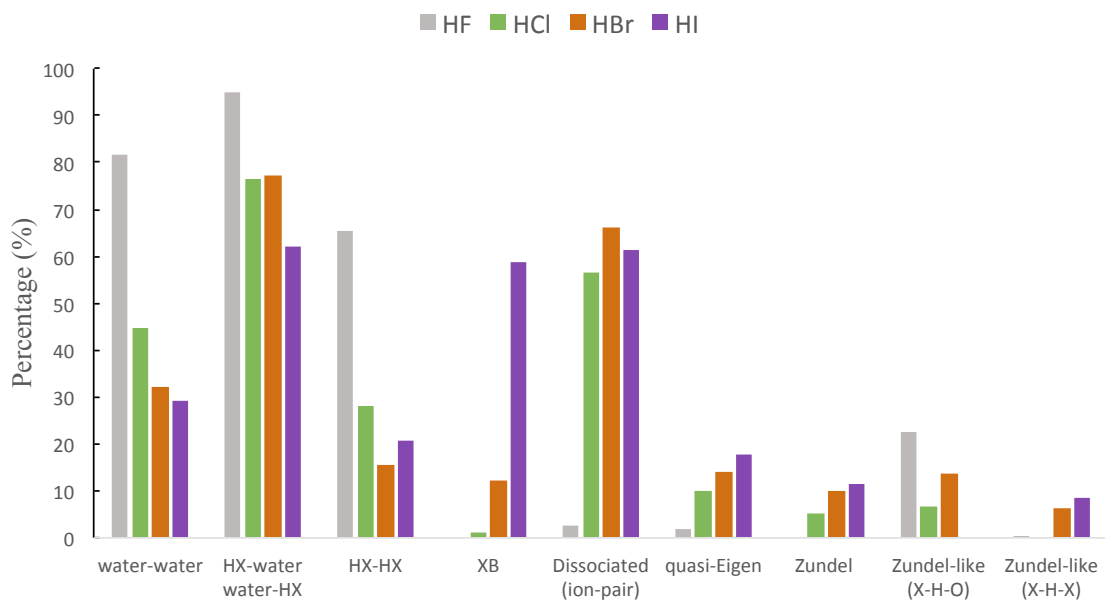


Figure E-7.7 Percentage of interactions in optimized structures of $(HX)_3(H_2O)_3$ clusters for $X =$ F, Cl, Br, and I, at PBE0-D3/def2-TZVP level.

PUBLICATIONS

This thesis is based on the following publications:

- Vargas-Caamal, A.; Ortiz-Chi, F.; Moreno, D.; Restrepo, A.; Merino, G.; Cabellos, J. L. “The rich and complex potential energy surface of the ethanol dimer” *Theor. Chem. Acc.* **2015**, 134, 16.
- Vargas-Caamal, A.; Pan, S.; Ortiz-Chi, F.; Cabellos, J. L.; Boto, R. A.; Contreras-Garcia, J.; Restrepo, A.; Chattaraj, P. K.; Merino, G. “How strong are the metallocene-metallocene interactions? Cases of ferrocene, ruthenocene, and osmocene” *Phys. Chem. Chem. Phys.* **2016**, 18, 550-556.
- Vargas-Caamal, A.; Cabellos, J. L.; Ortiz-Chi, F.; Rzepa, H. S.; Restrepo, A.; Merino, G. “How Many Water Molecules Does it Take to Dissociate HCl?” *Chem. Eur. J.* **2016**, 22, 2812- 2818.

In preparation:

- Vargas-Caamal, A.; Dzib, E.; Ortiz-Chi, F.; Restrepo, A.; Merino, G. “Acid dissociation in $(HX)_n(H_2O)_n$ clusters (X = F, Cl, Br, I; n= 2,3). Submitted.
- Vargas-Caamal, A.; Ortiz-Chi, F.; Restrepo, A.; Merino, G. “How many water molecules does it take to dissociate H-X acids? (X= F, Cl, Br, and I). In preparation.
- Vargas-Caamal, A.; Maldonado, A. F.; Aucar, G. A.; Merino, G. “Interactions and relativistic effects in HI and HAt-water complexes”. In preparation.

REFERENCES

1. Bondybey, V. E.; Beyer, M. K. *Int. Rev. Phys. Chem.* **2002**, *21* (2), 277-306.
2. Desiraju, G. R. *Nature* **2001**, *412*, 397.
3. Castleman, A. W.; Jena, P. *Proc. Natl. Acad. Sci.* **2006**, *103* (28), 10552.
4. Hobza, P.; Müller-Dethlefs, K., *Non-covalent interactions: Theory and experiment.* 2009.
5. Jellinek, J., *Theory of Atomic and Molecular Clusters : with a Glimpse at Experiments.* 1999.
6. Weber, K. H.; Tao, F.-M. *J. Phys. Chem. A* **2001**, *105* (7), 1208-1213.
7. Leopold, K. R., Hydrated Acid Clusters. In *Annual Review of Physical Chemistry, Vol 62*, Leone, S. R.; Cremer, P. S.; Groves, J. T.; Johnson, M. A., Eds. 2011; Vol. 62, pp 327-349.
8. Cramer, C. J., *Essentials of computational chemistry : theories and models.* West Sussex, England ; New York : J. Wiley, [2002] ©2002: 2002.
9. Florez, E.; Acelas, N.; Ramírez, F.; Hadad, C.; Restrepo, A. *Phys. Chem. Chem. Phys.* **2018**, *20* (13), 8909-8916.
10. Marques, J.; Pereira, F.; Llanio-Trujillo, J.; Abreu, P.; Albertí, M.; Aguilar, A.; Pirani, F.; Bartolomei, M. *Phil. Trans. R. Soc. A* **2017**, *375* (2092), 20160198.
11. Ayala, R.; Martínez, J. M.; Pappalardo, R. R.; Muñoz-Páez, A.; Sánchez Marcos, E. *Mol. Simul.* **2006**, *32* (12-13), 1035-1043.
12. Wilkinson, A.; McNaught, A. *International Union of Pure and Applied Chemistry* **1997**.
13. Ahn, D.-S.; Park, S.-W.; Jeon, I.-S.; Lee, M.-K.; Kim, N.-H.; Han, Y.-H.; Lee, S. *J. Phys. Chem. B* **2003**, *107* (50), 14109-14118.
14. Blanco, S.; López, J. C.; Lesarri, A.; Alonso, J. L. *J. Am. Chem. Soc.* **2006**, *128* (37), 12111-12121.
15. Truong, T. N.; Stefanovich, E. V. *Chem. Phys.* **1997**, *218* (1), 31-36.
16. Lewars, E. G., *Computational Chemistry. Introduction to the Theory and Applications of Molecular and Quantum Mechanics.* 2nd ed.; New York, 2011.
17. Cui, Z.-h.; Contreras, M.; Ding, Y.-h.; Merino, G. *J. Am. Chem. Soc.* **2011**, *133* (34), 13228-13231.
18. Klibanov, A. M. *Nature* **2001**, *409*, 241.
19. Ohtaki, H. *Monatshefte für Chemie / Chemical Monthly* **2001**, *132* (11), 1237-1268.
20. Forck, R. M.; Dauster, I.; Buck, U.; Zeuch, T. *J. Phys. Chem. A* **2011**, *115* (23), 6068-6076.

21. Nguyen, T.-N. V.; Peslherbe, G. H. *J. Phys. Chem. A* **2003**, *107* (10), 1540-1550.
22. Dauster, I.; Suhm, M. A.; Buck, U.; Zeuch, T. *Phys. Chem. Chem. Phys.* **2008**, *10* (1), 83-95.
23. Nielsen, S.; Andersen, L., *Properties of microsolvated ions: From the microenvironment of chromophore and alkali metal ions in proteins to negative ions in water clusters*. 2007; Vol. 124, p 229-37.
24. Salter, T. E.; Ellis, A. M. *Chem. Phys.* **2007**, *332* (1), 132-138.
25. Takis, P. G.; Papavasileiou, K. D.; Peristeras, L. D.; Boulougouris, G. C.; Melissas, V. S.; Troganis, A. N. *Phys. Chem. Chem. Phys.* **2017**, *19* (21), 13710-13722.
26. Ayala, R.; Martínez, J. M.; Pappalardo, R. R.; Sánchez Marcos, E. *J. Phys. Chem. A* **2000**, *104* (12), 2799-2807.
27. Marques, J.; Llanio-Trujillo, J.; Albertí, M.; Aguilar, A.; Pirani, F. *J. Phys. Chem. A* **2012**, *116* (20), 4947-4956.
28. Brutschy, B. *Chem. Rev* **2000**, *100* (11), 3891-3920.
29. Zwier, T. S. *Annu. Rev. Phys. Chem.* **1996**, *47* (1), 205-241.
30. Le Barbu, K.; Schiedt, J.; Weinkauff, R.; Schlag, E. W.; Nilles, J. M.; Xu, S. J.; Thomas, O. C.; Bowen, K. H. *J. Chem. Phys.* **2002**, *116* (22), 9663-9671.
31. Rao, J. S.; Zipse, H.; Sastry, G. N. *J. Phys. Chem. B* **2009**, *113* (20), 7225-7236.
32. Reddy, A. S.; Zipse, H.; Sastry, G. N. *J. Phys. Chem. B* **2007**, *111* (39), 11546-11553.
33. Mahadevi, A. S.; Sastry, G. N. *Chem. Rev* **2016**, *116* (5), 2775-2825.
34. Castleman, A.; Bowen, K. *J. Phys. Chem.* **1996**, *100* (31), 12911-12944.
35. Robertson, W. H.; Karapetian, K.; Ayotte, P.; Jordan, K. D.; Johnson, M. A. *J. Chem. Phys.* **2002**, *116* (12), 4853-4857.
36. Bachrach, S. M. *J. Phys. Chem. A* **2008**, *112* (16), 3722-3730.
37. Blom, M. N.; Compagnon, I.; Polfer, N. C.; von Helden, G.; Meijer, G.; Suhai, S.; Paizs, B.; Oomens, J. *J. Phys. Chem. A* **2007**, *111* (31), 7309-7316.
38. Balabin, R. M. *J. Phys. Chem. B* **2010**, *114* (46), 15075-15078.
39. Aikens, C. M.; Gordon, M. S. *J. Am. Chem. Soc.* **2006**, *128* (39), 12835-12850.
40. Chuhev, K.; BelBruno, J. J. *J. Mol. Struct.* **2008**, *850* (1-3), 111-120.
41. Kim, H.-S.; Ahn, D.-S.; Chung, S.-Y.; Kim, S. K.; Lee, S. *J. Phys. Chem. A* **2007**, *111* (32), 8007-8012.

42. Bachrach, S. M.; Nguyen, T. T.; Demoin, D. W. *J. Phys. Chem. A* **2009**, *113* (21), 6172-6181.
43. Göth, M.; Lermyte, F.; Schmitt, X. J.; Warnke, S.; von Helden, G.; Sobott, F.; Pagel, K. *Analyst* **2016**, *141* (19), 5502-5510.
44. Swarts, S. G.; Sevilla, M. D.; Becker, D.; Tokar, C. J.; Wheeler, K. T. *Radiation research* **1992**, *129* (3), 333-344.
45. Khattab, M.; Wang, F.; Clayton, A. H. *RSC Advances* **2017**, *7* (50), 31725-31735.
46. Ibarguen, C.; Manrique-Moreno, M.; Hadad, C. Z.; David, J.; Restrepo, A. *Phys. Chem. Chem. Phys.* **2013**, *15* (9), 3203-3211.
47. Tielrooij, K.; Garcia-Araez, N.; Bonn, M.; Bakker, H. *Science* **2010**, *328* (5981), 1006-1009.
48. Mundy, C. J.; Hutter, J.; Parrinello, M. *J. Am. Chem. Soc.* **2000**, *122* (19), 4837-4838.
49. Liu, C. W.; Gao, Y., *Understanding the Microsolvation of Salts in Molecular Clusters*. 2014; Vol. 115.
50. Xia, F.-F.; Zeng, D.; Yi, H.-B.; Fang, C. *J. Phys. Chem. A* **2013**, *117* (35), 8468-8476.
51. Marx, D. *ChemPhysChem* **2006**, *7* (9), 1848-1870.
52. Marx, D. *ChemPhysChem* **2007**, *8* (2), 209-210.
53. Domcke, W.; Sobolewski, A. L. *Science* **2003**, *302* (5651), 1693-1694.
54. Headrick, J. M. *Science* **2005**, *309* (5739), 1326-1326.
55. Headrick, J. M.; Diken, E. G.; Walters, R. S.; Hammer, N. I.; Christie, R. A.; Cui, J.; Myshakin, E. M.; Duncan, M. A.; Johnson, M. A.; Jordan, K. D. *Science* **2005**, *308* (5729), 1765-1769.
56. Hurley, S. M.; Dermota, T. E.; Hydutsky, D. P.; Castleman, A. W. *Science* **2002**, *298* (5591), 202-204.
57. Miyazaki, M.; Fujii, A.; Ebata, T.; Mikami, N. *Science* **2004**, *304* (5674), 1134-1137.
58. Robertson, W. H.; Diken, E. G.; Price, E. A.; Shin, J. W.; Johnson, M. A. *Science* **2003**, *299* (5611), 1367-1372.
59. Robertson, W. H.; Johnson, M. A. *Science* **2002**, *298* (5591), 69-69.
60. Shin, J. W.; Hammer, N. I.; Diken, E. G.; Johnson, M. A.; Walters, R. S.; Jaeger, T. D.; Duncan, M. A.; Christie, R. A.; Jordan, K. D. *Science* **2004**, *304* (5674), 1137-1140.
61. Stace, A. *Science* **2001**, *294* (5545), 1292-1293.

62. Voegelé, A. F.; Liedl, K. R. *Angew. Chem. Int. Ed.* **2003**, *42* (19), 2114-2116.
63. Zwier, T. S. *Science* **2004**, *304* (5674), 1119-1120.
64. Agmon, N. *Chem. Phys. Lett.* **1995**, *244* (5-6), 456-462.
65. Bondybey, V. E.; Beyer, M.; Achatz, U.; Joos, S.; Niedner-Schatteburg, G. *Isr. J. Chem.* **1999**, *39* (3-4), 213-219.
66. Hassanali, A. A.; Cuny, J.; Ceriotti, M.; Pickard, C. J.; Parrinello, M. *J. Am. Chem. Soc.* **2012**, *134* (20), 8557-8569.
67. Marx, D.; Chandra, A.; Tuckerman, M. E. *Chem. Rev* **2010**, *110* (4), 2174-2216.
68. Niedner-Schatteburg, G.; Bondybey, V. E. *Chem. Rev* **2000**, *100* (11), 4059-4086.
69. Rini, M.; Magnes, B. Z.; Pines, E.; Nibbering, E. T. J. *Science* **2003**, *301* (5631), 349-352.
70. Zahn, D.; Brickmann, J. *Isr. J. Chem.* **1999**, *39* (3-4), 469-482.
71. Farnik, M.; Weimann, M.; Suhm, M. A. *J. Chem. Phys.* **2003**, *118* (22), 10120-10136.
72. Gregory, J. K.; Clary, D. C.; Liu, K.; Brown, M. G.; Saykally, R. J. *Science* **1997**, *275* (5301), 814-817.
73. Guggemos, N.; Slavicek, P.; Kresin, V. V. *Phys. Rev. Lett.* **2015**, *114* (4), 5.
74. Gutberlet, A.; Schwaab, G.; Birer, O.; Masia, M.; Kaczmarek, A.; Forbert, H.; Havenith, M.; Marx, D. *Science* **2009**, *324* (5934), 1545-1548.
75. Hurley, S. M.; Dermota, T. E.; Hydutsky, D. P.; Castleman, A. W. *J. Chem. Phys.* **2003**, *118* (20), 9272-9277.
76. Kisiel, Z.; Bialkowska-Jaworska, E.; Pszczolkowski, L.; Milet, A.; Struniewicz, C.; Moszynski, R.; Sadlej, J. *J. Chem. Phys.* **2000**, *112* (13), 5767-5776.
77. Letzner, M.; Gruen, S.; Habig, D.; Hanke, K.; Endres, T.; Nieto, P.; Schwaab, G.; Walewski, L.; Wollenhaupt, M.; Forbert, H.; Marx, D.; Havenith, M. *J. Chem. Phys.* **2013**, *139* (15), 11.
78. Skvortsov, D.; Lee, S. J.; Choi, M. Y.; Vilesov, A. F. *J. Phys. Chem. A* **2009**, *113* (26), 7360-7365.
79. Weimann, M.; Farnik, M.; Suhm, M. A. *Phys. Chem. Chem. Phys.* **2002**, *4* (16), 3933-3937.
80. Amirand, C.; Maillard, D. *J. Mol. Struct.* **1988**, *176*, 181-201.
81. Ando, K.; Hynes, J. T. *J. Phys. Chem. A* **1999**, *103* (49), 10398-10408.
82. Ando, K.; Hynes, J. T., Acid-base proton transfer and ion pair formation in solution. In *Advances in Chemical Physics*, Prigogine, I.; Rice, S. A., Eds. 1999; Vol. 110, pp 381-430.
83. Ayotte, P.; Hebert, M.; Marchand, P. *J. Chem. Phys.* **2005**, *123* (18), 8.

84. Cabaleiro-Lago, E. M.; Hermida-Ramon, J. M.; Rodriguez-Otero, J. *J. Chem. Phys.* **2002**, *117* (7), 3160-3168.
85. Conley, C.; Tao, F. M. *Chem. Phys. Lett.* **1999**, *301* (1-2), 29-36.
86. Cuma, M.; Schmitt, U. W.; Voth, G. A. *Chem. Phys.* **2000**, *258* (2-3), 187-199.
87. Devlin, J. P.; Uras, N.; Sadlej, J.; Buch, V. *Nature* **2002**, *417* (6886), 269-271.
88. Gertner, B. J.; Peslherbe, G. H.; Hynes, J. T. *Isr. J. Chem.* **1999**, *39* (3-4), 273-281.
89. Kuo, J. L.; Klein, M. L. *J. Chem. Phys.* **2004**, *120* (10), 4690-4695.
90. Laasonen, K.; Klein, M. L. *J. Am. Chem. Soc.* **1994**, *116* (25), 11620-11621.
91. Laasonen, K.; Klein, M. L. *Mol. Phys.* **1996**, *88* (1), 135-142.
92. Lee, C. T.; Sosa, C.; Planas, M.; Novoa, J. J. *J. Chem. Phys.* **1996**, *104* (18), 7081-7085.
93. Lin, W.; Paesani, F. *J. Phys. Chem. A* **2013**, *117* (32), 7131-7141.
94. Mancini, J. S.; Bowman, J. M. *Phys. Chem. Chem. Phys.* **2015**, *17* (9), 6222-6226.
95. Mancini, J. S.; Samanta, A. K.; Bowman, J. M.; Reisler, H. *J. Phys. Chem. A* **2014**, *118* (37), 8402-8410.
96. Odde, S.; Mhin, B. J.; Lee, K. H.; Lee, H. M.; Tarakeshwar, P.; Kim, K. S. *J. Phys. Chem. A* **2006**, *110* (25), 7918-7924.
97. Odde, S.; Mhin, B. J.; Lee, S.; Lee, H. M.; Kim, K. S. *J. Chem. Phys.* **2004**, *120* (20), 9524-9535.
98. Pérez de Tudela, R.; Marx, D. *Phys. Rev. Lett.* **2017**, *119* (22), 223001.
99. Raugei, S.; Klein, M. L. *J. Am. Chem. Soc.* **2003**, *125* (30), 8992-8993.
100. Re, S.; Osamura, Y.; Suzuki, Y.; Schaefer, H. F. *J. Chem. Phys.* **1998**, *109* (3), 973-977.
101. Re, S. Y. *J. Phys. Chem. A* **2001**, *105* (42), 9725-9735.
102. Robertson, W. H.; Johnson, M. A. *Annu. Rev. Phys. Chem.* **2003**, *54*, 173-213.
103. Sato, H.; Hirata, F. *J. Am. Chem. Soc.* **1999**, *121* (14), 3460-3467.
104. Sillanpaa, A. J.; Simon, C.; Klein, M. L.; Laasonen, K. *J. Phys. Chem. B* **2002**, *106* (43), 11315-11322.
105. Simon, C.; Klein, M. L. *ChemPhysChem* **2005**, *6* (1), 148-153.
106. Smith, A.; Vincent, M. A.; Hillier, I. H. *J. Phys. Chem. A* **1999**, *103* (8), 1132-1139.
107. Vargas-Caamal, A.; Cabellos, J. L.; Ortiz-Chi, F.; Rzepa, H. S.; Restrepo, A.; Merino, G. *Chem. Eur. J.* **2016**, *22* (8), 2812-2818.
108. Walewski, L.; Forbert, H.; Marx, D. *J. Phys. Chem. Lett.* **2011**, *2* (24), 3069-3074.

109. Walewski, L.; Forbert, H.; Marx, D. *ChemPhysChem* **2013**, *14* (4), 817-826.
110. Xie, Z. Z.; Ong, Y. S.; Kuo, J. L. *Chem. Phys. Lett.* **2008**, *453* (1-3), 13-17.
111. Johnston, R. L., *Atomic and Molecular Clusters*. London, 2002.
112. der Waals, J. Over de Continuïteit van den Gas-en Vloeistofoestand (on the continuity of the gas and liquid state). Ph. D. thesis, Hoogeschool te Leiden, 1873.
113. London, F. Z. *phys. Chem* **1930**, *11*, 222-251.
114. Israelachvili, J., *Intermolecular and Surface Forces*. 3rd. Ed. ed.; London, 2011.
115. Knowles, R. R.; Jacobsen, E. N. *Proceedings of the National Academy of Sciences* **2010**, *107* (48), 20678.
116. Grimme, S. *Wiley Interdiscip. Rev.: Comput. Mol. Sci.* **2011**, *1* (2), 211-228.
117. Desiraju, G. R. *Angew. Chem., Int. Ed.* **2011**, *50*, 52-59.
118. Cavallo, G.; Metrangolo, P.; Pilati, T.; Resnati, G.; Terraneo, G., Halogen Bond: A Long Overlooked Interaction. In *Halogen Bonding I: Impact on Materials Chemistry and Life Sciences*, Metrangolo, P.; Resnati, G., Eds. Springer International Publishing: Cham, 2015; pp 1-17.
119. Desiraju, G. R.; Ho, P. S.; Kloo, L.; Legon, A. C.; Marquardt, R.; Metrangolo, P.; Politzer, P.; Resnati, G.; Rissanen, K. *Pure Appl. Chem.* **2013**, *85* (8), 1711-1713.
120. Wolters, L. P.; Schyman, P.; Pavan, M. J.; Jorgensen, W. L.; Bickelhaupt, F. M.; Kozuch, S. *Wiley Interdisciplinary Reviews-Computational Molecular Science* **2014**, *4* (6), 523-540.
121. Cavallo, G.; Metrangolo, P.; Milani, R.; Pilati, T.; Priimagi, A.; Resnati, G.; Terraneo, G. *Chem. Rev* **2016**, *116* (4), 2478-2601.
122. Metrangolo, P.; Resnati, G.; Pilati, T.; Biella, S., Halogen bonding in crystal engineering. In *Halogen Bonding: Fundamentals and Applications*, Metrangolo, P.; Resnati, G., Eds. Springer-Verlag Berlin: Berlin, 2008; Vol. 126, pp 105-136.
123. Hill, J. G.; Hu, X. J. *Chem. Eur. J.* **2013**, *19* (11), 3620-3628.
124. Palusiak, M. *Theochem-J. Mol. Struct.* **2010**, *945* (1-3), 89-92.
125. Aakeroy, C. B.; Fasulo, M.; Schultheiss, N.; Desper, J.; Moore, C. *Journal of the American Chemical Society* **2007**, *129* (45), 13772-+.
126. Alkorta, I.; Blanco, F.; Solimannejad, M.; Elguero, J. *J. Phys. Chem. A* **2008**, *112* (43), 10856-10863.

127. Hogan, S. W. L.; van Mourik, T. *Journal of Computational Chemistry* **2016**, *37* (8), 763-770.
128. Li, Q. Z.; Xu, X. S.; Liu, T.; Jing, B.; Li, W. Z.; Cheng, J. B.; Gong, B. A.; Sun, J. Z. *Physical Chemistry Chemical Physics* **2010**, *12* (25), 6837-6843.
129. Li, Q. Z.; Zhu, H. J.; Zhuo, H. Y.; Yang, X.; Li, W. Z.; Cheng, J. B. *Spectrochimica Acta Part a-Molecular and Biomolecular Spectroscopy* **2014**, *132*, 271-277.
130. Desiraju, G. R. *Angew. Chem.-Int. Edit.* **2011**, *50* (1), 52-59.
131. von Grothuß, T., *Mémoire sur la décomposition de l'eau et des corps qu'elle tient en dissolution à l'aide de l'électricité galvanique*. 1805.
132. Knight, C.; Voth, G. A. *Acc. Chem. Res.* **2012**, *45* (1), 101-109.
133. Hassanali, A. A.; Cuny, J.; Verdolino, V.; Parrinello, M. *Phil. Trans. R. Soc. A* **2014**, *372* (2011), 20120482.
134. Tuckerman, M.; Laasonen, K.; Sprik, M.; Parrinello, M. *J. Phys. Chem.* **1995**, *99* (16), 5749-5752.
135. Tuckerman, M.; Laasonen, K.; Sprik, M.; Parrinello, M. *J. Chem. Phys.* **1995**, *103* (1), 150-161.
136. Heuft, J.; Meijer, E. *Phys. Chem. Chem. Phys.* **2006**, *8* (26), 3116-3123.
137. Marx, D.; Tuckerman, M. E.; Hutter, J.; Parrinello, M. *Nature* **1999**, *397*, 601.
138. Acelas, N.; Hincapie, G.; Guerra, D.; David, J.; Restrepo, A. *J. Chem. Phys.* **2013**, *139* (4).
139. Guerra, D.; David, J.; Restrepo, A. *J. Comp. Methods in Sci. and Eng.* **2014**, *14* (1-3), 93-102.
140. Saunders, M. *J. Comput. Chem.* **2004**, *25* (5), 621-626.
141. Hadad, C.; Florez, E.; Acelas, N.; Merino, G.; Restrepo, A., *Microsolvation of small cations and anions*. 2018; p e25766.
142. Babin, V.; Paesani, F. *Chem. Phys. Lett.* **2013**, *580*, 1-8.
143. Buck, U.; Ettischer, I.; Melzer, M.; Buch, V.; Sadlej, J. *Phys. Rev. Lett.* **1998**, *80* (12), 2578-2581.
144. Gregory, J. K.; Clary, D. C. *J. Phys. Chem. A* **1997**, *101* (36), 6813-6819.
145. Hincapie, G.; Acelas, N.; Castano, M.; David, J.; Restrepo, A. *J. Phys. Chem. A* **2010**, *114* (29), 7809-7814.
146. Kuo, J. L.; Klein, M. L. *J. Chem. Phys.* **2005**, *122* (2), 9.

147. Perez, C.; Muckle, M. T.; Zaleski, D. P.; Seifert, N. A.; Temelso, B.; Shields, G. C.; Kisiel, Z.; Pate, B. H. *Science* **2012**, *336* (6083), 897-901.
148. Perez, J. F.; Hadad, C. Z.; Restrepo, A. *Int. J. Quantum Chem.* **2008**, *108* (10), 1653-1659.
149. Ramirez, F.; Hadad, C. Z.; Guerra, D.; David, J.; Restrepo, A. *Chem. Phys. Lett.* **2011**, *507* (4-6), 229-233.
150. Wang, Y. M.; Babin, V.; Bowman, J. M.; Paesani, F. *J. Am. Chem. Soc.* **2012**, *134* (27), 11116-11119.
151. Gadre, S. R.; Yeole, S. D.; Sahu, N. *Chem. Rev* **2014**, *114* (24), 12132-12173.
152. Hartke, B. *J. Phys. Chem.* **1993**, *97* (39), 9973-9976.
153. Deaven, D. M.; Ho, K.-M. *Phys. Rev. Lett.* **1995**, *75* (2), 288.
154. Johnston, R. L. *Dalton Transactions* **2003**, (22), 4193-4207.
155. Jensen, F., *Introduction to Computational Chemistry*. 1999.
156. Frenkel, D.; Smit, B. *Understanding molecular simulations: from algorithms to applications*; Academic press: 2002.
157. Buehl, M.; Wipff, G. *ChemPhysChem* **2011**, *12* (17), 3095-3105.
158. Chaban, G. M.; Gerber, R. B.; Janda, K. C. *J. Phys. Chem. A* **2001**, *105* (36), 8323-8332.
159. Emmeluth, C.; Dyczmons, V.; Kinzel, T.; Botschwina, P.; Suhm, M. A.; Yanez, M. *Phys. Chem. Chem. Phys.* **2005**, *7* (5), 991-997.
160. Masia, M.; Forbert, H.; Marx, D. *J. Phys. Chem. A* **2007**, *111* (49), 12181-12191.
161. Oncak, M.; Slavicek, P.; Farnik, M.; Buck, U. *J. Phys. Chem. A* **2011**, *115* (23), 6155-6168.
162. Takayanagi, T.; Takahashi, K.; Kakizaki, A.; Shiga, M.; Tachikawa, M. *Chem. Phys.* **2009**, *358* (3), 196-202.
163. Jeffrey, G. A., *An Introduction to Hydrogen Bonding*. New York, 1997.
164. Samanta, A. K.; Wang, Y.; Mancini, J. S.; Bowman, J. M.; Reisler, H. *Chem. Rev* **2016**, *116* (9), 4913-4936.
165. Chen, F.; Gülbakan, B.; Weidmann, S.; Fagerer Stephan, R.; Ibáñez Alfredo, J.; Zenobi, R. *Mass Spectrometry Reviews* **2015**, *35* (1), 48-70.
166. Mackenzie, R. B.; Dewberry, C. T.; Leopold, K. R. *Science* **2015**, *349* (6243), 58-61.
167. Miller, T. A. *Science* **1984**, *223* (4636), 545-553.
168. Sylla, F.; Veltcheva, M.; Kahaly, S.; Flacco, A.; Malka, V. *Review of Scientific Instruments* **2012**, *83* (3), 033507.

169. Murphy, H. R.; Miller, D. R. *J. Phys. Chem.* **1984**, *88* (20), 4474-4478.
170. Rizzuto, A. M.; Cheng, E. S.; Lam, R. K.; Saykally, R. J. *The Journal of Physical Chemistry C* **2017**, *121* (8), 4420-4425.
171. Kirkpatrick, S.; Gelatt, C. D.; Vecchi, M. P. *Science* **1983**, *220* (4598), 671-680.
172. Perez, J. F.; Florez, E.; Hadad, C. Z.; Fuentealba, P.; Restrepo, A. *J. Phys. Chem. A* **2008**, *112* (25), 5749-5755.
173. Cabellos, J.; Ortiz-Chi, F.; Ramírez, A.; Merino, G. *Bilatu 1.0 Cinvestav Mérida, Yuc. México. 2013.*
174. Grande-Aztatzi, R.; Martínez-Alanis, P. R.; Cabellos, J. L.; Osorio, E.; Martínez, A.; Merino, G. *J. Comput. Chem.* **2014**, *35* (32), 2288-2296.
175. Frisch, M.; Trucks, G.; Schlegel, H.; Scuseria, G.; Robb, M.; Cheeseman, J.; Scalmani, G.; Barone, V.; Mennucci, B.; Petersson, G.; Nakatsuji, H.; Caricato, M.; Li, X.; Hratchian, H.; Izmaylov, A.; Bloino, J.; Zheng, G.; Sonnenberg, J.; Hada, M.; Ehara, M.; Toyota, K.; Fukuda, R.; Hasegawa, J.; Ishida, M.; Nakajima, T.; Honda, Y.; Kitao, O.; Nakai, H.; Vreven, T.; JA, M.; Peralta, J.; Ogliaro, F.; Bearpark, M.; Heyd, J.; Brothers, E.; Kudin, K.; Staroverov, V.; Kobayashi, R.; Normand, J.; Raghavachari, K.; Rendell, A.; Burant, J.; Iyengar, S.; Tomasi, J.; Cossi, M.; Rega, N.; Millam, N.; Klene, M.; Knox, J.; JB, C.; Bakken, V.; Adamo, C.; Jaramillo, J.; Gomperts, R.; Stratmann, R.; Yazyev, O.; Austin, A.; Cammi, R.; Pomelli, C.; Ochterski, J.; Martin, R.; Morokuma, K.; Zakrzewski, V.; Voth, G.; Salvador, P.; Dannenberg, J.; Dapprich, S.; Daniels, A.; Farkas, O.; Foresman, J.; Ortiz, J.; Cioslowski, J.; Fox, D. *Gaussian09, Revision D.01 Gaussian, Inc., Wallingford, CT. 2013.*
176. Ramírez-Manzanares, A.; Pena, J.; Azpiroz, J. M.; Merino, G. *J. Comput. Chem.* **2015**, *36* (19), 1456-1466.
177. Chen, X.; Zhao, Y.-F.; Wang, L.-S.; Li, J. *Computational and Theoretical Chemistry* **2017**, *1107*, 57-65.
178. Grimme, S.; Antony, J.; Schwabe, T.; Muck-Lichtenfeld, C. *Org. Biomol. Chem.* **2007**, *5* (5), 741-758.
179. Steinmann, S. N.; Corminboeuf, C. *J. Chem. Theory Comput.* **2010**, *6* (7), 1990-2001.
180. Tkatchenko, A.; DiStasio, R. A.; Car, R.; Scheffler, M. *Phys. Rev. Lett.* **2012**, *108* (23).
181. Tkatchenko, A.; Scheffler, M. *Phys. Rev. Lett.* **2009**, *102* (7).

182. Weinberger, C. R. T., G. J., *Multiscale Materials Modeling for Nanomechanics*. Switzerland, 2016.
183. Řezáč, J.; Hobza, P. *Chem. Rev* **2016**, *116* (9), 5038-5071.
184. Grimme, S. *J. Chem. Phys.* **2006**, *124* (3), 16.
185. Grimme, S.; Ehrlich, S.; Goerigk, L. *J. Comput. Chem.* **2011**, *32* (7), 1456-1465.
186. Mayer, I., *Simple Theorems, Proofs, and Derivations in Quantum Chemistry*. 2003.
187. Mayer, I. *J. Comput. Chem.* **2007**, *28* (1), 204-221.
188. Datta, S.; Trindle, C.; Illas, F., *Theoretical and Computational Aspects of Magnetic Organic Molecules*. 2014.
189. Glendening Eric, D.; Landis Clark, R.; Weinhold, F. *J. Comput. Chem.* **2013**, *34* (16), 1429-1437.
190. Wiberg, K. B. *Tetrahedron* **1968**, *24*, 1083-1096.
191. Phipps, M.; Fox, T.; Tautermann, C.; Skylaris, C.-K., *Energy decomposition analysis approaches and their evaluation on prototypical protein–drug interaction patterns*. 2015; Vol. 44.
192. von Hopffgarten, M.; Frenking, G. *Wiley Interdisciplinary Reviews-Computational Molecular Science* **2012**, *2* (1), 43-62.
193. Su, P. F.; Li, H. *J. Chem. Phys.* **2009**, *131* (1).
194. Morokuma, K. *J. Chem. Phys.* **1971**, *55* (3), 1236-1244.
195. Jeziorski, B.; Moszynski, R.; Szalewicz, K. *Chem. Rev* **1994**, *94* (7), 1887-1930.
196. Schmidt, M. W.; Baldrige, K. K.; Boatz, J. A.; Elbert, S. T.; Gordon, M. S.; Jensen, J. H.; Koseki, S.; Matsunaga, N.; Nguyen, K. A.; Su, S. J.; Windus, T. L.; Dupuis, M.; Montgomery, J. A. *J. Comput. Chem.* **1993**, *14* (11), 1347-1363.
197. te Velde, G.; Bickelhaupt, F. M.; Baerends, E. J.; Guerra, C. F.; Van Gisbergen, S. J. A.; Snijders, J. G.; Ziegler, T. *J. Comput. Chem.* **2001**, *22* (9), 931-967.
198. Ziegler, T.; Rauk, A. *Theor. Chim. Acta* **1977**, *46* (1), 1-10.
199. Kitaura, K.; Morokuma, K. *Int. J. Quantum Chem.* **1976**, *10* (2), 325-340.
200. Johnson, E. R.; Keinan, S.; Mori-Sanchez, P.; Contreras-Garcia, J.; Cohen, A. J.; Yang, W. *J. Am. Chem. Soc.* **2010**, *132* (18), 6498-6506.
201. Contreras-Garcia, J.; Yang, W. T.; Johnson, E. R. *J. Phys. Chem. A* **2011**, *115* (45), 12983-12990.

202. Contreras-Garcia, J.; Johnson, E. R.; Keinan, S.; Chaudret, R.; Piquemal, J.-P.; Beratan, D. N.; Yang, W. *J. Chem. Theory Comput.* **2011**, *7* (3), 625-632.
203. Limbach, H. H.; Tolstoy, P. M.; Perez-Hernandez, N.; Guo, J.; Shenderovich, I. G.; Denisov, G. S. *Isr. J. Chem.* **2009**, *49* (2), 199-216.
204. Gonzalez, J. D.; Florez, E.; Romero, J.; Reyes, A.; Restrepo, A. *J. Mol. Model.* **2013**, *19* (4), 1763-1777.
205. Provencal, R. A.; Casaes, R. N.; Roth, K.; Paul, J. B.; Chapo, C. N.; Saykally, R. J.; Tschumper, G. S.; Schaefer, H. F. *J. Phys. Chem. A* **2000**, *104* (7), 1423-1429.
206. Wassermann, T. N.; Suhm, M. A. *J. Phys. Chem. A* **2010**, *114* (32), 8223-8233.
207. Dyczmons, V. *J. Phys. Chem. A* **2004**, *108* (11), 2080-2086.
208. Gonzalez, L.; Mo, O.; Yanez, M. *J. Chem. Phys.* **1999**, *111* (9), 3855-3861.
209. Perchard, J. P.; Josien, M. L. *J. Chim. Phys. Phys. Chim. Biol.* **1968**, *65* (10), 1834-&.
210. Perchard, J. P.; Josien, M. L. *J. Chim. Phys. Phys. Chim. Biol.* **1968**, *65* (10), 1856-&.
211. Ehbrecht, M.; Huisken, F. *J. Phys. Chem. A* **1997**, *101* (42), 7768-7777.
212. Haber, T.; Schmitt, U.; Suhm, M. A. *Phys. Chem. Chem. Phys.* **1999**, *1* (24), 5573-5582.
213. Hearn, J. P. I.; Cogley, R. V.; Howard, B. J. *J. Chem. Phys.* **2005**, *123* (13).
214. Durig, J. R.; Larsen, R. A. *J. Mol. Struct.* **1990**, *238*, 195-222.
215. Adamo, C.; Barone, V. *J. Chem. Phys.* **1999**, *110* (13), 6158-6170.
216. Dunning, T. H. H., P. J. , *Modern Theoretical Chemistry*. New York, 1977.
217. Zhao, Y.; Truhlar, D. G. *Theor. Chem. Acc.* **2008**, *120* (1-3), 215-241.
218. Weigend, F.; Ahlrichs, R. *Phys. Chem. Chem. Phys.* **2005**, *7* (18), 3297-3305.
219. Pople, J. A.; Headgordon, M.; Raghavachari, K. *J. Chem. Phys.* **1987**, *87* (10), 5968-5975.
220. Zapata-Escobar, A.; Manrique-Moreno, M.; Guerra, D.; Hadad, C. Z.; Restrepo, A. *J. Chem. Phys.* **2014**, *140* (18).
221. Laury, M. L.; Carlson, M. J.; Wilson, A. K. *J. Comput. Chem.* **2012**, *33* (30), 2380-2387.
222. Murillo, J.; David, J.; Restrepo, A. *Phys. Chem. Chem. Phys.* **2010**, *12* (36), 10963-10970.
223. David, J.; Guerra, D.; Restrepo, A. *J. Phys. Chem. A* **2009**, *113* (38), 10167-10173.
224. Simončič, M.; Urbic, T. *Chem. Phys.* **2018**, *507*, 34-43.
225. Loru, D.; Peña, I.; Sanz, M. E. *Journal of Molecular Spectroscopy* **2017**, *335*, 93-101.
226. Umer, M.; Kopp, W. A.; Leonhard, K. *J. Chem. Phys.* **2015**, *143* (21), 214306.
227. Kealy, T. J.; Pauson, P. L. *Nature* **1951**, *168* (4285), 1039-1040.

228. Fischer, E. O.; Pfab, W. Z. *Naturforsch., B: J. Chem. Sci.* **1952**, 7 (7), 377-379.
229. Miller, S. A.; Tebboth, J. A.; Tremaine, J. F. *J. Chem. Soc.* **1952**, (FEB), 632-635.
230. Wilkinson, G.; Rosenblum, M.; Whiting, M. C.; Woodward, R. B. *J. Am. Chem. Soc.* **1952**, 74 (8), 2125-2126.
231. Laszlo, P.; Hoffmann, R. *Angew. Chem., Int. Ed.* **2000**, 39 (1), 123-+.
232. van Staveren, D. R.; Metzler-Nolte, N. *Chem. Rev* **2004**, 104 (12), 5931-5985.
233. Fouda, M. F. R.; Abd-Elzaher, M. M.; Abdelsamaia, R. A.; Labib, A. A. *Appl. Organomet. Chem.* **2007**, 21 (8), 613-625.
234. Ornelas, C. *New J. Chem.* **2011**, 35 (10), 1973-1985.
235. Alt, H. G.; Koppl, A. *Chem. Rev* **2000**, 100 (4), 1205-1221.
236. Arrayas, R. G.; Adrio, J.; Carretero, J. C. *Angew. Chem., Int. Ed.* **2006**, 45 (46), 7674-7715.
237. Astruc, D.; Ornelas, C.; Ruiz, J. *Acc. Chem. Res.* **2008**, 41 (7), 841-856.
238. Bochmann, M. *J. Chem. Soc., Dalton Trans.* **1996**, (3), 255-270.
239. Brintzinger, H. H.; Fischer, D.; Mulhaupt, R.; Rieger, B.; Waymouth, R. M. *Angew. Chem., Int. Ed.* **1995**, 34 (11), 1143-1170.
240. Dai, L. X.; Tu, T.; You, S. L.; Deng, W. P.; Hou, X. L. *Acc. Chem. Res.* **2003**, 36 (9), 659-667.
241. Kaminsky, W. *Macromol. Chem. Phys.* **1996**, 197 (12), 3907-3945.
242. Kaminsky, W.; Arndt, M., Metallocenes for polymer catalysis. In *Polymer Synthesis / Polymer Catalysis*, 1997; Vol. 127, pp 143-187.
243. Kaminsky, W.; Laban, A. *Appl. Catal., A* **2001**, 222 (1-2), 47-61.
244. Maschmeyer, T.; Rey, F.; Sankar, G.; Thomas, J. M. *Nature* **1995**, 378 (6553), 159-162.
245. Barlow, S.; Bunting, H. E.; Ringham, C.; Green, J. C.; Bublitz, G. U.; Boxer, S. G.; Perry, J. W.; Marder, S. R. *J. Am. Chem. Soc.* **1999**, 121 (15), 3715-3723.
246. Barlow, S.; Marder, S. R. *Chem. Commun.* **2000**, (17), 1555-1562.
247. Calabrese, J. C.; Cheng, L. T.; Green, J. C.; Marder, S. R.; Tam, W. *J. Am. Chem. Soc.* **1991**, 113 (19), 7227-7232.
248. Long, N. J. *Angew. Chem., Int. Ed.* **1995**, 34 (1), 21-38.
249. Manias, E.; Touny, A.; Wu, L.; Strawhecker, K.; Lu, B.; Chung, T. C. *Chem. Mater.* **2001**, 13 (10), 3516-3523.

250. Bogdanovic, G. A.; Novakovic, S. B. *CrystEngComm* **2011**, *13* (23), 6930-6932.
251. Allen, F. H. *Acta Crystallogr. Sect. B-Struct. Sci.* **2002**, *58*, 380-388.
252. Perdew, J. P.; Burke, K.; Ernzerhof, M. *Phys. Rev. Lett.* **1996**, *77* (18), 3865-3868.
253. Grimme, S. *J. Comput. Chem.* **2006**, *27* (15), 1787-1799.
254. Irikura, K. K. a. F., D. J., "Computational Thermochemistry: Prediction and Estimation of Molecular Thermodynamics" Society, A. C., Ed. ACS Symposium Series 677: Washington, DC, 1998.
255. Irikura, K. K. National Institute of Standards and Technology. <http://thermo.pl/>.
256. Zhang, Y. K.; Yang, W. T. *Phys. Rev. Lett.* **1998**, *80* (4), 890-890.
257. Brock, C. P.; Fu, Y. G. *Acta Crystallogr. Sect. B-Struct. Sci.* **1997**, *53*, 928-938.
258. J. R. Grover, E. A. W., E. T. Hui. *J. Phys. Chem.* **1987**, *91*, 3233.
259. Janowski, T.; Pulay, P. *Chem. Phys. Lett.* **2007**, *447* (1), 27-32.
260. Park, Y. C.; Lee, J. S. *J. Phys. Chem. A* **2006**, *110* (15), 5091-5095.
261. Feyereisen, M. W.; Feller, D.; Dixon, D. A. *J. Phys. Chem.* **1996**, *100* (8), 2993-2997.
262. Ludwig, R. *Angew. Chem., Int. Ed.* **2001**, *40* (10), 1808-1827.
263. Frenking, G.; Caramori, G. F. *Angew. Chem., Int. Ed.* **2015**, *54* (9), 2596-2599.
264. W. Klopper, J. v. D.-v. d. R., F. B. Duijneveldt. *Phys. Chem. Chem. Phys.* **2000**, *2*, 2227-2234.
265. Míguez-Lago, S.; Cid, M. M.; Alonso-Gómez, J. L. *European Journal of Organic Chemistry* **2016**, *2016* (34), 5716-5721.
266. Pal, R.; Mebs, S.; Shi, M. W.; Jayatilaka, D.; Krzeszczakowska, J. M.; Malaspina, L. A.; Wiecko, M.; Luger, P.; Hesse, M.; Chen, Y.-S. *Inorganic chemistry* **2018**, *57* (9), 4906-4920.
267. Bianco, R.; Hynes, J. T. *Acc. Chem. Res.* **2006**, *39* (2), 159-165.
268. Huthwelker, T.; Ammann, M.; Peter, T. *Chem. Rev* **2006**, *106* (4), 1375-1444.
269. McNeill, V. F.; Loerting, T.; Geiger, F. M.; Trout, B. L.; Molina, M. J. *Proc. Natl. Acad. Sci. U. S. A.* **2006**, *103* (25), 9422-9427.
270. Forbert, H.; Masia, M.; Kaczmarek-Kedziera, A.; Nair, N. N.; Marx, D. *J. Am. Chem. Soc.* **2011**, *133* (11), 4062-4072.
271. Lesch, V.; Jeremias, S.; Moretti, A.; Passerini, S.; Heuer, A.; Borodin, O. *J. Phys. Chem. B* **2014**, *118* (26), 7367-7375.

272. Morrison, A. M.; Flynn, S. D.; Liang, T.; Douberly, G. E. *J. Phys. Chem. A* **2010**, *114* (31), 8090-8098.
273. Rzepa, H. *The Winnower* **2015**.
274. Schindler, T.; Berg, C.; Niederschattburg, G.; Bondybey, V. E. *Chem. Phys. Lett.* **1994**, *229* (1-2), 57-64.
275. Yoon, Y. K.; Carpenter, G. B. *Acta Crystallogr.* **1959**, *12* (1), 17-20.
276. Zischang, J.; Skyortsov, D.; Choi, M. Y.; Mata, R. A.; Suhm, M. A.; Vilesov, A. F. *J. Phys. Chem. A* **2015**, *119* (11), 2636-2643.
277. Goerigk, L.; Grimme, S. *J. Chem. Theory Comput.* **2011**, *7* (2), 291-309.
278. Siu, C. K.; Fox-Beyer, B. S.; Beyer, M. K.; Bondybey, V. E. *Chem. Eur. J.* **2006**, *12* (24), 6382-6392.
279. Boda, M.; Patwari, G. N. *Phys. Chem. Chem. Phys.* **2017**, *19* (11), 7461-7464.
280. Chen, J.; Jiang, S.; Liu, Y.-R.; Huang, T.; Wang, C.-Y.; Miao, S.-K.; Wang, Z.-Q.; Zhang, Y.; Huang, W. *RSC Advances* **2017**, *7* (11), 6374-6388.
281. Krishnakumar, P.; Maity, D. K. *New J. Chem.* **2017**, *41* (15), 7195-7202.
282. Krishnakumar, P.; Maity, D. K. *Mol. Phys.* **2017**, *115* (24), 3224-3233.
283. Soria, J.; Sanz, J.; Torralvo, M.; Sobrados, I.; Garlisi, C.; Palmisano, G.; Çetinkaya, S.; Yurdakal, S.; Augugliaro, V. *Applied Catalysis B: Environmental* **2017**, *210*, 306-319.
284. Zuraski, K.; Kwasniewski, D.; Samanta, A. K.; Reisler, H. *The journal of physical chemistry letters* **2016**, *7* (21), 4243-4247.
285. Zuraski, K.; Wang, Q.; Kwasniewski, D.; Bowman, J. M.; Reisler, H. *J. Chem. Phys.* **2018**, *148* (20), 204303.
286. De Haan, D. O.; Brauers, T.; Oum, K.; Stutz, J.; Nordmeyer, T.; Finlayson-Pitts, B. J. *Int. Rev. Phys. Chem.* **1999**, *18* (3), 343-385.
287. Jencks, W. P., *Catalysis in Chemistry and Enzymology*. McGraw-Hill: 1969.
288. Keesee, R. G. *J. Geophys. Res.: Atmos.* **1989**, *94* (D12), 14683-14692.
289. Müller, A.; Ratajczak, H.; Junge, W.; Diemann, E., *Electron and proton transfer in chemistry and biology*. Elsevier Science Publishers: 1992.
290. Peter, T. *Annu. Rev. Phys. Chem.* **1997**, *48*, 785-822.
291. Rokita, S. E. *Q. Rev. Biol.* **1992**, *67* (3), 357-357.
292. Steiner, T. *Angew. Chem. Int. Ed.* **2002**, *41* (1), 48-76.

293. Cotton, F. A.; Wilkinson, G., *Advanced Inorganic Chemistry*. Wiley New York: 1988; Vol. 594.
294. Weast, R. C.; Astle, M. J.; Beyer, W. H., *CRC Handbook of chemistry and physics*. CRC press, Boca raton FL: 1989; Vol. 1990.
295. Giguere, P. A.; Turrell, S. *J. Am. Chem. Soc.* **1980**, *102* (17), 5473-5477.
296. Rojas-Valencia, N.; Ibarguen, C.; Restrepo, A. *Chem. Phys. Lett.* **2015**, *635*, 301-305.
297. Salazar-Cano, J. R.; Guevara-Garcia, A.; Vargas, R.; Restrepo, A.; Garza, J. *Phys. Chem. Chem. Phys.* **2016**, *18* (34), 23508-23515.
298. Zakai, I.; Varner, M. E.; Gerber, R. B. *Phys. Chem. Chem. Phys.* **2017**, *19* (31), 20641-20646.
299. Scheiner, S., *Hydrogen bonding: a theoretical perspective*. Oxford University Press on Demand: 1997.
300. Esrafil, M. D.; Beheshtian, J.; Hadipour, N. L. *Int. J. Quantum Chem.* **2011**, *111* (12), 3184-3195.
301. Dannenberg, J. J. *J. Mol. Struct.* **2002**, *615* (1-3), 219-226.
302. Guevara-Vela, J. M.; Romero-Montalvo, E.; Gómez, V. A. M.; Chávez-Calvillo, R.; García-Revilla, M.; Francisco, E.; Pendás, Á. M.; Rocha-Rinza, T. *Phys. Chem. Chem. Phys.* **2016**, *18* (29), 19557-19566.
303. Kemp, D. D.; Gordon, M. S. *J. Phys. Chem. A* **2010**, *114* (3), 1298-1303.
304. Jiang, G. J.; Anderson, G. R. *J. Chem. Phys.* **1974**, *60* (8), 3258-3263.
305. Emsley, J. *Chem. Soc. Rev.* **1980**, *9* (1), 91-124.
306. Grabowski, S. J.; Ugalde, J. M.; Andrada, D. M.; Frenking, G. *Chem. Eur. J.* **2016**, *22* (32), 11317-11328.
307. Grabowski, J. S. *Crystals* **2016**, *6* (1).
308. Pylaeva, S. A.; Elgabarty, H.; Sebastiani, D.; Tolstoy, P. M. *Phys. Chem. Chem. Phys.* **2017**, *19* (38), 26107-26120.